# Robotic Catheters for Beating Heart Surgery

**Robert D. Howe**
Thesis Advisor

**Samuel B. Kesner**
Author

# Robotic Catheters for Beating Heart Surgery

## Abstract

Compliant and flexible cardiac catheters provide direct access to the inside of the heart via the vascular system without requiring clinicians to stop the heart or open the chest. However, the fast motion of the intracardiac structures makes it difficult to modify and repair the cardiac tissue in a controlled and safe manner. In addition, rigid robotic tools for beating heart surgery require the chest to be opened and the heart exposed, making the procedures highly invasive. The novel robotic catheter system presented here enables minimally invasive repair on the fast-moving structures inside the heart, like the mitral valve annulus, without the invasiveness or risks of stopped heart procedures.

In this thesis, I investigate the development of 3D ultrasound-guided robotic catheters for beating heart surgery. First, the force and stiffness values of tissue structures in the left atrium are measured to develop design requirements for the system. This research shows that a catheter will experience contractile forces of 0.5 – 1.0 N and a mean tissue structure stiffness of approximately 0.1 N/mm while interacting with the mitral valve annulus. Next, this thesis presents the catheter system design, including force sensing, tissue resection, and ablation end effectors. In order to operate inside the beating heart, position and force control systems were developed to compensate for the

catheter performance limitations of friction and deadzone backlash and evaluated with *ex vivo* and *in vivo* experiments. Through the addition of friction and deadzone compensation terms, the system is able to achieve position tracking with less than 1 mm RMS error and force tracking with 0.08 N RMS error under ultrasound image guidance. Finally, this thesis examines how the robotic catheter system enhances beating heart clinical procedures. Specifically, this system improves resection quality while reducing the forces experienced by the tissue by almost 80% and improves ablation performance by reducing contact resistance variations by 97% while applying a constant force on the moving tissue.

.

# Contents

## Acknowledgements

During my journey to complete this PhD research and dissertation, I have had the privilege to learn from a number of amazing and gifted individuals. This work would not have been possible without their contributions and support.

First, I must thank my PhD advisor and mentor, Professor Robert Howe. From our very first meeting, Professor Howe encouraged me to become an independent thinker and researcher and develop my own interests and skills. While working together on undergraduate classes, writing grants and papers, brainstorming new project ideas, and discussing confusing experimental results, my work with Professor Howe has been the most formative experiences in my educational career. I hope to emulate his joy of research and intellectual exploration throughout the rest of my life.

I also want to thank my PhD committee for their support and guidance. First, I would like to thank Professor Alex Slocum from MIT for introducing me to medical device design. Through our work on the Endoblend surgical tool during my Masters Degree studies, I learned about the exciting opportunities and challenges of developing new medical devices. Professor Rob Wood provided me not only great mentorship and advice, but also with access to his unmatched laboratory facilities and the expertise of his graduate students and postdocs. Professor Pierre Dupont has also been a supportive mentor during the course of my PhD, initially as a member of our NIH funding grant partnership and now as collaborator at Children's Hospital Boston, by allowing me to share his laboratory space. Thank you all for your help in guiding me to this stage in my career.

The members of the Harvard Biorobotics lab have been there for me every day over the last four years. There is no way to sufficiently thank them for the countless conversations and research assistance that shaped my work. I would especially like to thank Dr. Shelten Yuen, Dr. Peter Hammer, Professor Mahdi Tavakoli, Leif Jentoft, Paul Loschak and Laura Brattain for their help and advice. I could not have completed this body of research without their assistance and support.

I would also like to thank the people at Children's Hospital Boston. I have had the honor to work with a number of highly talented and patient surgeons, especially Dr. Nikolay Vasilyev, Dr. Haruo Yamauchi, and Dr. Mitsuhiro Kawata. The knowledge they have generously provided me regarding cardiology, surgery, and clinical medicine is arguably the most valuable education I have received during the course of my PhD program. In addition to these surgeons, I would like to thank Dr. Pedro del Nido for making this entire research project possible and Dr. Andrew Gosline for his advice, tools, and support as I prepared for my *in vivo* experiments. This work was supported by the U. S. National Institute of Health under grant NIH R01 HL073647.

My family has always been there for me with love and support. I could not have made it this far in life without them. Sue, Rich, and Henry: thank you so much for teaching me the importance of education, hard work, and compassion. This PhD is a tribute to your nurturing and guidance. I love you all.

Finally, all of the energy and effort that went into completing this thesis was inspired by my wife Jessica, the love of my life. Everything is sweeter when she is with me. Her support, encouragement, and love have been the driving force that allowed me to reach this day. Thank you, Jessie, for your love, patience, and everything.

# Dedication

*To my family: Mom, Dad, Henry, and the lovely Mrs. Jessie.*

# Chapter 1

# Introduction

## 1.1. Motivation

Heart disease is the leading cause of death in most industrialized nations [1]. Physicians and engineers are developing a myriad of new procedures, drugs, and technologies to treat ailments that can affect the health and function of the human heart. One of the most significant advances in cardiac therapies is the use of cardiac catheters to give clinicians direct intracardiac access, or access to the inside of the beating heart, via the vascular system. The alternative to catheterization is open-heart intervention, an invasive procedure where the chest is opened to expose and stop the heart while the blood is artificially oxygenated and pumped throughout the body using a cardiopulmonary bypass (CPB) machine. In addition to the significant post-operative recovery time from an open-chest procedure, CPB has the additional risks of stroke and long-term cognitive deficiencies for the patient [2, 3].

Open-chest cardiac intervention without the use of CPB is known as beating heart surgery. These procedures, often conducted to repair vessels on the outside of the heart,

offer a number of advantages, including reduced post-operative recovery time and decreased medical costs [4, 5]. Beating heart surgery also allows clinicians to evaluate the quality of the repair while the heart is still beating. This is especially useful when evaluating the function of dynamic structures in the heart, such as the active opening and closing of the mitral valve [6].

Cardiac catheters are the only clinically available technology that enables beating heart diagnosis and treatment inside the heart without the use of highly invasive open-heart surgical techniques. Cardiac catheters are long and thin flexible tubes and wires that are inserted into the vascular system and passed into the heart. Innovations in catheter technology have greatly expanded the range of procedures that interventional cardiologists can perform inside the heart using minimally invasive techniques. Procedures that are now performed using catheters include measuring cardiac physiological function, dilating vessels and valves, and implanting prosthetics and devices [7]. While catheters can perform many tasks inside the heart, they do not as yet allow clinicians to interact with heart tissue with the same level of skill as in open-heart surgery. A primary reason for this limitation is that current catheters do not have the dexterity, speed, and force capabilities to perform complex tissue modifications on moving cardiac tissue.

It is the goal of this work to enable catheter-based surgical repairs inside the heart with the same efficacy as traditional open-chest and stopped-heart surgical techniques. A crucial enabling technology that allows robotic catheter devices to operate inside the beating heart and interact with moving tissue structures is real-time 3D ultrasound (3DUS) imaging. 3DUS imaging is able to track the fast tissue motion so that the

catheter can be servoed to compensate for the cardiac motions [8, 9]. Motion compensation stabilizes the tissue relative to the catheter tool, allowing the surgical tool end effector at the catheter tip to interact with the fast-moving structures as if they were fixed in space. The combination of this motion compensation technology and robotic catheters allows the system to achieve the goal of minimally invasively performing surgical repairs inside the beating heart.

The following thesis presents the design, control, and *in vivo* evaluation of the 3DUS image-guided robotic catheter system. The catheter system demonstrates the effectiveness of beating heart surgery through representative surgical tasks.

## 1.2. Background and Prior Art

Robotic catheter systems have the potential to revolutionize cardiac treatment and repair. Commercially available robotic cardiac catheters now on the market include the Artisan Control Catheter (Hansen Medical, Mountain View CA, USA), the CorPath Vascular Robotic System (Corindus Vascular Robotics, Natick MA, USA), and the Catheter Robotics Remote Catheter Manipulation System (Catheter Robotics, Inc., Budd Lake, NJ, USA) [10, 11], [12]. These devices build upon the robotic catheter modeling and teleoperation research conducted by Jayender, Fukuda, Camarillo, and others [10, 13-16]. The Artisan Control Catheter and Catheter Robotics system allow clinicians to position an ablation catheter inside the heart at manual speeds via a teleoperated actuation system [17]. The CorPath System also uses a teleoperated catheter to remove the need for the clinician to manually position the device inside the patient. However, this system is designed to perform percutaneous coronary interventions (PCI) such as deploying stents or balloons inside the coronary vessels [11]. These devices offer the advantage of

enabling the positioning of a catheter while the human operator is safely away from the potentially harmful radiation produced by fluoroscopy imaging [17]. However, these actuated catheters do not provide sufficient speeds to allow the catheters end effectors to keep up with the fast motion of intracardiac structures [8, 18].

Motion compensation is required when operating on the inside of the beating heart because it enables far more dexterous tissue-tool interactions. Motion compensation also limits the risk of injury from catheter collisions with fast-moving tissue structures. Researchers have developed robotic approaches to compensate for the motion of the beating heart [19-21], but these techniques are directed at procedures that repair coronary arteries on the external surface of the heart. In previous work, Yuen et al. developed robotic devices that compensate for the motion of internal heart structures with a handheld robotic instrument inserted through incisions in the heart wall [8, 22-24]. The motion of the tissue target is tracked in real-time using 3D ultrasound (3DUS) imaging [24], [25]. 3DUS imaging is utilized in this work because it is the only imaging modality that allows for real-time volumetric imaging of soft tissue structures through the blood pool at video frame rates (28 Hz) [24, 25]. Ultrasound also has the benefit of being safe, clinically available, and non-irradiating.

The previous work on 3DUS-guided beating heart surgery showed that single degree of freedom (DOF) servoing is sufficient to accurately track the motion of certain cardiac structures, including the human mitral valve annulus [18, 22]. The handheld rigid tool approach enables beating heart procedures that alleviate the risks associated with stopped heart techniques [3, 26], but the necessity of creating incisions through the chest and into the heart wall requires intubation and deep anesthesia. Therefore, the rigid tool

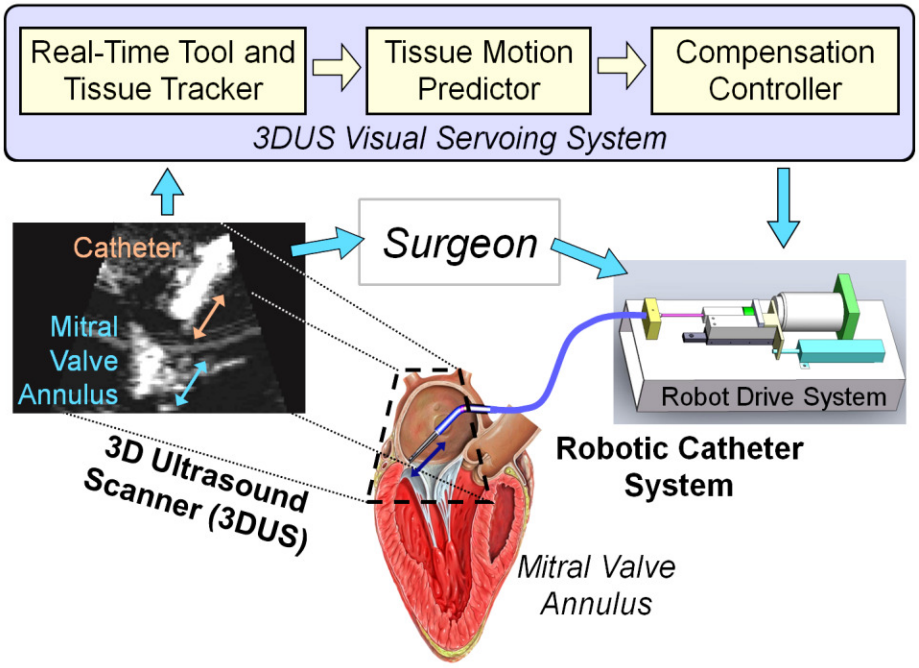


Figure 1.1 The robotic catheter system consists of a drive system, a catheter module, and a 3DUS visual servoing system. The system compensates for the fast motion of the cardiac tissue using 3D ultrasound imaging and a visual servoing system while the surgeon performs the repair procedure.

approach is still relatively invasive.

The robotic catheter system overcomes these limitations by combining the advantages of beating heart surgery under 3DUS guidance with the minimally invasive techniques of catheters. The system consists of a 3DUS imaging system, a visual servoing and control system, a robotic drive system, and a catheter module that is inserted into the heart. See Figure 1.1 for a diagram of the entire robotic catheter system.

## 1.3. Thesis Contributions

The work presented in this thesis constitutes the first time a catheter system has actively compensated for the fast motion of intracardiac tissue structures, actively regulated the forces it applies to the inside of the heart, and utilized ultrasound-guidance

and motion compensation to perform cardiac surgical procedures. The results provide a clearer understanding of the requirements and challenges of performing surgery on the beating heart with a robotic catheter and a pathway to realize this objective. This work is built upon the robotics and image-guidance research conducted by Yuen et al. [22, 23, 25, 27] and Novotny *et al* [24, 28, 29].

A number of topics and challenges were investigated in order to realize the goal of a catheter system capable of performing beating heart surgery. First, the intracardiac environment where the catheter system operates was examined to produce design specifications, including force and displacement requirements. Based on these specifications, the mechanical design of the robotic catheter system and three catheter tip end effectors were developed and evaluated. The major robotic control contributions of this work are the characterization of the catheter performance limitations of friction and backlash and the use of compensation controller terms to reduce the effects of these limitations on the catheter tip position accuracy and force regulation. The robotic catheter system developed for this project was employed to investigate users' ability to discern the stiffness properties of moving tissue using haptic feedback and motion compensation. Finally, the entire motion compensated catheter system was demonstrated through clinically relevant surgical tasks, including tissue resection and ablation.

## 1.4. Thesis Outline

This thesis presents the development of the 3D ultrasound-guided robotic catheter system from initial concept to pre-clinical *in vivo* evaluation experiments.

Chapter 2 discusses the mechanical properties of the tissue structures inside the heart chambers where the catheter system operates. First, the basic cardiac physiology is

briefly described to inform the reader about the structures encountered by the catheter inside the heart. In order to specify the performance requirements of the robotic system, *in vivo* experiments were conducted to evaluate the stiffness and forces associated with the tissue structures around the mitral valve and left atrium. These experiments determined that the stiffness of the cardiac structures in the left atrium are approximately 0.1 N/mm and the forces experienced by a tool interacting with these structures varies from 0.5 – 1.0 N.

Chapter 3 presents the mechanical design of the robotic catheter system, including the system level design, actuation, image guidance, and catheter component selection. A number of end effectors have been developed for the catheter system including a force sensor, a tissue resection tool, and a radio frequency (RF) ablation tool that also functions as a force sensor. The force sensors were developed using rapid prototyping technologies and are able to measure forces with a precision of 0.2 N RMS, or 2% of its full 10 N scale. The chapter concludes with a discussion of braced manipulation and catheter bracing strategies inside the heart. Bracing is required to apply larger forces against the cardiac tissue and improve tissue tracking.

Chapter 4 and Chapter 5 discuss the position and force control of robotic catheters, respectively. The dominant performance limitations identified for the catheter transmission system are friction and backlash. The success of the control systems is closely connected to accurately compensating for these performance limitations. A position control system designed specifically to reduce the impact of friction and backlash on catheter tip position was developed and successfully evaluated *ex vivo* and *in vivo*, with position tracking errors < 1 mm RMS. The position control system was then

extended to force control with the addition of a catheter tip force sensor and a control scheme that wrapped a force control feedback loop around the existing position control system. This force control method was successfully demonstrated to be able to safely maintain a constant force on a moving target under ultrasound guidance with force tracking errors as low as 0.08 N RMS.

Chapter 6 presents a study evaluating the increases to human perception sensativity provided by motion compensation, force sensing robotic catheters, and haptic feedback while interacting with moving cardiac structures. Currently, clinicians experience almost no tactile feedback while conducting procedures with cardiac catheters. Force sensing catheters allow clinicians to both sense tissue-tool interaction forces and to perceive the tissue as if it were stationary through the use of motion compensation. This approach was evaluated with a user study and haptic teleoperation with the catheter system was demonstrated *in vivo* on the beating heart.

Chapter 7 presents applications of the robotic catheter system to clinically-relevant surgical procedures and the design of procedure-specific end effectors. The ability to accurately resect moving tissue structures with low forces was demonstrated *ex vivo*. Maintaining ablation contact with fast-moving cardiac structures was successfully achieved in a water tank and the ablation system was evaluated *in vivo*. Both of these applications are examples of essential procedure tasks for beating heart surgery.

Finally, Chapter 8 summarizes the contributions of the work, discusses the design and control insights found during the course of this research, and lays out the future work for this project.

# Chapter 2

# Intracardiac Structural Properties

This chapter describes the conditions and structures inside the beating heart, the intracardiac environment, where the robotic catheter will operate. The following sections present the basic cardiac physiology and function as well as an *in vivo* study of the mechanical structural properties of the mitral valve annulus and left atrium.

## 2.1. Cardiac Physiology

The human heart is a semi-hollow, muscular organ that circulates blood throughout the body. The inside of the heart is composed of four chambers: the right atrium (RA), the left atrium (LA), the right ventricle (RV), and the left ventricle (LV). Flow between these chambers and the rest of the body is regulated by the four valves indicated in Figure 2.1: the tricuspid valve (TV), the pulmonary valve (PV), aortic valve (AV), and the mitral valve (MV). During each heart beat, the cardiac muscle contracts to pump blood to the lungs and throughout the body in the directions indicated by the arrows in Figure 2.1. Deoxygenated blood returns from the body into the RA, passes through the TV in to the RV, and is then pumped into the lungs through the PV via the

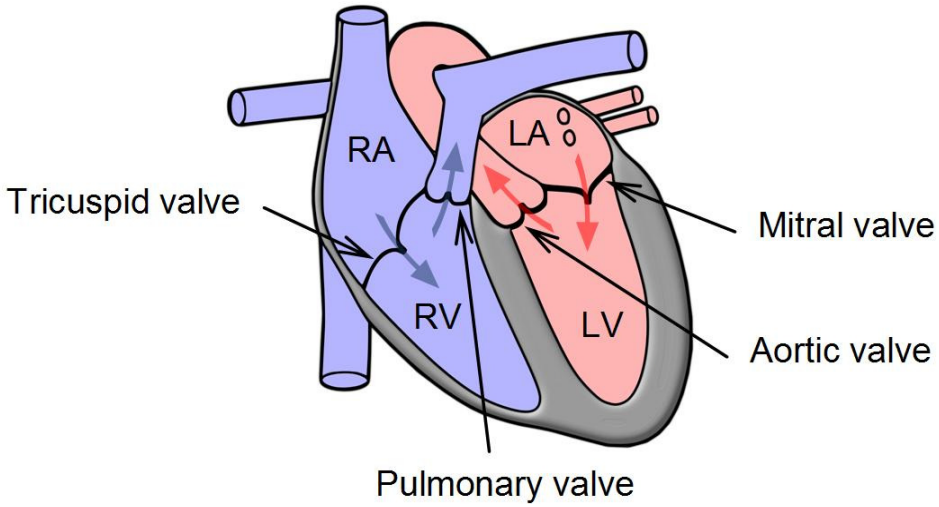


Figure 2.1 Basic cardiac physiology. The arrows indicate the direction of oxygenated (red) and deoxygenated (blue) blood flow. Image adapted from the dissertation "Simulating heart valve mechanical behavior for planning surgical repair" by P E Hammer, 2011.

pulmonary artery where it is oxygenated. The oxygenated blood returns to the heart via the pulmonary vein into the LA, enters LV through the MV, and finally is pumped into the rest of the body through the AV and the aorta. The timing and coordination of the heart beating cycle is controlled by a complex electrical conduction system embedded in the cardiac muscle structures. See *Gray's Anatomy of the Human Body* for more details on structures inside of the heart [30].

Catheter devices can be maneuvered to operate in all four chambers inside the heart. However due to the significant motion of the TV and MV annuli (up to 20 mm each heart cycle), clinicians do not regularly attempt to manipulate these structures with catheters [18][7]. Because these valves prevent backflow from the ventricles, the chambers responsible for the majority of the cardiac output, they see significant pressures and are crucial for cardiac health [6], [31]. Failure or poor operation of these valves can

result in serious health conditions, including heart failure and death [31]. In addition, people with compromised cardiac function are often too frail for invasive surgery or the use of CPB. Thus, there is a significant need to find solutions to repair or replace the TV and MV without stopped-heart and open-chest techniques, such as minimally invasive catheter technologies.

## 2.2. Tissue Structural Mechanics

There is currently a great deal of interest in percutaneous mitral valve repair [32]. These percutaneous approaches have the potential to repair one of the major valves in the heart while avoiding the morbidity associated with large chest incisions and the use of cardiopulmonary bypass (CPB) to artificially pump and oxygenate the blood [33][2, 31]. Examples of percutaneous MV repair devices include: the Carillon device (Cardiac Dimension, Inc., Kirkland, Washington), which decreases the mitral valve diameter by compressing the coronary sinus [32], the Mitralign system (Mitralign, Tewksbury, Massachusetts), which decreases the circumference of the mitral valve via cinching the valve [32], and the robotic catheter system developed to manipulate and reshape the mitral valve annulus [34]. These devices must interact with the tissue structures around the mitral valve to reshape the annulus and complete the annuloplasty procedure [32]. To successfully accomplish this procedure, it is important to know the required forces to reshape, manipulate, and affix devices to the annulus. However, many of these values are currently unknown. For example, the forces required to decrease the MV diameter by pulling on the annulus radially or the forces applied to an annuloplasty device due to cardiac muscle contractions are currently unknown. These properties must be better understood to effectively repair the valve.

Furthermore, the forces and stiffness of the intracardiac environment are currently unknown. An instrument introduced into the beating heart will encounter rapidly varying pressures and blood flows, cardiac muscle contractile forces, and tissues with properties that vary over the cardiac cycle. Other researchers have investigated certain properties of the tissue structures inside the beating heart. For example, researchers have implanted sensors to measure specific forces experienced by implants, including the forces on a rigid mitral valve ring implant and a mitral valve chordae [35-37]. However, none of the previous studies directly measured the forces and displacements resulting from an instrument interacting with the tissue structures inside the beating heart or around the mitral valve. The absence of research in this area is due to the limitations of real-time intracardiac tissue imaging and the challenges of making accurate mechanical measurements of fast-moving structures.

The work presented here directly investigates structural properties of the mitral annulus especially relevant to beating heart and percutaneous valve repair. A position and force sensing instrument was introduced into the porcine beating heart and the forces of a repair procedure were approximated by palpating the tissue structures in the left atrium. Real-time 3D ultrasound imaging enabled instrument navigation and measured the motion of the tissue structures (Figure 2.2). The measurements represent the forces applied to a surgical instrument due to interaction with contracting cardiac tissues and the mechanical stiffness of structures around the MV in the LA.

In a separate experiment, the forces required to tear sutures from the MV annulus were measured on fresh ex vivo hearts. This suture tear out experiment provides an upper bound for the maximum forces supported by a device attached to the annulus. Sutures

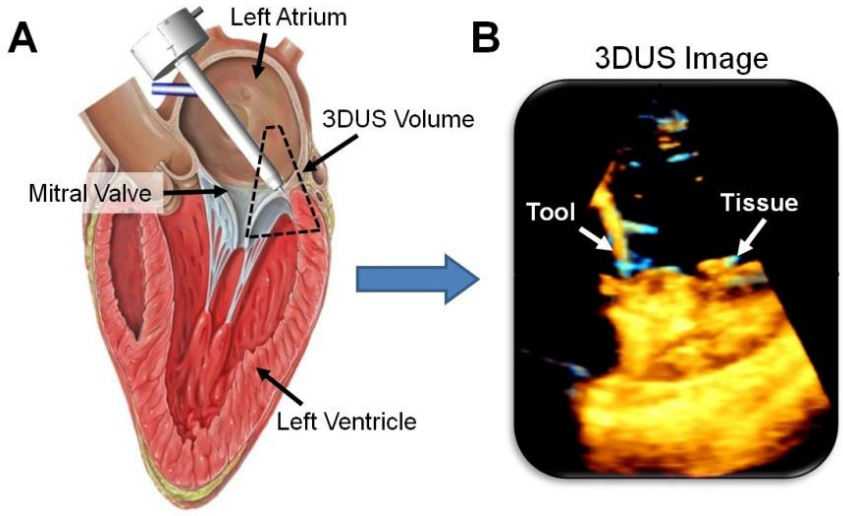


Figure 2.2 A: The left atrium of the human heart (adapted from Creative Commons) with an instrument inserted and making contact with the mitral valve annulus. B: The 3DUS image displays a similar instrument-tissue configuration and is an example of the imaging quality and resolution possible with this technology.

are a standard method for attaching prosthetic rings to the MV in open-heart repair procedures [38].

The following section describes the experimental methods, including the measurement instruments and procedures developed for the study. The section that follows presents the results of the intracardiac palpation and suture pull out experiments. The chapter concludes with a discussion of the results as well as insights into the design and control of surgical tools for beating heart mitral valve repair.

### *2.2.1.* Methods

The work presented here was conducted in two parts. First, a position and force sensing instrument was introduced into the beating porcine heart to palpate the tissue structures in the left atrium. Second, the forces required to tear out a suture from the MV

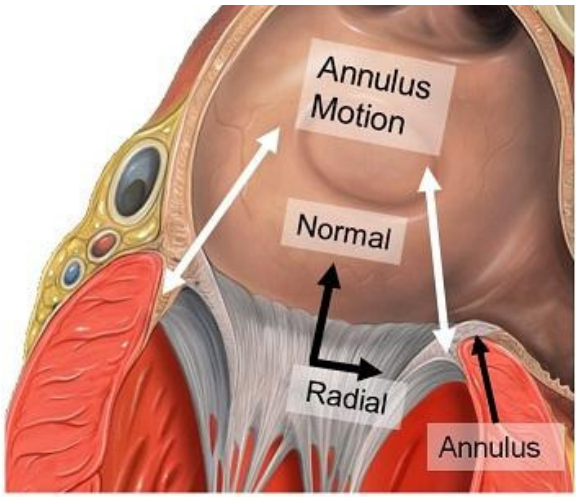


Figure 2.3 The mitral valve annulus. The motion of the annulus is approximately along one degree of freedom [18]. The annulus properties were examined in the direction normal to the plane of the valve and radially towards the center of the valve (Illustration adapted from the original by Patrick J. Lynch, medical illustrator, Creative Commons).

annulus were recorded using fresh, ex vivo porcine hearts. In this section, the equipment and methods utilized in these experiments are presented in detail.

**Equipment**

The goal of this study is to measure clinically relevant mechanical properties of the mitral annulus. Tradition annuloplasty may involve interaction with the entire circumference of the mitral valve [38]. For complete characterization of the MV annulus, the measurements should be made in directions both within and normal to the plane of the annulus (Figure 2.3). In addition, heart contractions during beating produce large displacements (> 20 mm), primarily along a single degree of freedom [18]. Therefore, an instrument with high stiffness is beneficial. The instrumentation must also withstand the pressure and flow within the intracardiac environment while minimizing disruptions to cardiac function.

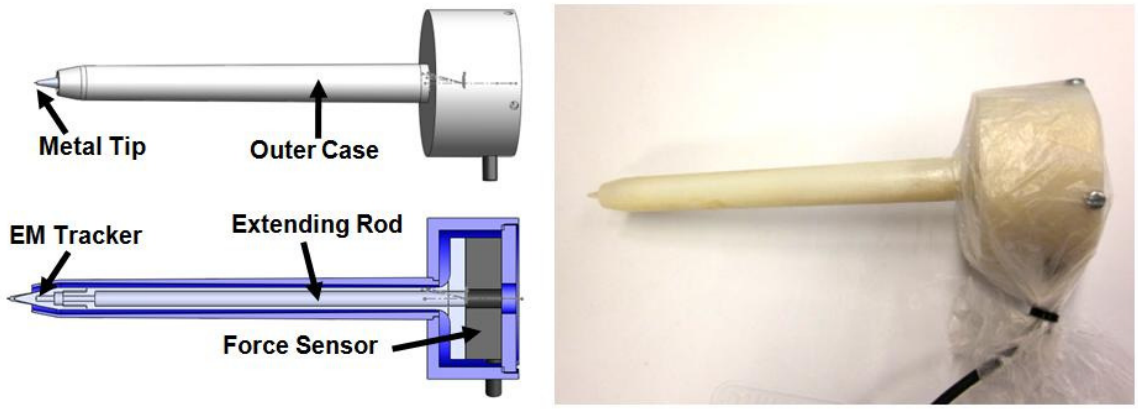


Figure 2.4 The tissue measurement instrument consists of a commercial force sensor, an EM tracker, and a rod that to allows the tool to enter the beating heart via a small incision in the LA wall.

To reach the entire workspace with the required dexterity and stiffness, the measurement instrument is designed to be inserted through an incision in the top of the LA. The instrument consists of a handle, an outer case, a rod with a sharpened tip, a 6 degree of freedom (DOF) force-torque sensor, and a 6 DOF electromagnetic (EM) position tracker (Figure 2.4). The EM tracker (Model 180 sensor, 3D Guidance trakSTAR system, Ascension Technology Corp., Burlington VT, USA, Resolution: 0.11 mm) is located inside the tip of the instrument at the point of tissue contact. The force-torque sensor (Mini40, ATI Industrial Automation, Apex NC, USA, Resolution: < 0.02 N) is located in the handle of the instrument. The position sensor was selected because it can accurately track position without visual access. The force sensor was selected for its compact size and accuracy. However, the rod was required to extend the sensor inside the heart because it is too large to fit in the LA. A small metal spike (diameter: 0.25 mm, length: < 1 mm) is attached to the tip of the rod to ensure it engages the tissue without slipping. The outer case serves to block forces generated at the incision through the heart wall from affecting the force reading. The rod is sufficiently

stiff to prevent any contact between the rod and outer case during the experiment. The region between the rod and the outer case was packed with silicone grease to prevent blood from filling the instrument while allowing the rod to move freely and transmit forces to the force sensor. Force and position sensing performance was confirmed with extensive bench calibration of the final design.

**Experimental Methods**

The in vivo experiments were conducted on three approximately 60 kg pigs in compliance with the regulations and supervision of Children's Hospital Boston animal research committee. The in vivo protocol consisted of sedating and intubating the animals, performing a left thoracotamy, and introducing the sensing instrument into the left atrium through a purse-string suture in the left atrium wall. 3DUS imaging (iE33 with X7 imaging probe, Philips Healthcare, Andover, MA, USA) provided intracardiac guidance and enabled recording the gross motion of the tissue during the experiment. During each trial, the experimenter first used 3DUS to align the instrument and the tissue target and then the EM position, force sensing, and 3DUS imaging were recorded simultaneously while the experimenter slowly moved the instrument tip ($\leq$ 5 mm/s) towards the tissue target of interest, indented the tissue until a reaction force of approximately 1-2 N was generated and held at that position for several seconds. At the end of the trial (approximately 10 s), the instrument was quickly withdrawn to provide a synchronizing event in all three sensor signals (force, EM position, and 3DUS). Sampling rates were 100 Hz, 100 Hz, and 28 Hz for the force, EM position, and 3DUS signals, respectively.

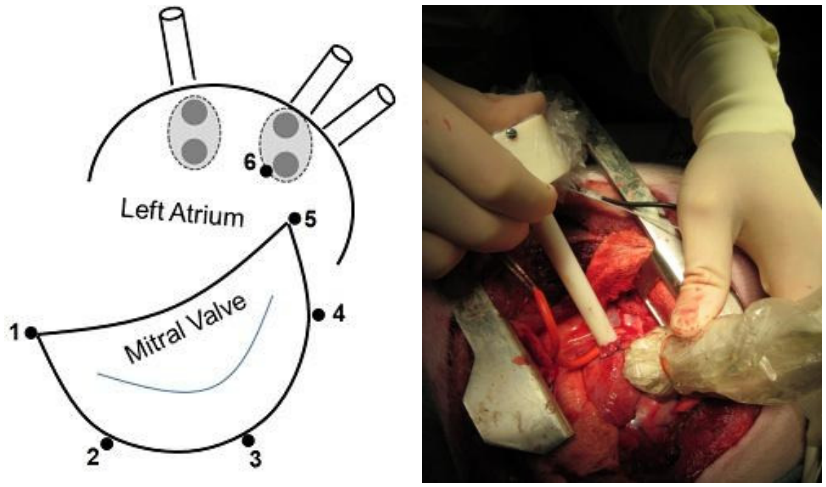


Figure 2.5 Left: The areas in the left atrium examined during the in vivo experiment. Multiple points around the mitral valve annulus were palpated in both the normal and radial direction and the LA wall was palpated in the normal directions. Right: An image of the in vivo experiment. The experimenter introduced the instrument into the LA while 3DUS probe imaged the intracardiac environment.

Position and force measurements were collected at locations around the MV annulus while palpating in the normal direction (towards the apex of the heart), and in the radial direction (towards the center of the valve) (Figure 2.3, Figure 2.5). In addition, measurements were made on the LA wall in the normal direction (perpendicular to the heart wall) (Figure 2.5). The LA was examined to understand the way in which percutaneous tools will interact with the heart wall while navigating around the MV and to evaluate catheter bracing in the LA. The total number of trials for each experiment and location in the heart is presented in the results section below. After each study was completed, the heart was excised and examined for tissue damage and to confirm the absence of structural abnormalities.

The suture tear out experiments were conducted ex vivo on three recently excised

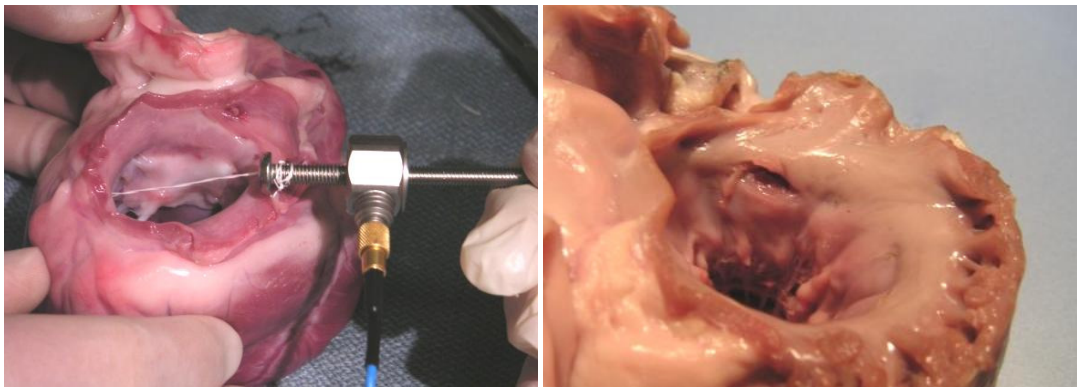

Figure 2.6 The suture tear out experiment: The heart was affixed in place, the left atrium wall was removed and a suture bite was introduced into the atrium, and an increasing tensile force was applied to a suture bite using a load cell (left) until the suture ripped out of the tissue (right).

porcine hearts from large (≥ 60 kg), recently sacrificed research animals (< 60 minutes after sacrifice). The hearts were drained and washed, fixated to a rigidly mounted stand, and the left atrium was removed to expose the mitral valve (Figure 2.6). Next, a surgeon applied suture bites at the anterior, posterior, and trigone regions around the MV annulus. The suture bites were 7-8 mm in length and 1-2 mm in depth, except for the bites into the trigones, which were 5-6 mm in length and 1-1.5 mm in depth. These suture bite sizes are similar to ones employed while implanting annuloplasty rings [38]. Finally, the sutures were tied to a 1 DOF load cell (Model 9212, Kistler Instrument Corp., Amherst NY, USA, non-linearity: ± 0.5%) and a force was applied through the load cell until the suture fully ripped out of the tissue (Figure 2.6). For each heart, 3 to 5 trials were conducted, for a total of 12 data points.

### *2.2.2.* Results

The tissue indentation evaluations were conducted in the locations indicated in Figure 2.5. While the displacements and forces measured with the instrument were

primarily along one DOF approximately parallel or perpendicular to the single DOF motion of the MV annulus (Figure 2.3) [18], they were not necessarily aligned with the axes of the sensors. Therefore, the 3 DOF displacement and force data were rotated to align with the principle direction of the position and force signals using a standard principle component analysis (PCA) method.

In each data set, the experimenter slowly moved the instrument tip towards the tissue target of interest, indented the tissue until a mean reaction force of approximately 1-2 N was generated, held the instrument at that position for several seconds, and then quickly pulled the instrument back. The force curves recorded during these experiments are challenging to interpret because of the movement of the tissue, as illustrated by the schematic plot of tissue position and tissue-instrument interaction force in Figure 2.7. The relationship of the instrument indentation depth in Figure 2.7 to the tissue surface motion is explained in Figure 2.8. Initially, the instrument only detects forces at the extreme of the tissue motion, as shown in curve (1). As the instrument continues to advance and indent the tissue, the tissue motion decreases and interaction force increases, as shown in curves (2) and (3). The point at which the instrument is always in contact with the tissue according to the force values, curve (2), is taken as the initial position point for the tissue displacement calculations.

Figure 2.9 presents a typical plot of the principle component of the position and force sensor measurements recorded while indenting the MV annulus in the normal direction in the posterior leaflet region. A number of values can be calculated from these data sets. The three parameters selected in this study are (a) the mean tissue displacement, (b) the mean tissue reaction force, and (c) the peak-to-peak tissue beating force. The

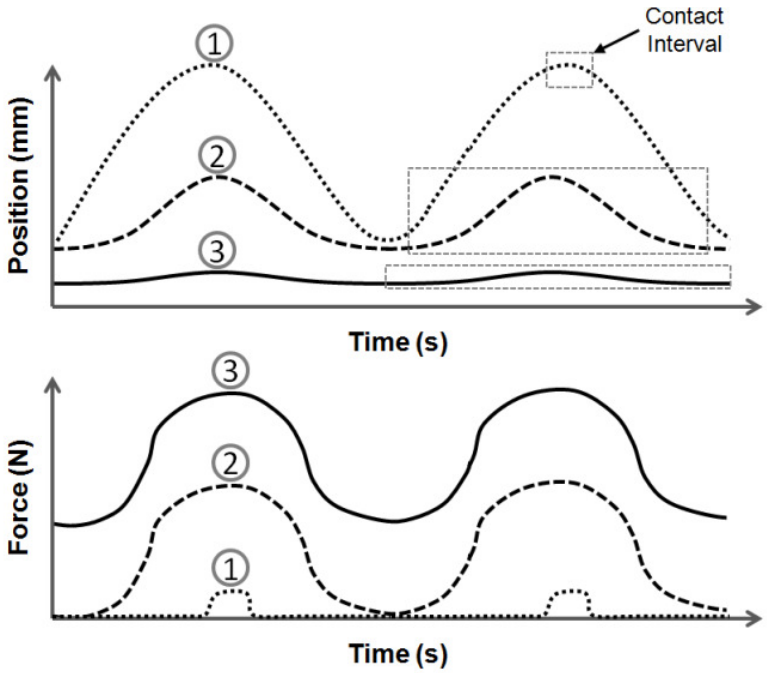


Figure 2.7 The cardiac tissue position and tissue-instrument forces as the instrument comes into contact and indents the moving tissue. The three curves indicate three levels of indentation and the dashed boxes indicate typical tissue-instrument contact intervals. Curve (1) represents the instrument only making contact at the extremes of the tissue displacement. This intermittent contact results in a force for (1) that is zero except at the maximum tissue positions. Curve (2) represents the minimum instrument displacement depth that the instrument is always in contact with the tissue, and curve (3) represents the force and tissue position at a displacement depth when the instrument is significantly indenting the tissue.

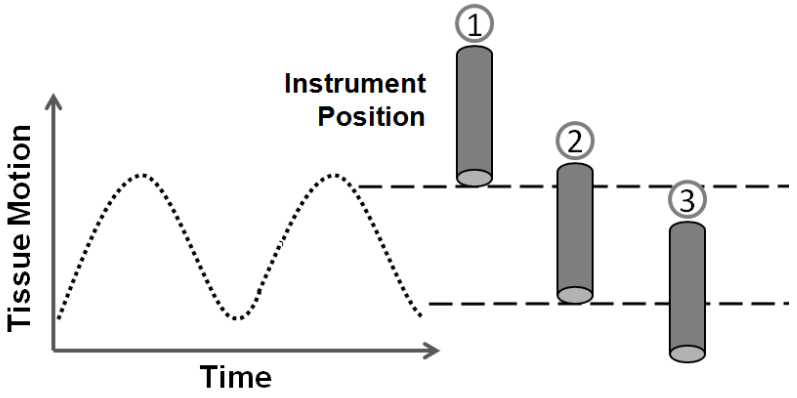


Figure 2.8 A diagram of the tissue motion range with no instrument contact and the instrument indentation depths for the three curves in Figure 2.7

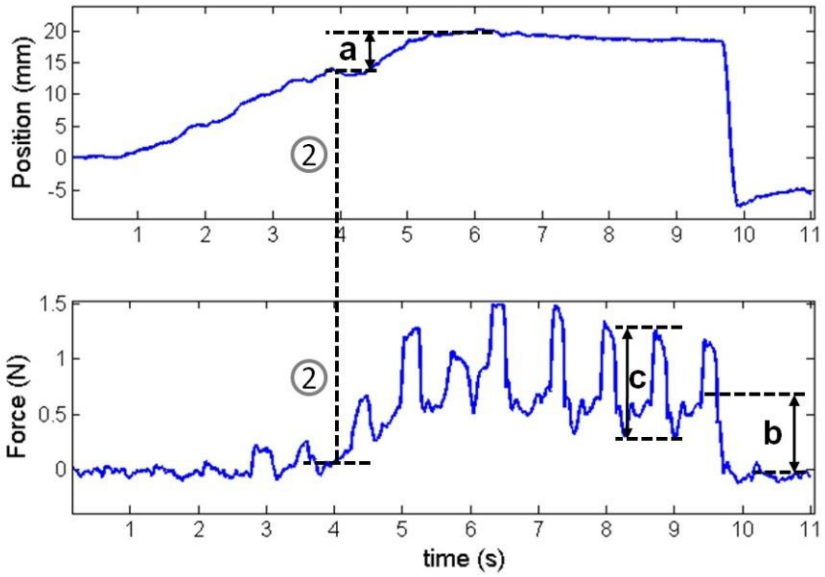


Figure 2.9 Typical principle component curves for the position and force measurements recorded by the instrument during one trial. The data was recorded while palpating the MV annulus in the normal direction in the posterior leaflet area. Note the changes in force caused by the periodic hearting beating and the instrument pull off. In this figure, (a) is the mean tissue displacement, (b) is the mean reaction force, and (c) is the beating heart force. Dashed line (2) correlates to curve (2) in Figure 2.7.

mean tissue displacement is the distance the instrument indents and displaces the tissue across the cardiac cycle. It is defined as the distance the instrument advances from the point of complete contact (curve (2) in Figure 2.7) to the point of maximum indentation. The tissue reaction force is defined as the difference between the mean force measurement at the maximum instrument displacement and after the instrument has been pulled away from the tissue.

Because of the rapidly changing force measurements, the force values before and after the point of interest are averaged across integer numbers of complete heart cycles (2-4 beats) to approximate the mean value. This technique is also used if the displacement reading is affected by the heart beating motion. The stiffness of the tissue

structure was calculated for each data set by dividing the mean tissue-instrument interaction force by the mean tissue displacement. This calculation assumes a linear stiffness model for the tissue structures at the force values applied in this study.

Finally, the heart beating force is defined as the peak-to-peak (minimum to maximum) force range applied to the instrument during the point of maximum instrument displacement. This force amplitude value represents the magnitude of the periodic forces applied by the beating heart to the measurement instrument. Examples of the indentation force, tissue displacement, and beating force values are indicated in Figure 2.9.

The results below are presented as box plots. For each value, the median is presented as a solid line surrounded by a box that represented the 25th and 75th percentiles of the data set at the top and bottom edge of the box, respectively. Whiskers extend from the top and bottom of the box to the most extreme data sample not considered an outlier. Outliers, denoted by the + symbol, are considered samples that are more than 1.5 times the interquartile range away from the top or bottom of the box. For each result data set, the mean value as well as the 95% confidence interval (CI) range is presented as a closed interval [a,b], indicating that the confidence interval for the mean falls within the range ($a \leq \text{mean} \leq b$).

**Mitral Valve Annulus: Normal Direction**

The first objective of the in vivo experiments was palpating the MV annulus in the normal direction. The MV annulus was examined in a number of locations, including the posterior and anterior commissures and the posterior leaflet annulus (Figure 2.5). The results, presented in Figure 2.10 ($n$=43), are grouped into the commissure regions and the

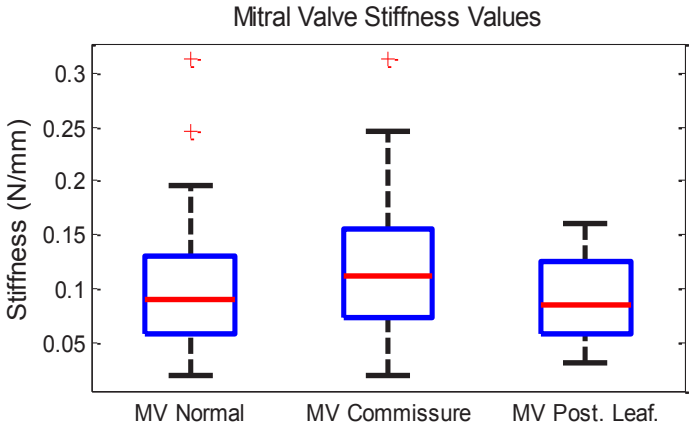


Figure 2.10 The stiffness of the mitral valve annulus in the normal direction

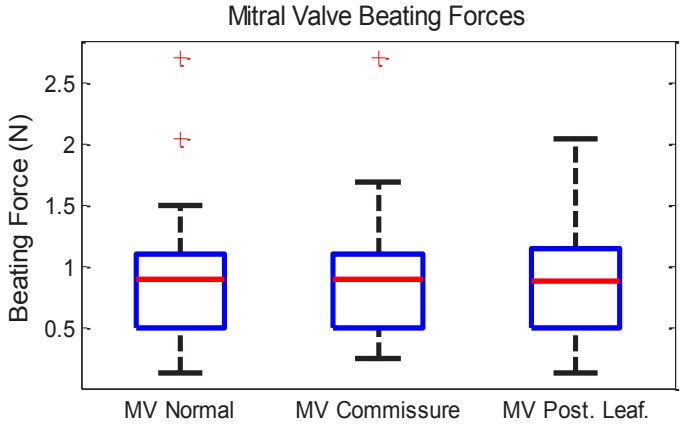


Figure 2.11 The beating forces applied by the mitral valve annulus in the normal direction.

posterior leaflet region (P1-P3). These values were grouped because they are two distinct tissue structure regions and have different requirements for proper MV function. Mean values for the entire MV are 0.103 N/mm [0.085, 0.120], 0.121 N/mm [0.091, 0.150] for the commissures, and 0.089 N/mm [0.073, 0.105] for the posterior leaflet region. The beating forces experienced by the instrument in these same areas is presented in Figure 2.11 ($n$=43). The mean values for the entire MV = 0.92 N [0.75, 1.09], commissures = 0.95 N [0.71, 1.18], posterior leaflet = 0.85 N [0.66, 1.03].

**Mitral Valve Annulus: Radial Direction**

In addition to palpating the MV annulus in the normal direction, the instrument was also used to examine the radial stiffness of the annulus structure. In these experiments, the tissue testing instrument first engaged the tissue in the normal direction and then pulled the instrument tip towards the center of the valve. The lateral forces were applied through the small metal spike at the tip of the tissue instrument. Application of force in the radial direction caused the heart to shift laterally in the body cavity perpendicular to the great vessels. This gross heart motion was not experienced during the normal direction experiments. Any data sets where the instrument tip slipped or did not apply forces in the correct direction were eliminated from the analysis. Trials were eliminated if the experimenter experienced slippage via tactile perception or data sets where the instrument displacement increased while the measured forces decreased, indicating slippage or tearing of the tissue.

The radial direction stiffness values for the entire annulus are plotted in (Figure 2.12). Mean radial stiffness is 0.078 N/mm [0.058, 0.099], ($n$=22). The beating forces applied to the instrument in the radial direction (Figure 2.13) have a mean force of 0.62 N [0.51, 0.73], ($n$=22).

**Left Atrium Wall**

The wall of the left atrium was palpated in the normal direction in the posterior region near the right pulmonary veins (Figure 2.5). The same technique as was used to examine the MV annulus in the normal direction was employed. The mean stiffness

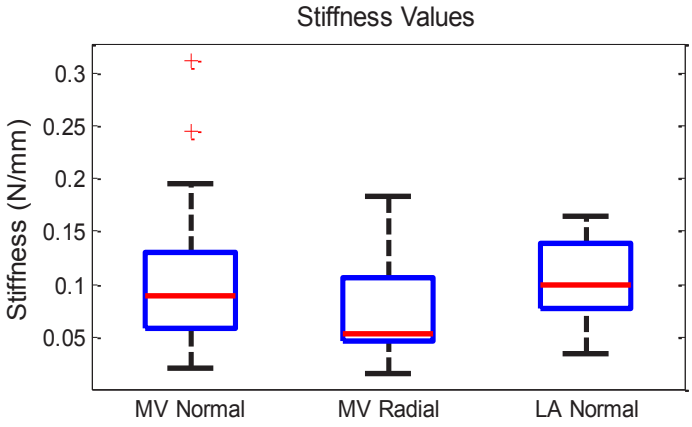


Figure 2.12 The stiffness values for the three regions examined in this study: (1) the MV annulus in the normal and (2) radial directions and (3) the LA in the normal direction.

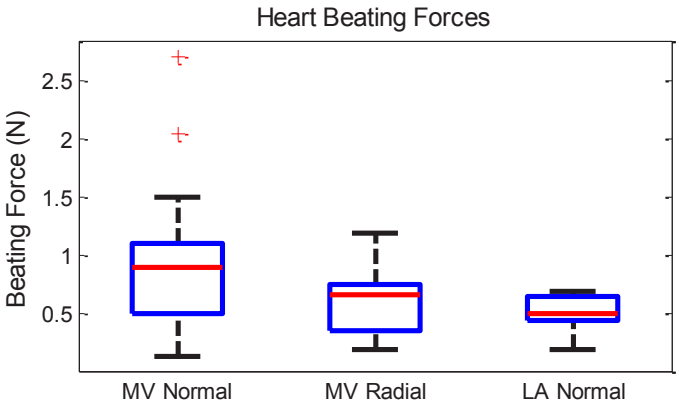


Figure 2.13 The heart beating forces generated by the three regions examined in this study: (1) the MV annulus in the normal and (2) radial directions and (3) the LA in the normal direction.

value (Figure 2.12) is 0.105 N/mm [0.081, 0.129], ($n$=12), and the mean heart beating force value (Figure 2.13) is 0.52 N [0.43, 0.61], ($n$=12).

**Applied Force Dependence**

The stiffness values for the MV annulus in the normal ($n$=43) and radial directions ($n$=22) and the LA wall ($n$=12) are plotted as a function of the force applied by

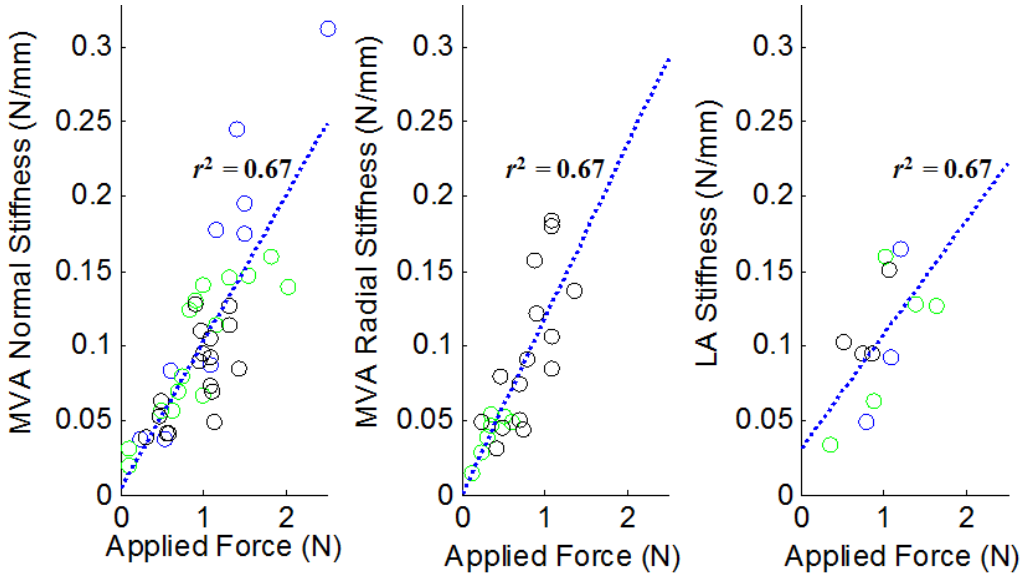


Figure 2.14 Stiffness of the locations in the heart as a function of applied force. Note the approximate linear dependence of stiffness on applied force, presented as a linear regression line (RMS error $\leq$ 0.03 N/mm for all plots). The results indicate a nonlinear force-displacement relationship for these regions in the heart.

the instrument in Figure 2.14. A linear regression line and the coefficients of determination ($r^2$) are included for each plot.

**Suture Tear out**

The force values required to tear out the sutures from the annulus are presented in Figure 2.15. For the trigone regions, the mean tear out force = 22.8 N [15.6, 30.0]), ($n$=7). The mean tear out force value for the other locations on the annulus = 7.7 N [4.51, 7.73], ($n$=5).

### *2.2.3.* Discussion

The goal of this work is to determine the forces and tissue stiffness values required to safely repair the mitral valve and operate in the LA. The results presented

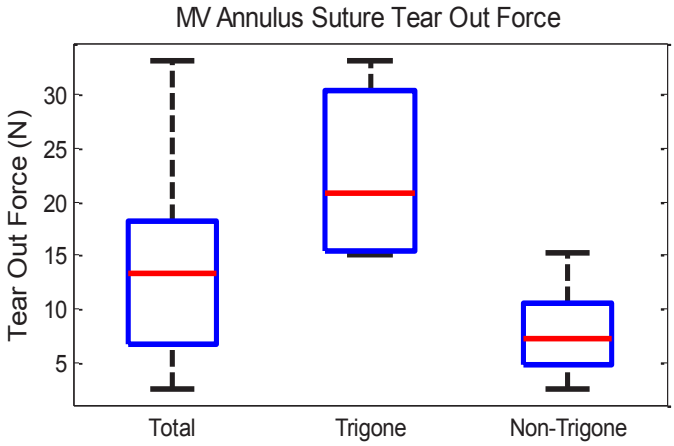


Figure 2.15 The forces required to tear a suture out of the MV annulus. The trigone regions can support an almost 3x greater forces than the other regions.

above demonstrate that the experiments were able to successfully ascertain these values for the beating porcine heart. Porcine research animals have been shown to have similar cardiac physiology to the human heart, thus the results of these experiments are germane to human MV repair [39]. However, the precise corresponds between the human and porcine cardiac physiology is unknown.

It should be noted that measuring multiple mechanical parameters in multiple directions within the beating heart is extremely challenging. The measurements require careful interaction with fast-moving cardiac structures and accessing a wide range of locations using only low-resolution ultrasound imaging for guidance while avoiding disruption of cardiac function. The instrument developed for this study successfully dealt with these constraints to provide the first in vivo measurements of the mechanical properties of the mitral valve annulus structure.

The work described above produced a number of interesting results with implications to the design and control of beating heart surgical tools. For example, the measured stiffness values increase with applied force. The stiffness values for each of

the three tissue targets are plotted as a function of the applied force in Figure 2.14. This result indicates that the tissue structures become stiffer as greater forces are applied to them. Possible explanations for this behavior include the fact that the tissue structures are linked to other anatomical structures (ventricles, major vessels, etc.). As forces are applied by the instrument, the tissues deform and interact with other parts of the anatomy, further distributing the deformation forces. Another explanation is the nonlinear mechanics of the types of tissues that compose these structures. For example, cardiac muscle displays a nonlinear stress-strain relationship due to the non-homogeneous nature of the underlying tissue and the complex alignment of the collagen network inside the myocardium [40]. This behavior is exhibited by many tissue structures due to the directionally of tissue fiber alignment [41].

**Implications**

In addition to presenting this stiffness trend, this work also has implications for the design of devices for percutaneous MV repair and beating heart surgery. First, the beating heart force results suggest that a tool will have to tolerate force variations of at least 1 N while interacting with the structures in the LA. This means that in order to accurately manipulate the tissue, a tool will have to either be compliant enough to flex like a catheter, be rigid enough to minimally deflect under the applied load, or actively compensate for the changing tissue forces using closed-loop force sensing and actuation [27, 42].

The stiffness values found in this work are also useful for the development of beating heart medical procedures. For example, the MV annulus stiffness in the normal

direction, approximately 0.1 N/mm (Figure 2.10), indicates how far the MV will displace on average when a tool pushes on the valve to drive a staple or suture into the tissue. This is required to perform beating heart annuloplasty as is described in [22, 43]. The results also provide a method for calculating how much force must be applied in the radial direction in order to change the shape and shift the mitral valve. This information is important for surgical planning and robotic surgery guidance.

The stiffness and beating force values from interacting with the LA wall are useful for a number of applications, including predicting the tissue displacement while applying a force with an ablation catheter or determining the forces associated with bracing against the LA wall.

Finally, the suture pullout results illustrate the possible failure modes of attaching a prosthetic device, such as an artificial value or annuloplasty ring, to the MV annulus. The tear out forces suggest that if the fixation devices can sustain the forces measured here, they are likely to keep the implant safely in place. This is especially the case if the implant is anchored to both tough, cartilaginous trigones.

It should also be noted that the suture bite lengths were different for the trigone and the other regions of the MV annulus (5-6 mm vs. 7-8 mm). This range of lengths are similar to the techniques used to attach mitral valve annuloplasty devices and are limited by the geometry and dimensions of the MV annulus. Although these are not general results that can be applied to all methods of attaching devices to the mitral valve annulus, the tear out values do provide an upper bound for the maximum forces the annulus tissue can withstand

**Limitations**

While this study has determined some of the properties of MV and LA tissue structures, there remain a number of limitations to this work. The primary limitation of the study is the sensing technologies. The EM tracker, force sensor, and 3DUS are all affected by the challenges of the intracardiac and operating room environment. These include metal interference for the EM tracker; friction, off axis, and viscous forces for the force sensor; and the limited resolution and field of view of the 3DUS. These limitations, as well as the challenges of precisely setting up and operating sensors in a surgical environment, impact the accuracy of the values calculated in this study.

The accuracy of the EM tracking technology is affected by the ferrous and magnetic materials in the operating room. For example, Wilson et al. found that the tracking accuracy of a previous generation EM tracking system varied from 0.38 mm in a radiology suite to 1.00 mm in a pulmonology suite [44]. Alternative sensing modalities such as sonomicrometry within the heart and optical tracking of the instrument handle are potential alternatives for future studies that may enhance position resolution.

A number of restrictions of the in vivo setup also complicate this experiment. For example, the surgical access into the LA through the external wall limits the 3DUS imaging view and the access of the instrument to all points of the MV. As a result, the experimenters were not able to apply a radial force on all points of the MV annulus and certain data sets were rejected due to slippage. Furthermore, the radial force not only compressed the valve, as in an annuloplasty procedure, it also shifted the annulus in the direction of the applied force as the entire heart organ deformed and moved. This shifting further complicated the ability to 3DUS image the tissue structure from a fixed

viewpoint during the entirety of each experimental trial. The fact that the entire heart moved while applying the radial force suggest that all of measurements not only examined the local tissue structures, but also the mechanics of all of the structures surrounding the heart. The normal direction experiments, for example, also examine the stiffness of the great vessels supporting the heart in the chest in addition to the properties of the MV annulus.

Despite these limitations, the values found in this study are a good starting point for the design of surgical tools and percutaneous devices for beating heart surgery.

# Chapter 3

# Mechanical Design

The following chapter presents the mechanical design of the robotic catheter system, including the system level design, force sensors, and intracardiac bracing strategies.

## 3.1. System Level Design

The robotic catheter system is designed to compensate for the motion of the outer annulus of the mitral valve, the major valve between the left atrium and ventricle. This valve exhibits some of the largest motions and greatest velocities of any structure inside the heart. Previous work on compensating for the mitral valve annulus has shown that the motion is primarily along one axis of motion, thus a single DOF system can be used to sufficiently compensate for the valve motion [18].

The actuated catheter system performance parameters were derived from human mitral valve physiology values [18, 22]. The principal functional requirements are a single actuated linear degree of freedom with at least 20 mm of travel and velocity and acceleration of at least 210 mm/s and 3800 mm/s$^2$, respectively. The catheter

components should have the same dimensions and materials as current clinical cardiac catheters. Finally, the system should be able to apply a sufficient force to modify cardiac tissue, approximately 4 N.

The system can be divided into three main modules: The drive system that actuates the catheter, the catheter module that is inserted into the heart, and the 3D ultrasound visual servoing system that tracks the tissue and commands the catheter to follow the motion. A user control interface is also required for clinical use, provided in this system by the image processing and control computer and manual catheter positioning controls. See Figure 1.1 for a diagram of the entire system.

### *3.1.1.* Drive System

The catheter drive system (Figure 3.1) is composed of a linear voice coil actuator (NCC20-18-02-1X, H2W Technologies Inc, Valencia CA; 50.8 mm travel, 26.7 N peak force), a linear ball bearing slide (BX3-3, Tusk Direct, Inc., Bethel CT), and a linear potentiometer position sensor (LP-50F, Midori America Corp, Fullerton CA, linearity: ±0.5%). In addition, a force sensor (LCFD-1KG, Omega Engineering, Stamford CT; range: 10 N, accuracy: +/-0.015 N) measures the catheter friction for evaluation purposes.

### *3.1.2.* Catheter Module

The catheter module consists of a sheath, a guidewire, and the end effectors required for each specific repair procedure. The sheath is an 85 cm long section of flexible Teflon or Nylon tubing that encloses the guidewire, a close-wound stainless steel spring that is easily bent but can apply significant compressive forces without buckling. During the procedure, the sheath is inserted from a peripheral blood vessel (typically the

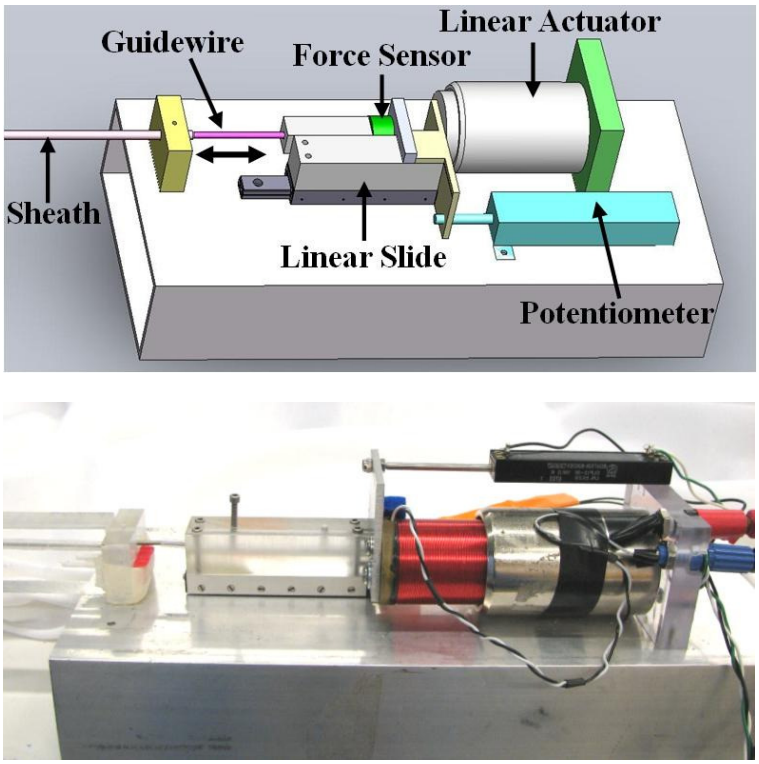


Figure 3.1 The catheter drive system consists of a linear actuator, slide, potentiometer, and a force sensor to evaluate the friction experienced by the catheter guidewire. The system servos the guidewire inside the fixed sheath.

femoral vein leading into the RA) into the heart, and then fixed in place while the drive system servos the guidewire inside the sheath to compensate for the heart motion. The gap *G*, defined as the difference between the guidewire outer diameter and the sheath inner diameter (Figure 3.2), is a major determinant of system performance. The impact of gap size on system performance is described in detail in Chapter 4.

### *3.1.3.* 3D Ultrasound Visual Servoing System

The ultrasound servoing system streams 3D image volumes from the ultrasound scanner to an image processing computer via Ethernet (Figure 1.1). A GPU-based Radon transform algorithm finds the catheter axis in real-time. The target tissue is then located

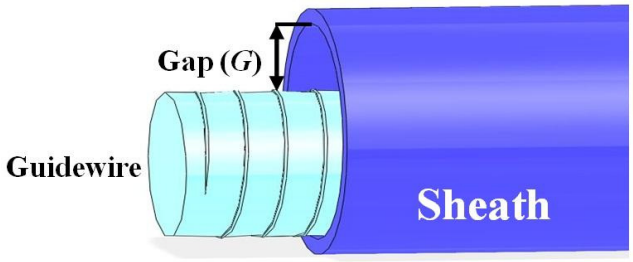


Figure 3.2 A catheter guidewire emerging from a sheath. The distance between the outer diameter of the guidewire and the inner diameter of the sheath is defined as the gap size ($G$).

by projecting the axis forward through the image volume until tissue is encountered; this allows the clinician to designate the target to be tracked by simply pointing at it with the catheter. To compensate for the 50-100 ms delay in image acquisition and processing, an extended Kalman filter (EKF) estimates the current tissue location based on a Fourier decomposition of the cardiac cycle. Previous *in vivo* experiments using this servoing system showed that a rigid instrument system was capable of accurate tracking within the heart, with an RMS error of 1.0 mm. See [22-25] for a detailed description of the 3DUS visual servoing system.

A PID control system running at 1 kHz controls the position of the linear actuator in the drive system. Commands to the linear actuator are amplified by a linear current power amplifier (AMPAQ, Quanser Inc., Markham, Ontario, Canada).

### *3.1.4.* Clinician Controls

The robotic catheter system automatically compensates for the fast motion of the cardiac tissue, thus allowing a clinician to operate on a virtually stationary tissue structure. The procedure is then performed by adjusting the position of the motion compensated tool relative to the moving tissue target. The manual inputs available to the

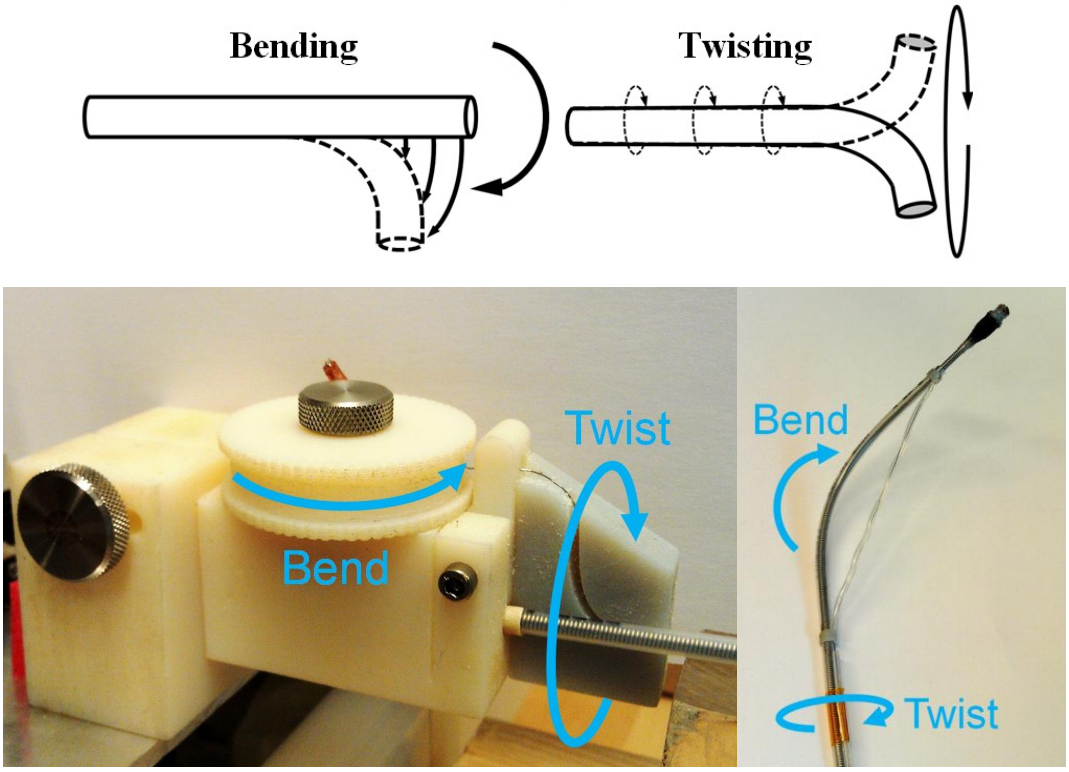


Figure 3.3 The catheter manual bending and twisting controls. These inputs, in addition to the linear joystick input, allow the clinician to position the catheter relative to the tissue target of interest. The bent and twisted configuration can be fixed by tightening the thumbscrews on the input mechanism attached to the catheter drive system.

clinician include a linear joystick to adjust the DC offset of the guidewire in the direction of fast servoing (along the axis of the tool) and bending and twisting the distal segment of the catheter sheath in the lateral directions (Figure 3.3). The bending and twisting mechanism, shown in Figure 3.3, is attached to the robotic drive system at the proximal end of the catheter and allows the catheter to be locked in its bent and twisted position via thumbscrews. These manual controls seek to reproduce conventional steerable catheter control inputs. The combination of the adjustable sheath and the superposition of the joystick position on the motion compensation trajectory allow the clinician to orient the guidewire relative to the tissue and perform repair procedures such as tissue resection.

## 3.2. Force Sensing

Force sensors are crucial components in a large range of devices and systems, including robotics, manufacturing, transportation, and human-machine interfaces. General purpose force sensors, however, are not adapted to application-specific needs, resulting in systems that are overly large, expensive, and fragile. There is a clear need for inexpensive and easily customized force sensors for a range of applications where force information can greatly improve performance but high precision measurements are not a primary design consideration. For example, force sensing at the distal tip of a robotic catheter could enable more precise tool-tissue interactions. However, no off-the-shelf force sensing options are compatible with the specific requirements of the catheter system.

This section describes design principles and approaches for fabricating new and customizable force sensors using 3D printing, an increasingly commonplace rapid prototyping technology. The advantages of 3D printed sensors are that they are fast to develop and build, easy to customize, and can be shared with the larger design and research community in an open source fashion. This sensor design approach is applied below to the development of a force sensing end effector for the catheter robotic system.

In addition to the force sensors, two other catheter tip end effectors have also been developed for the robotic catheter system: a resection cutting tool and a radio frequency ablation burning tool. The design and evaluation of these devices are described in detail in Chapter 7.

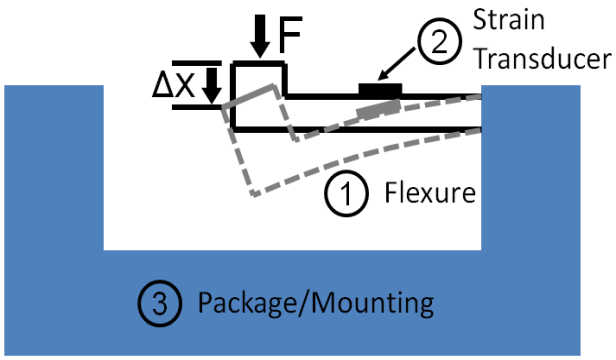


Figure 3.4 A generic force sensor design consists of (1) a flexure, (2) a strain transducer, and (3) a packaging enclosure that allows for sensor mounting.

### *3.2.1.* Design Principles and Methods

Force sensors convert applied forces into electronic signals by measuring the displacement or strain of an internal structural element called a flexure. A general force sensor design consists of three components: a flexure, a transducer that converts the displacement into an electrical signal, and packaging to protect the components and facilitate mechanical connection to the rest of the system (Figure 3.4). Traditional force sensors and load cells use metal flexures, strain gauges or piezoelectric transducers, and metal enclosures [45].

Conventional force sensors have limitations that restrict their utility in many applications. General purpose commercial force sensors must be designed to work with a wide range of systems and loading situations. This requires rigid packaging elements to avoid internal deflections under any anticipated load. The mounting provisions on the system side of the force sensor interface must also be designed to ensure rigidity in the connection to the force sensor. This usually results in excessive size and mass compared with a sensor that is tailored to a specific system. In addition, sensing multiple directions of force or torque often requires complicated rigid structures to couple multiple

conventional sensors. It is also challenging to design miniature force sensors using conventional approaches because of the difficulty of machining small and delicate metal flexures and bonding strain gauges to small structures.

3D printing is a rapid prototyping method that creates three dimensional objects from computer aided design models. This technique is an additive manufacturing method where material is deposited in layers to build up the part. A number of printing materials are available, including metal particles, ceramics, and plastics [46]. Force sensors fabricated with 3D printing offers a number of advantages over discrete general purpose sensors. For example, 3D printed sensors can be tailored to the configuration of the overall system, reducing or eliminating the need for a rigid mounting interface with the sensor. Also, 3D printing allows for a sensor to be quickly and inexpensively optimized through iterative prototyping and redesign. This allows for quick translation of a design from concept to useful device. Miniaturization is enabled by the ability to print small, light weight, and intricate structures. Sensors can be easily adapted for specialized applications, e.g. without ferrous metal parts for compatibility with Magnetic Resonance Imaging (MRI) or for chemically corrosive environments [47-49].

**Flexures**

Flexures convert forces applied to the sensor along a specific direction to a displacement or strain that can be measured by the transducer (Figure 3.4). The mechanical properties, size, and shape of the flexures determine the sensitivity, accuracy, and directional response of the sensor.

The stiffness, and therefore the amount of deflection, of the flexures is determined by the dimensions and material properties of the components. Traditionally, force sensor use high-stiffness flexures that produce small maximum displacements and small strains, usually on the order of $10^{-3}$%. This enables measurement by small strain transducers like strain gauges and piezoelectric elements. These transducers have the advantages of good linearity and higher resonant frequency. However, the use of small strain transducers also entails complexity and expense due to the difficulty of assembling the sensor and the need for sophisticated electronics for small signals.

Rapid prototyping allows for the use of flexures that have larger deflections and simple displacement sensors that enable operation in challenging environments, such as MRI machines or electrosensitive environments. Compliant flexures allow for more control over mechanical impedance of the sensor than traditional, stiff flexures used with strain transducers. This is beneficial in situations where lower structural stiffness is preferable, such as compliant grippers for robotic end effectors. The use of highly compliant flexures also reduces the relative effects of thermal expansion. However, compliant flexures have the limitations of lower resonant frequency, nonlinear response requiring a more complex calibration process, and increased risk of contaminating the force reading due to contact between the flexure and other structures.

As with conventional force sensors, the geometry of the flexure design is crucial for performance. The flexures should be compliant along the degree of freedom (DOF) of interest, but stiff in all other DOF to prevent off-axis measurement errors. Also, the flexures should be designed to never undergo plastic deformation, which will impair the sensor calibration and potentially destroy the sensor. The ability to create detailed

structural geometry using rapid prototyping techniques enables optimizing the flexures and their support structures for each application.

In general, it is advantageous to avoid using 3D printed structures as flexures. 3D printing materials, especially plastics, are susceptible to viscoelastic and hysteretic properties and often have low yield strength. While these issues can be reduced through design improvements or corrected through calibration as in [49], it is easier to instead incorporate flexures with better materials properties into the sensor. For example, metal flexures can be easily inserted into specifically designed slots in 3D printed structures. This allows for the use of materials with excellent elastic properties in a variety of sizes and stiffnesses. This approach allows the same sensor design to be configured to measure different force ranges depending on the flexures selected. Superelastic alloy flexures can also be used to increase the sensor displacement for a given force or add additional overloading protection. However, such materials can introduce other undesirable properties, including material property changes due to thermal effects and loading hysteresis for large strains [50].

**Transducers**

Traditional force sensors and load cells use strain gauges or piezoelectric transducers to create an output signal related to the applied load [45]. While such technologies are feasible for 3D printed sensors, they present a number of challenges. In particular, they require complex signal conditioning and elaborate mounting techniques [51]. The need for electrical wiring and potentially dangerous voltages and currents

makes these technologies unsuitable for the electrically sensitive applications, such as intracardiac or MRI applications [45].

The ideal transducer technology for 3D printed sensors is simple to install for rapid design iteration and compatible with a range of flexure displacements and dimensions. For the reasons outlined in the above, displacement sensors are a suitable transducer technology for the complaint flexures used in this design approach due to the relatively large strains. Two measurement technologies that are strong candidates are fiber optic sensors and Hall effect sensors [45][52]. These inexpensive transducers are simple, noncontact, and useful for a range of flexure designs and sensitivities. A vast number of fiber optic transduction mechanisms have been developed, including intensity modulation, interferometric, and spectrally-based sensors [47, 52], [48]. The design example presented here uses intensity-based "fiber optic lever" or numerical-aperture based transduction as it is simple and inexpensive to implement and may be readily adapted to many sensor geometries. These transducers measure displacement by determining the amount of light reflected from a surface as it moves relative to the sensor. The fiber optic cables transmit the incident light from an emitter and the reflected light back to a sensor that can be located at a remote location [52, 53]. This means that the fibers that are inserted into the force sensor are electrically, magnetically, and chemically inert. To incorporate the transducer only the fibers need to be inserted into the force sensor, allowing for quick prototyping iterations.

Hall Effect sensors use the motion of a magnet attached to the flexure to detect displacement [54, 55]. Low cost and simplicity of implementation make this approach

attractive, but these sensors cannot operate around magnetic materials and are essentially single DOF sensors because they respond to the magnitude of the magnetic field.

**Packaging and Mounting**

Force sensor packaging protects the flexure and transducer and provides a means to mount to other structures. In the context of 3D printed sensors, the packaging and mounting should be stiff and resist any forces that might affect the sensor measurement or damage the sensor. The package should also provide environmental isolation, e.g. waterproof for liquid or medical environments, or rubber-coated for impact protection. The packaging should also allow for easy assembly and integration with the rest of the system structure. For example, no additional mounting is needed if the force sensor packaging is 3D printed directly as part of a mechanism, such as a machine linkage or a robot arm.

**Manufacturing and Calibration**

One of the advantages of manufacturing with a 3D printer is that the sensor can be designed for easy assembly. For example, small features can be added to help align the flexures and transducers and aid in the assembly of the outer packaging. In addition to traditional pins and holes, the packaging can include slots, guides, and other features to reduce alignment errors during assembly.

Force sensors must be calibrated to accurately relate the applied force to the displacement transducer output. This process is not trivial, as the best fitting calibration law may not be linear and the sensor output might have dynamic or hysteretic

components depending on the sensing technology and design of the flexures. Flexure designs that involve larger deformations or superelastic materials like Nickel Titanium (NiTi) will most likely require nonlinear calibration laws or calibration models that include loading hysteresis [49].

Mounting the force sensors can introduce offset strains in the system and alter calibration values. Particularly for sensors with a nonlinear response, it is best to calibrate the sensors after they are mounted and integrated with the system. Increasing the stiffness of the packaging can reduce the significance of mounting variability.

**Sensor Limitations**

The limitations of 3D printed sensors include contact between internal components, unintended deformations of the packaging or mounting structures caused by loading or the environment, and plastic deformation of the flexures caused by overloading. Contact between the components in the sensor during loading can produce friction that alters the elastic response of the flexing components. This fiction effect usually manifests as hysteresis in the sensor response. If too great a force is applied, the flexures may yield and plastically deform. While the sensor may still be useable after it is overloaded or deformed by applied forces, the calibration will no longer be valid.

Other potential limitations of 3D printed sensors include thermal sensitivity of the 3D printing materials, local deformation of the 3D printed components where the flexures are mounted to the sensor body, and manufacturing quality variations caused by the imperfect nature of 3D printing. However, these potential challenges are acceptable

when creating a fast prototype or specialized research device for applications where high sensing precision is not the primary design consideration.

### *3.2.2.* Catheter Force Sensor Design

The process of creating a 3D printed force sensor requires designers to consider the force measurement objectives and system constraints in determining how to best use the 3D printing technology. The following section demonstrates the sensor design process through the example of a force sensor end effector for the robotic catheter system.

The functional requirements of this sensor are that it (1) measures forces in one DOF along the axis of the tool with enough accuracy to allow for force control feedback, (2) is small enough to maneuver inside the heart, (3) is able withstand the forces, fluids, and pressures inside the heart, and (4) does not use electrical elements because of the electrical sensitivity of the heart.

The design specifications for this force sensor were created from the above functional requirements and limitations of the 3D printing technology. The sensor should have a less than 6 mm outer diameter, deflect less than 1 mm when forces are applied, can accommodate an electromagnetic (EM) tracking sensor, and can be easily integrated with the robotic catheter. The system should also resist lateral forces, measure a maximum 10 N force, and measure forces with an RMS error less that 0.2 N (<2% of the maximum force).

Figure 3.5 presents a schematic diagram of the catheter force sensor based on these specifications. NiTi wires flexures (0.25 mm diameter) were arranged in a perpendicular configuration (Figure 3.6). This flexure design allows for large defections

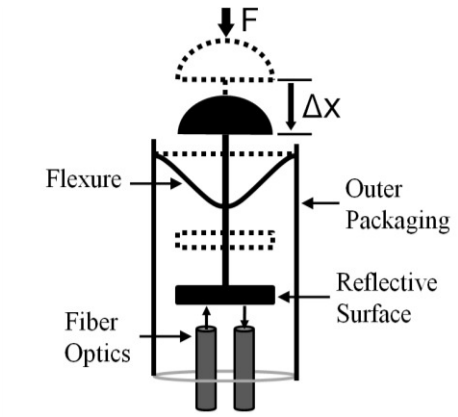


Figure 3.5 Catheter tip force sensor configuration.

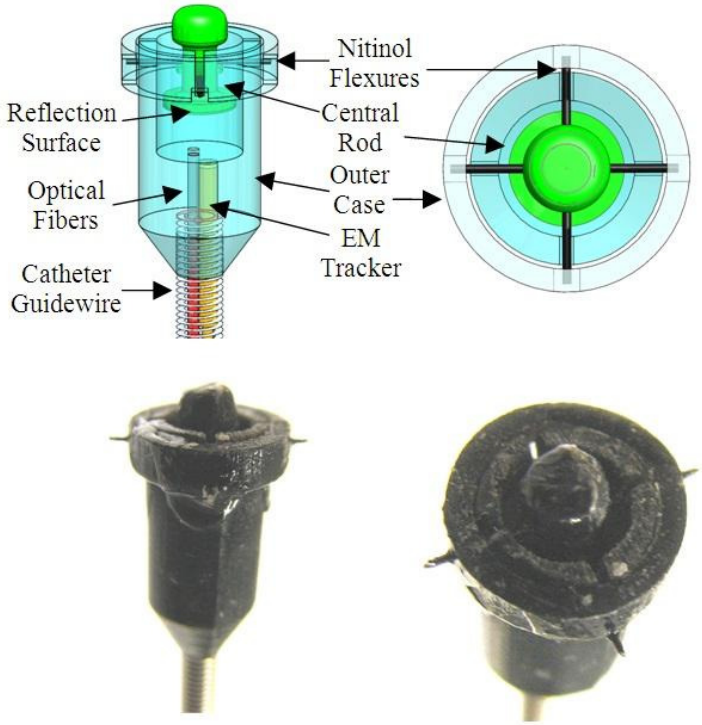


Figure 3.6 Solid model (side and top views) of the 3D printed force sensor integrated with the catheter and EM tracker and images of the assembled sensor.

along the axis of the tool but resists lateral deflections, has little hysteresis, and prevents rubbing of the sensor components. Superelastic NiTi flexures were selected for overload protection. Figure 3.6 presents a solid model of the sensor design and images of the final assembled sensor.

A fiber optic transducer was selected for this sensor because it is inexpensive, easy to implement, and requires no electrical components within the catheter [45]. Integrating the transducer into the sensor is as simple as inserting the fibers and fixing them in place with adhesive.

The Objet Connex500 3D printer (Objet Geometries Ltd, Billerica, MA, USA) was used to fabricate the catheter force sensor. This printer has a minimum resolution of 16 microns and can print with a range of photopolymers, from a stiff acrylic plastic to a rubber-like, flexible plastic (see [56]). For this work, the Veroblack photopolymer was selected because it is a stiff plastic (2 GPa) with a high tensile strength (50 MPa). It is also opaque, thus minimizing light transmission through the sensor packaging that could potentially affect the fiber optic transducer signal [56].

Careful consideration of assembly of the 3D printed components is required because of their small size. For example, slots and raised features were added to the central rod to help insert and align the NiTi flexures (Figure 3.6). Because the 250 micron diameter holes for the NiTi wire can only be seen clearly with a microscope, these additional features allow components of the sensors to be assembled by touch alone.

### *3.2.3.* Sensor Evaluation

The catheter tip sensor was calibrated and tested with a commercial 6-axis force torque sensor (Mini40, ATI Industrial Automation, Apex, NC, USA). The 3D printed sensor was manually loaded against the ATI sensor with a varying force profile. The signal from the fiber optic sensor was amplified with a digital fiber amplifier (E3X-DA21-N, Omron Electronics LLC Industrial Automation, Schaumburg, IL, USA) before digital acquisition (DAQCard-6024E, National Instruments Corp., Austin TX, USA).

A quadratic equation was selected to relate the fiber optic sensor output to the force input

$$F = Ax^2 + Bx + C \tag{3.1}$$

where $F$ is the output force, $x$ is the fiber optic sensor output voltage, and $A$, $B$, and $C$ are constant coefficients. This calibration law modeled the deformations of the NiTi flexures. Linear and higher-order functions, as well as time varying models that considered the viscoelasticity of the material, were investigated but they did not perform as well as the quadratic law. This design experienced smaller flexure deformations (<0.25 deflections or <1% strain), so a model that considered the hysteresis of the NiTi material was not required.

The coefficients in (3.1) were found by least squares estimation on a calibration data set. Figure 3.7 shows representative examples of the calibration forces applied to the sensor and the forces from the 3D printed sensor calculated by the calibration law. The RMS error for this calibration set is 0.21 N, approximately 2% of the maximum range of the data set and sufficient for the robotic catheter applications [27], [42]. The sensor consistently produced accuracy values of 2-4% of the full sensor range over long data sets (>30 s). The maximum deflection of the sensor tip is approximately 0.25 mm. The sensor also exhibits good insensitivity to lateral forces and each prototyping iteration takes under 3 hours to 3D print, clean, assembly, and calibrate.

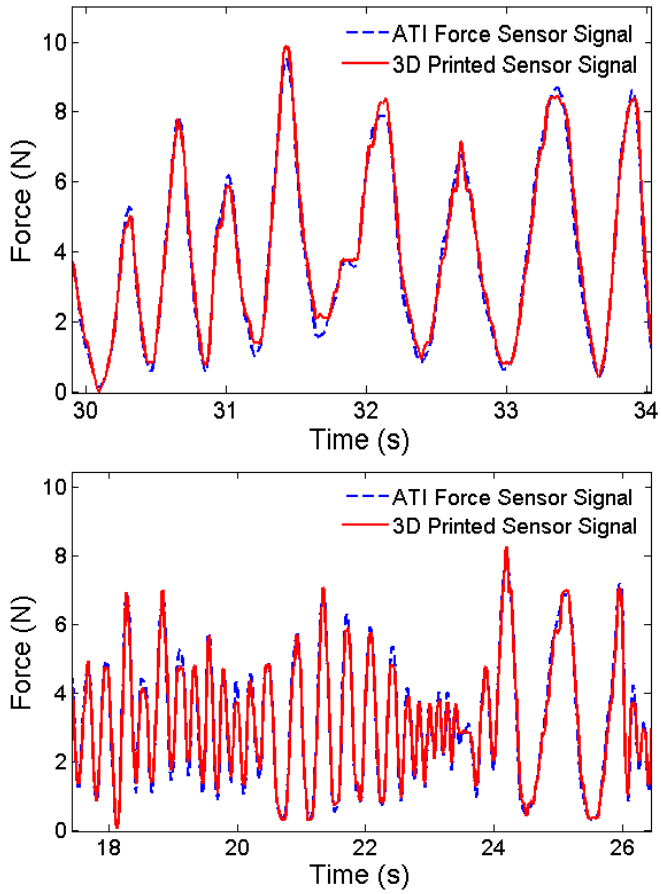


Figure 3.7 3D printed force sensor response to time-varying loading.

### *3.2.4. In Vivo* Evaluation

The catheter tip force sensor was also tested *in vivo* during a porcine cardiac surgery. The sensor successfully measured forces and transmit signals along the length of the catheter via the fiber optics. The seals and adhesives used to construct the sensor also performed successfully during the procedure and blood did not penetrate the body of the sensor. The sensor drift, resolution, and sensitivity observed *in vivo* were similar to the sensor performance in *ex vivo* conditions. The force readings supplied by the sensor provided catheter-tissue interaction forces for haptic teleoperation and procedure guidance.

## 3.3. Bracing

Due to the long and flexible nature of catheters, bracing the distal end inside the heart is required for the catheter tool to apply large forces**.** Without bracing, the catheter shaft will instead deflect away from the heart wall and apply only small forces to the tissue structures. The following section presents a survey of braced manipulation prior work and strategies for bracing the robotic catheter inside the heart.

### *3.3.1.* Braced Manipulation

Braced manipulation is a technique used to improve the performance of a manipulator by constraining its motion in some beneficial way. A classic example of braced manipulation is the manner in which humans support their wrists while writing. The reason for supporting one's wrist is to improve fine control of the writing tool to ensure clear and legible handwriting. In this simple example, the hand is mechanically constrained to travel along the plane of the writing surface by the force of gravity and the reaction force provided by the surface, thus improving the end effectors position accuracy (Figure 3.8).

The three motivations found in the literature for utilizing braced manipulation are (1) to reduce manipulator mass, (2) to increase manipulator accuracy or repeatability, and (3) to ground the manipulator relative to the workpiece or target.

Bracing the manipulator can reduce a manipulator's mass because an equivalent or greater manipulator stiffness can be achieved with a lighter, more flexible arm if the arm is braced to a supporting structure [57]. West found that bracing can increase the stiffness at the end effector of a manipulator by a factor of 50 [58]. Thus, adding bracing

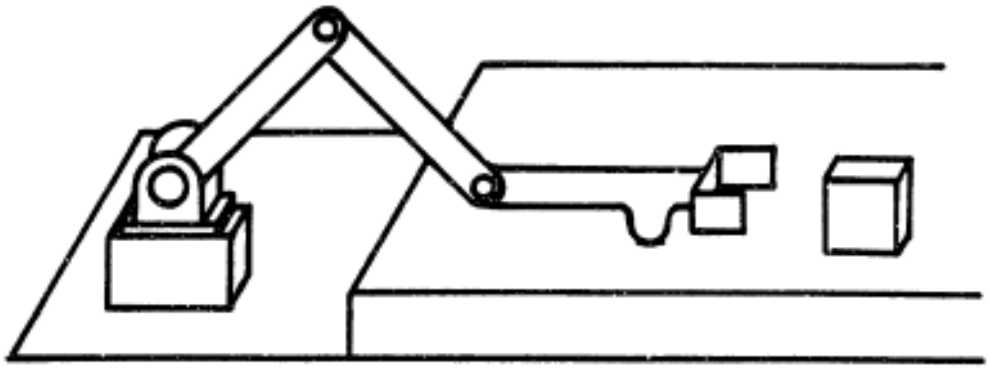

Figure 3.8 A manipulator constrained to move in the plane of the table [59].

can reduce the manipulator mass by allowing a lighter, more flexible manipulator arm to transport a mass with the same accuracy as a stiffer and heavier arm if it can brace itself against a rigid structure close to the end effector [57, 59].

Bracing can also improve accuracy and repeatability of manipulation operations. Bajd et al. found that bracing improves fine-motion accuracy for both humans and robotic manipulators [60]. The authors investigated the effects of bracing by comparing the position repeatability of a robotic arm manipulator and a human arm with and without bracing and found that bracing the Asea Irb 6 industrial manipulation robot improved its repeatability by approximately 50% and that bracing improved the human operator's repeatability by approximately 25% [60].

Finally, grounding a robot relative to the workpiece immobilizes a section of the manipulator to improve performance or controllability. This strategy is often applied to macro-micro or coarse-fine manipulation robots, which divide up tasks so that coarse motions are achieved by a robot arm with a large workspace and the finer motions are realized by a more precise wrist and end effector [57, 59, 61]. Grounding the manipulator is advantageous for these macro-micro manipulators because by

immobilizing the coarse manipulator, only the control of the fine manipulator needs to be considered. Grounding the manipulator relative to the work piece also improves the robot's ability to control the interactions between the manipulator and the workpiece. This strategy is utilized by industrial manipulators that perform drilling or grinding operations on flexible or delicate materials [58, 62].

There are a number of possible bracing approaches to achieve the goals mentioned above. A manipulator can be braced via a mechanical constraint, such as a rigid connection to another structure, or via a virtual constraint, such as a modification of the control system that limits the manipulator's degrees of freedom (DOF). The most basic bracing method is to constrain the manipulator against a surface as shown in Figure 3.8. This method constraints the manipulator to move in the plane of the surface, increasing its stiffness perpendicular to the surface and reduces the degrees of freedom. Figure 3.9 illustrates another mechanical bracing approach where a special mechanism, often referred to as a "jig hand", is used to connect the manipulator to the work piece or some other structure. The jig hand mechanism can be designed to specify the constrained degrees of freedom of the manipulator and also provide other benefits, such as orienting and positioning the work piece relative to the end effector.

Mechanical bracing of a manipulator can be achieved in a number of ways. A simple method, illustrated in Figure 3.8, is to brace the manipulator by using actuators or gravity to apply a normal force on the bracing structure to keep the manipulator in the plane of the workpiece. More complicated methods include using an actuated clamping system, a suction-based brace, or permanent magnets [57]. A mechanical bracing option not discussed in the literature is to use of the surface adhesion techniques developed by

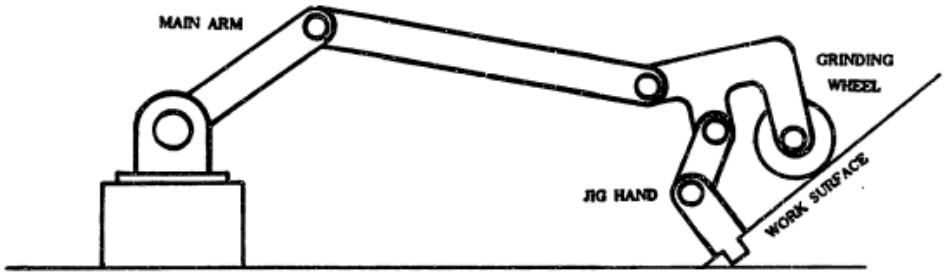


Figure 3.9 A manipulator grounded to the work surface with a "jig hand" [59].

the wall-climbing robotics research community. These technologies include pressure-sensitive adhesives, wet adhesives, and microstructure adhesion elements similar to those used by wall-climbing geckos [63]. Real world applications of these bracing technologies includes automotive manufacturing, aligning laminated substrates [61], deburring systems [58], and drilling large aerospace parts without templates [62].

### *3.3.2.* Catheter Bracing

In the context of catheter-based robotic surgery, braced manipulation has the advantages of allowing flexible catheter devices to apply greater forces against the compliant heart tissue without deflecting significantly. Grounding the device against the moving tissue of interest or tissue structures with similar motion will also aid in tracking the intracardiac tissue. The following section discusses possible implementations of catheter braced manipulation.

Bracing the catheter device inside the heart poses a different set of challenges than what is seen in the industrial robot applications discussed above. As opposed to the rigid metal work surfaces seen in the industrial applications, the heart walls are compliant, actively contracting, and quickly moving structures as discussed in Chapter 2.

Bracing a surgical catheter device against the dynamic heart tissue may further increase the end effector control complexity.

Another challenge of bracing inside the heart in addition to the tissue motion is the fact that the cardiac tissue is electrically and mechanically sensitive. Applying forces to certain areas of the heart can create unpredictable arrhythmias or permanent tissue damage [64]. Therefore, the bracing method and strategy must be carefully designed to interact with only certain areas of the heart and apply forces that will not damage the underlying tissues, such as the atrial appendage and the apex of the heart.

Given these constraints, there are a number of possible bracing strategies that could be employed to improve robotic catheter performance. The most basic bracing approach is to take advantage of the physiological structures used during the catheter approach into the heart. For example, the catheter sheath could attach to the approaching vessels with a deployable mechanism similar to a stent or a semi-rigid introducer sheath. Another anatomical structure often encountered during a catheter approach into the left heart is the atrial septum [7]. This structure is often pierced using a needle and crossed when the catheter approaches the left atrium via the right atrium (Figure 2.1). The catheter could be braced relative to this structure using a mechanism similar to the devices used to close congenital defects or holes inside of the septum, such as the AMPLATZER septal occlude device (AGA Medical Corp., Plymouth, Minnesota, USA). These devices clamp onto the thin septum membrane without creating significant tissue damage and would act to anchor the flexible catheter relative to the cardiac structures.

Another bracing strategy is to attach rigid, extendable wires to the catheter sheath and use the wires to anchor the system. One option is to insert the wires into other

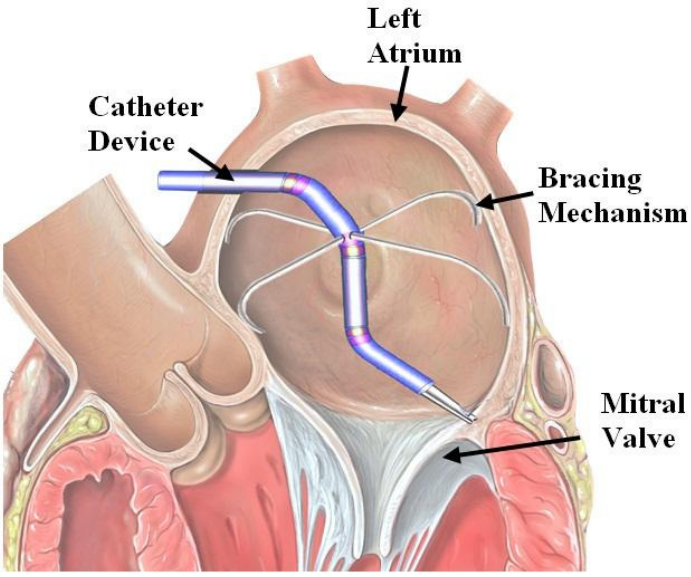


Figure 3.10 Conceptual image of the robotic catheter device supported by a deployable bracing mechanism inside the left atrium.

structures or vessels around the heart, such as the pulmonary veins going into the left atrium (Figure 2.1). This technique keeps the catheter in place relative to the vessels that also anchor the heart in the body. The wires would also allow for the catheter to brace against the tissue surfaces inside the heart, such as the atrial appendage or the apex, by attaching the wires to the tissue using expandable structures, suction, graspers, or other releasable mechanisms. Figure 3.10 illustrates this concept with an expandable structure applying normal forces against the interior of the left atrium while the catheter interacts with the mitral valve annulus.

For the *in vivo* experiments presented Chapters 4, 6, and 7, an introducer sheath is used to brace the catheter system inside the heart relative to the vessels and the heart wall. Future research into this area, include *in vivo* animal experiments, will be required to further define the requirements of a bracing system for catheter-based intracardiac surgery.

# Chapter 4

# Position Control

This chapter investigates the accurate control of the robotic catheter tip position through analysis of the performance limitations, system modeling, control methods, and *ex vivo* and *in vivo* evaluations.

## 4.1. Performance Limitations

Operation of the actuated catheter system reveals two principal performance limitations: the friction forces on the guidewire and the backlash behavior of the guidewire-sheath system. These two phenomena degrade the trajectory tracking accuracy and response time of the actuated catheter tip. Figure 4.1 shows an example of an uncompensated catheter tip inaccurately tracking a desired trajectory.

To determine the major factors that are responsible for these limitations, a parametric study was conducted on the catheter system. The experimental variables examined in this study include the gap size between the sheath and guidewire (Figure 3.2) and the bending configuration of the catheter, characterized by the bend radii and

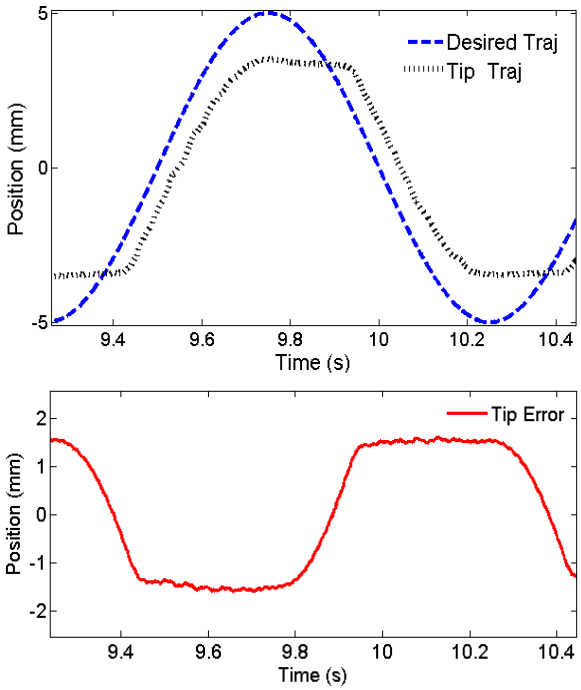


Figure 4.1 Top: Typical catheter tip trajectory tracking accuracy limitations due to friction and backlash. Bottom: Tip trajectory tracking error.

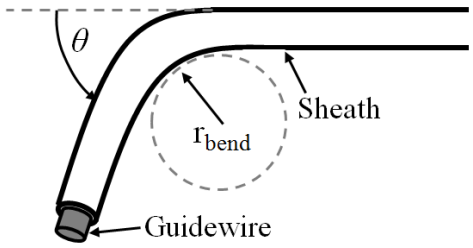


Figure 4.2 The catheter sheath configurations used to evaluate the friction and backlash performance limitations.

bend angles of the sheath (Figure 4.2). The catheter material properties and the external forces were held constant.

For evaluation purposes, the friction forces in the catheter system and the catheter tip position were directly measured. The friction forces between the guidewire and actuation mechanism were measured with a small load cell (LCFD-1KG, Omega Engineering, Stamford CT) connected to a differential amplifier (AM502, Tektronix, Beaverton OR). The catheter tip position was measured with an ultra-low friction rotary

potentiometer (CP-2UTX, Midori America Corp, Fullerton CA, linearity: ±1%). The linear motion of the tip was converted into rotation of the potentiometer through a long, lightweight lever arm that connects the tip of the catheter to the sensor. In a clinical setting, tip position can be measured with an electromagnetic tracker or ultrasound imaging.

### *4.1.1.* Friction

The first set of experiments examined the catheter system friction as a function of four different sheath-guidewire gap sizes (Table 4.1), three bending angles (90°,180°, and 360°), and two bend radii (25 and 50 mm). The sheaths are made of flexible Teflon tubing and the guidewires are manufactured from uncoated stainless steel. The friction was calculated by commanding a series of constant velocities from the actuator in both the positive and negative directions. Force sensor readings during the constant velocity portion of the trajectory were averaged and plotted against the velocities. The friction data was summarized for each configuration by taking the average of the friction values for each velocity. The data was analyzed with a three-way analysis of variance (ANOVA).

**Friction Results**

Figure 4.3 presents a typical friction-velocity curve for this system. The observed behavior can be approximated as constant dynamic friction plus a component that varies linearly with velocity. For this case, the Coulomb term can be approximated as 1.0 N of friction, and the velocity dependent term as 0.006 N/(mm/s). In this study friction is modeled as Coulombic friction because the velocity dependant contributions are small

TABLE 4.1
EXPERIMENTAL CATHETER DIMENSIONS

| Sheath Inner Diameter | Guidewire Diameter | Gap Size ($G$) |
|---|---|---|
| 1.59 mm | 0.76 mm | 0.83 mm |
| 1.59 mm | 1.50 mm | 0.09 mm |
| 2.38 mm | 1.50 mm | 0.88 mm |
| 2.38 mm | 2.23 mm | 0.15 mm |

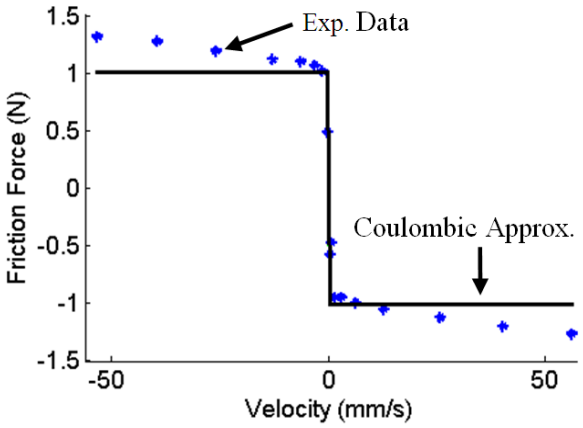


Figure 4.3 The catheter friction forces and Coulombic friction approximation as a function of guidewire velocity.

(<10%) for the majority of velocities required to track the heart motion. Configurations with less than 0.05 N of friction were assumed to be frictionless because the friction was on the order of the sensor drift for the duration of the experiment.

The results of the friction experiments, summarized in Figure 4.4, contain a number of trends. The gap size has the strongest influence on guidewire friction ($p < 0.0001$, $F = 107.62$). This parameter directly affects the normal forces applied to the guidewire by the sheath. The normal force is created by any sections of the sheath that might be pinched, locations where the guidewire is constrained to conform to the inner wall of the bending sheath, and places where kinks in the guidewire or sheath cause the two components to come into contact. A small gap size amplifies these issues because

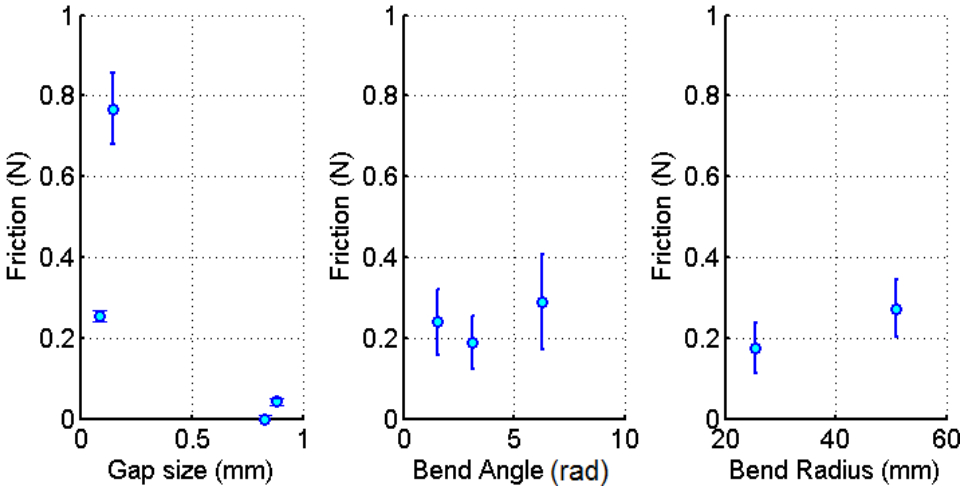


Figure 4.4 Friction results as a function of gap size, bend angle, and bend radius. Friction is assumed to be Coulombic and the symbols are the mean values and bars are the standard error.

smaller deformations in the catheter system cause the sheath and guidewire to interact. Large gap sizes, on the other hand, allow more space for misalignments. Therefore, increasing the gap size decreases the friction experienced by the guidewire.

The results also show that bend angle has an effect on the friction forces ($p = 0.004$, $F = 6.47$). Although the magnitude of the effect is small, it is clearly illustrated when the data is partitioned by gap size as in [65]. One reason for this trend is that bending causes the sheaths' cross sections to deform slightly. This deformation can pinch the guidewire, thus increasing the applied normal forces. Also, the bending of the sheath forces the inner guidewire to bend in order to conform to the outer sheath. The reaction forces generated by the conforming guidewire increase the normal force and therefore the friction on the guidewire.

The bending radii used in this study, which span the typical range for cardiac catheters, do not appear to have a significant impact on the friction measurements ($p = 0.64$, $F = 0.23$).

These results indicate that for certain conditions, only the gap size and catheter bending are required to estimate the friction in the system. However, additional factors that contribute to the total friction experienced by the guidewire, including the sheath and guidewire materials and dimensions, the catheter seals and connectors, and the external forces applied to the system, complicate the development of a general model of system friction.

### *4.1.2.* Backlash

The backlash properties of the sheath-guidewire system were investigated with the same experimental variables (gap size, bend angle, bend radius) as the friction experiments above. The backlash was examined by commanding the base of the catheter system to follow a 1 Hz sinusoidal trajectory (Figure 4.1). This trajectory is a highly simplified version of a mitral valve annulus motion of a heart beating at 60 beats per minute. The hysteresis curve for the system plots the input trajectory versus the measured tip position trajectory (Figure 4.5).

The amount of backlash was quantified for each experiment by the width of the backlash hysteresis curve. For example, the hysteresis curve in Figure 4.5 has a width of approximately 3 mm. The width of the hysteresis is the amount of displacement commanded at the base of the catheter that does not result in any movement at the tip. The backlash data was analyzed with a three-way ANOVA.

**Backlash Results**

The experimental data presented in Figure 4.6 summarizes the effect of the three experimental parameters on the backlash. Bend angle has the clearest effect on backlash

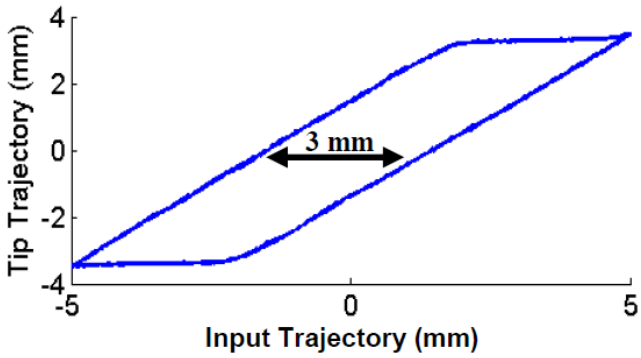


Figure 4.5 A hysteresis plot of the trajectory at the drive system versus the catheter tip. The width of this hysteresis curve is referred to as the backlash deadzone, equal to 3 mm in this example.

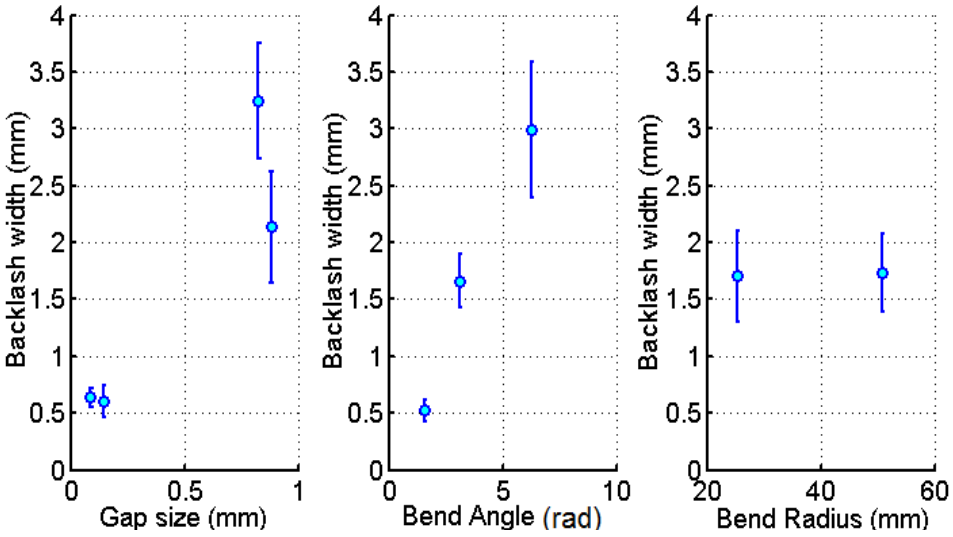


Figure 4.6 The backlash results as a function of gap size, bend angle, and bend radius. Symbols are the mean values and bars are the standard error.

($p < 0.0001$, F = 28.11). The backlash width was found to be approximately proportional to the bend angle. The other parameter that was found to affect the backlash was the gap size ($p < 0.0001$, $F = 32.28$). The data indicates that the larger the gap size, the larger the backlash. Bend radius did not have a significant effect on the backlash width ($p = 0.53$, $F = 0.41$).

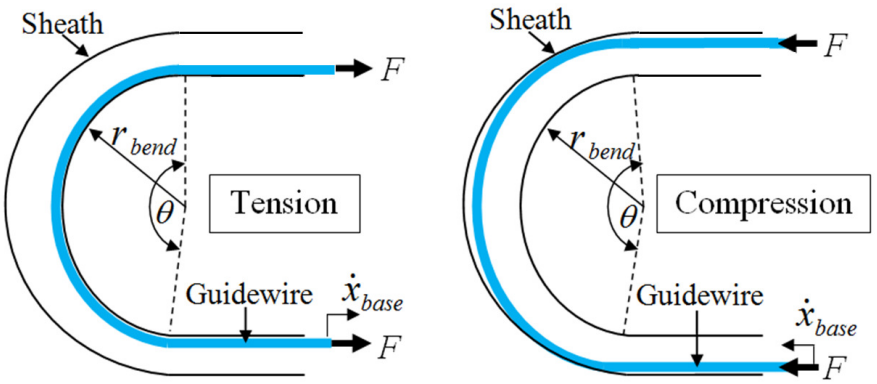


Figure 4.7 Guidewire position in the sheath under tension (left) and compression (right). Backlash behavior is created by this change of position inside the sheath during transitions from tension to compression.

**Backlash Model**

A model was developed to explain the backlash width values in these experimental results. The catheter guidewires utilized in this system are different from tendon transmission mechanisms because unlike tendons, the guidewires are used both in tension and compression, which can result in buckling [66-68]. Unlike backlash models that describe the effects of backlash on displacement and force transmission, our model predicts the size of the backlash deadzone [69].

The model determines the change in length of the guidewire required to conform to the curvature inside the catheter sheath. Under tension, the guidewire uses the inside of the curve as a bearing surface and slides along this inner surface of the sheath. When the applied force changes directions to compression, the guidewire is forced to switch positions and conform to the outside of the sheath. This behavior is illustrated in Figure 4.7.

As the force $F$ switches from pulling the guidewire in tension to pushing it in compression, the guidewire tip does not initially move despite the translation of the base because the guidewire must first change positions inside the sheath. The length of the guidewire required to change positions depends on the physical configuration and dimensions of the system. The backlash width $w$ can be predicted as the change in curve length

$$\begin{aligned} w &= \theta(r_{bend} + D_{sh} - \tfrac{1}{2} D_{gw}) - \theta(r_{bend} + \tfrac{1}{2} D_{gw}) \\ &= \theta(D_{sh} - D_{gw}) \end{aligned} \tag{4.1}$$

where $\theta$ is the total bend angle of the sheath, $r_{bend}$ is the bend radius of the sheath, $D_{sh}$ is the inner diameter of the sheath, and $D_{gw}$ is the diameter of the guidewire (Figure 4.7).

The backlash model (4.1) was evaluated with the backlash data presented in Figure 4.6. The model predicted values, $w$, are plotted against the experimental backlash values, $w_e$, in Figure 4.8. The root mean square (RMS) error for the model is 0.4 mm and the coefficient of determination, $r^2$, is 0.93.

The results in Figure 4.8 show that the model accurately predicts the backlash width. The model slightly underestimates the backlash for lower backlash values and overestimates for larger values. This trend is most likely caused by the effects of friction on the catheter.

Systems with smaller gap sizes have greater friction, which causes the guidewire to buckle in compression during operation and deforms the outer flexible sheath, thus increasing the backlash width. Systems with larger gaps experience decreased friction forces, which in turn reduce the forces that drive the guidewire to conform to the inner wall of the sheath. An analysis of compliant guidewires buckling inside rigid sheaths

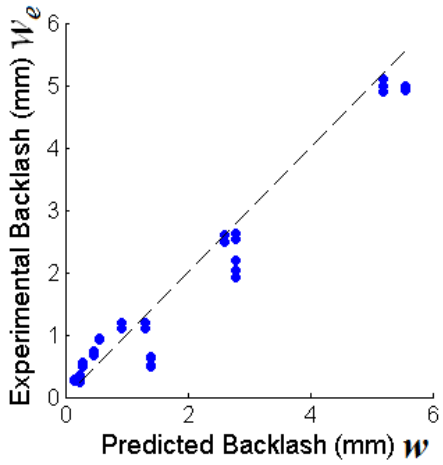


Figure 4.8 Model-predicted backlash values versus experimental values. The model agrees with the experimental values with an $r^2$ of 0.93.

was examined in [70], which could be extended to account for the sheath deformation observed here.

**Backlash-Friction Dependence**

The hypothesis presented above is that the catheter friction applies resistance forces to the guidewire that can cause it to deform as it moves, thus increasing the backlash behavior of the catheter tip. To evaluate this hypothesis, a range of normal forces were applied to the sheath at the tip end of the catheter while the guidewire was driven to follow a sinusoidal trajectory, thus varying the friction level. The sheath configuration was held constant.

The results of this experiment (Figure 4.9) confirm that backlash increases with applied friction, thus causing the model in Eqn. (4.1) to further underestimate the backlash. This understanding of how the friction affects backlash can be used to improve backlash compensation.

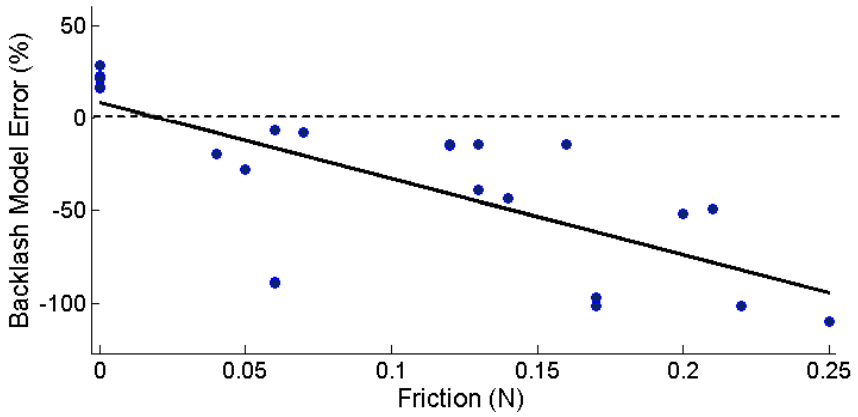


Figure 4.9 Backlash model error versus the catheter friction force. The results confirm that the model underestimates the backlash as the friction increases. The coefficient of determination ($r^2$) for the linear fit is 0.54.

## 4.2. Compensation Methods

The above results demonstrate the major factors that affect catheter system trajectory tracking performance. These factors can be used to improve performance through both mechanical design and control system modifications to reduce the impact of friction and backlash on the system.

### *4.2.1.* Mechanical Design

**Friction**

Friction in the catheter system arises from the mechanical rubbing and sticking contacts between the guidewire and the sheath. Friction can be reduced through material selection, material coatings, and lubrication. Catheter sheaths can be made out of plastics that offer both flexibility and low friction surfaces, such as polytetrafluoroethylene (PTFE). Clinical guidewires are often coated with low coefficient of friction polymers, such as Teflon, to reduce friction forces. Finally, saline is a possible lubrication method

for the catheter system. Clinical catheter systems use saline to flush air bubbles out of the catheter and prevent blood from backflowing out through the catheter. The saline is also crucial for preventing blood from entering the gap between the guidewire and sheath and coagulating inside the sheath.

**Backlash**

The backlash behavior in the catheter system can be decreased by reducing the gap between the guidewire and the sheath. However, reducing the gap will also increase the friction experienced by the guidewire. This design tradeoff should be considered by selecting the guidewire and sheath with the smallest gap that does not introduce enough friction to significantly increase the backlash width.

### *4.2.2.* Control System

**Friction**

The system backlash and friction can also be reduced through improvements to the control system. For example, feedforward Coulomb friction compensation can be used to reduce the friction force effects in the base module [71]. This method uses a friction predictor that observes the desired catheter velocity and the average friction resistance, and then feeds forward an additional force that the actuator applies to the catheter to compensate for the friction. The feedforward predictor used in this case employs a Coulombic model, which was shown to reasonably approximate the friction forces experienced by the catheter (Figure 4.3).

One limitation of friction compensation is that it primarily improves the trajectory tracking of the drive system module. It is not able to reduce the main source of trajectory

tracking error at the catheter tip, the backlash behavior of the guidewire inside the sheath. While backlash is related to friction resistance in the catheter, compensating for friction at the drive system does not reduce the backlash effects on the guidewire.

**Backlash**

An enhanced control system can reduce the backlash behavior by modifying the trajectory commanded at the base of the catheter. The trajectory can be extended to ensure that the tip of the catheter overcomes the backlash deadzone and reaches the desired location. The general approach is to add an offset, $\delta$, to the desired trajectory, $x_d(t)$, to create a new trajectory for the drive system to follow that will ensure that the tip of the catheter achieves the desired trajectory. The modified trajectory, $x_m(t)$, can be written as

$$x_m(t) = x_d(t) + \delta(x_d, x_m, w) \tag{4.2}$$

The offset value $\delta$ can be determined by a number of methods and can vary as a function of the desired trajectory, the previous modified trajectory, the predicted or experimental backlash width, and a range of other system parameters.

Here we consider two leading trajectory modification control methods, inverse compensation and model-based compensation.

**Inverse Compensation**

Inverse compensation commands the system to follow a new trajectory created by adding the tracking error to the original desired trajectory. This method measures the backlash and uses the inverse value to specify the offset $\delta$ [69]. Figure 4.1 presents an example of the tracking error caused by backlash in the catheter system. Limitations of

this method include the assumption that the system is able to traverse the deadzone region instantaneously and that the backlash behavior is constant and not velocity-dependent [69]. Another challenge with this method is that it requires knowledge of the error before the trajectory can be modified, which requires initially running the system without compensation.

**Model-Based Compensation**

Another backlash compensation method is to use the backlash model prediction in Eqn. (4.1) to adjust the desired trajectory. Given a known gap size and sheath bend configuration, this model-based controller can estimate the backlash width and then feedforward a trajectory correction to the drive system controller. This method has the advantage that it can adjust the compensation in real-time as the bend configuration changes. The sheath configuration measurement can be updated either through imaging or mechanical sensors as the catheter position changes during the procedure.

For this control method, the offset value $\delta$ is a function of the desired and modified trajectories, the width of the backlash deadzone region, $w$, calculated with the model in Eqn. (4.1), and a smoothing term, $\tau$.

$$\delta = \begin{cases} +w-\tau \\ -w+\tau \end{cases} \tag{4.3}$$

The sign of the offset is determined by which side of the deadzone the model predicts the catheter tip should be commanded to travel. The additional term $\tau$ is included to smooth the transition of the offset when the desired trajectory requires that the catheter to travel to the other side of the deadzone. Without this smoothing term, the catheter tip would attempt to instantaneously traverse the deadzone and potentially overshoot.

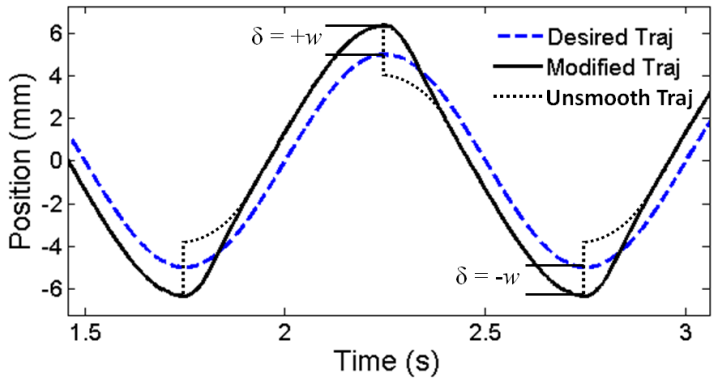


Figure 4.10 The desired sinusoidal trajectory and the modified trajectory created with the model-based backlash compensation method. Note the smoothed and unsmoothed transitions between the positive and negative offset.

A gradual, smooth transition can be achieved if a transition term τ is included to modify the backlash offset:

$$\tau = 2w(1 - e^{(-\Delta x/G)}) \tag{4.4}$$

where $\Delta x$ is the distance traveled from the previous side of the backlash deadzone and $G$ is a gain value used to select how quickly the offset travels across the deadzone. $\tau$ is set based on the system bandwidth to allow the catheter to transition as fast as possible without causing any significant overshoot. Figure 4.10 presents an example of the modified trajectory calculated for a given backlash width and a sinusoidal desired trajectory with and without the smoothing term.

## 4.3. Compensation Methods Evaluation

Backlash and friction compensation are required to improve the catheter system trajectory tracking accuracy. Both inverse and model-based deadzone compensation were tested. A feedforward Coulombic friction compensator was used in addition to

these methods. This compensator's primary function is to ensure that the drive system overcomes the friction resistance and accurately follows the desired trajectory.

### *4.3.1.* Inverse Compensation

The inverse compensation method was evaluated on the actuated catheter system in conditions that simulated a cardiac intervention. All of the trajectories tracking evaluations were longer than 10 s in duration. In this experiment, a 0.76 mm diameter guidewire and a 1.59 mm inner diameter sheath were constrained to a configuration with two 90° bends that simulated a realistic anatomical approach of passing the catheter from the inferior vena cava into the right atrium with a 50 mm bending radius, crossing the atrial septum, and then turning towards the mitral valve with a 25 mm bend radius. A rubber seal attached to the end of the sheath simulated a seal used to prevent the gap between the sheath and guidewire from filling with blood.

Inverse compensation was first applied to the 1 Hz sinusoidal trajectory. Initially, the tip position trajectory tracking mean absolute error (MAE) for the sinusoidal trajectory was 1.28 mm. The inverse compensation trajectory improved the tip position trajectory tracking by 80%, to the MAE of 0.26 mm.

The compensation method was applied to a typical mitral valve annulus trajectory taken from human ultrasound data [18] (Figure 4.11). Without compensation, the catheter tip failed to track the extremes of the mitral valve trajectory. However, the tip trajectory tracking greatly improved when the inverse compensation trajectory was applied to the system (Figure 4.11). The inverse method reduced the mean absolute error from 1.19 mm to 0.24 mm, an improvement of almost 80%.

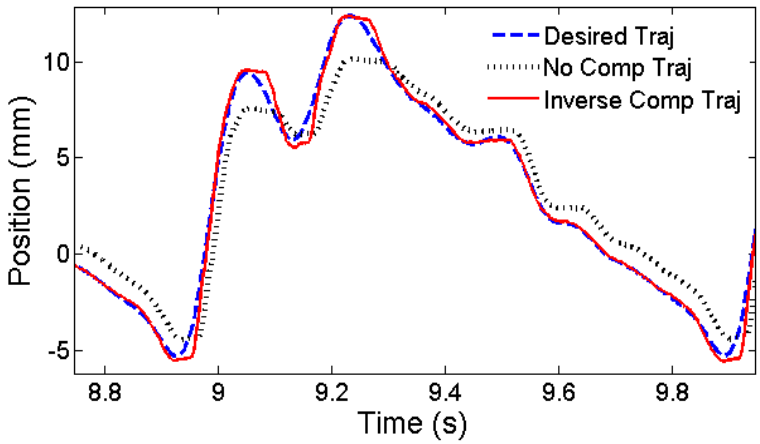


Figure 4.11 The recorded human mitral valve annulus trajectory, the tip trajectory, and the inverse compensation improved tip trajectory.

### *4.3.2.* Model-based Compensation

The model-based deadzone compensation method was tested with a 1.50 mm guidewire and a 2.38 mm inner diameter sheath. The sheath was configured to a 180° bend with an approximately 50 mm bend radius, similar to the experiment above. These values were applied to the model in Eqn. (4.1) to predict the width of the backlash region. Each evaluation trial was longer than 10 s in duration.

The results presented in Figure 4.12 show that this compensation method greatly improved the catheter trajectory tracking. For tracking a sinusoidal trajectory, the MAE without compensation was 2.34 mm and the MAE with model-based compensation was 0.24 mm, an improvement of almost 90%.

### *4.3.3.* Compensation Methods Discussion

The two backlash compensation methods presented here both significantly improve the catheter tip trajectory tracking. One limitation of inverse compensation is that it requires the system to first follow the commanded trajectory inaccurately and then

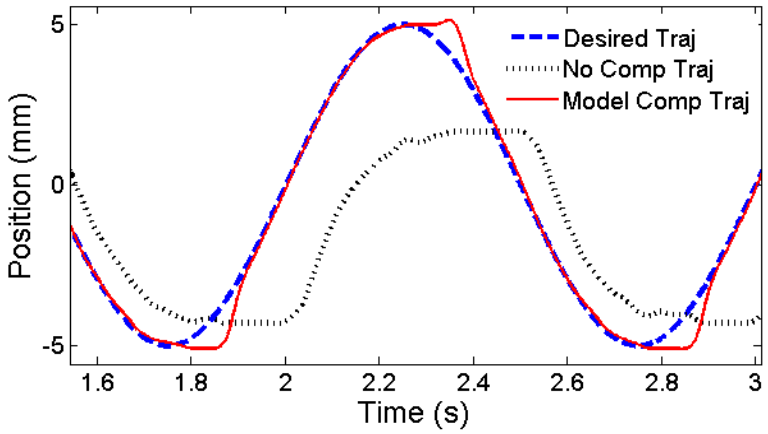


Figure 4.12 The sinusoidal trajectory, the tip trajectory, and improved tip trajectory with model-based compensation.

calculate how to alter the trajectory to improve tracking. This approach is impractical for the real-time control because it assumes that backlash is constant during operation, which is not that case when the bend angle and radius change during a procedure. The model-based method, on the other hand, only requires an accurate knowledge of the sheath configuration, which can be found through fluoroscopic imaging or sensors embedded in the catheter sheath. Furthermore, the sheath should not require regular readjustment once the catheter is inside the heart during the procedure. Therefore, the model-based approach is a more appropriate compensation method for the clinical setting.

## 4.4. *In Vivo* Validation

To investigate the clinical feasibility of image-based catheter control, we integrated the actuated catheter system with the ultrasound visual servoing system developed in previous work [18, 23-25] and evaluated it *in vivo*. Controlling a catheter to follow the motion of internal cardiac structures requires real-time sensing of both the catheter tip and tissue target positions. 3D ultrasound must be used for guidance because

it is currently the only real-time volumetric imaging technique that can image tissue through blood. In the previous image guidance system, the tip of a hand-held instrument with a rigid shaft was introduced through a small incision in the heart wall. The instrument successfully demonstrated *in vivo* the ability to track the tissue motion, control the interaction forces, and place anchors in the mitral valve annulus [8, 22]. The goal of the present study is to reduce the invasiveness of this approach by performing these tasks with a catheter.

The image guidance system was evaluated *in vivo* on a 75 Kg porcine animal model. For this initial study, the actuated catheter was inserted into the beating heart via the top of the left atrium rather than the vasculature to give the surgeon easy access to the mitral valve. The 3D ultrasound scanner probe (X4 Ultrasound Transducer for the SONOS 7500, Philips Healthcare, Andover, MA, USA) was placed epicardially. After the catheter was introduced into the heart, the surgeon used the ultrasound image to aim the catheter at the mitral valve annulus. The catheter was aimed by pivoting the sheath about the insertion point in the LA. The bending and twisting mechanism described in Section 3.1.4 were not included in this prototype. The imaging system was then initialized and tracked the valve motion. See Figure 4.13 for an image of the catheter device inserted into the porcine left atrium and a 3DUS image of the catheter *in vivo*.

The catheter module consisted of a sheath with 1.6 mm inner diameter and a guidewire with a 1.5 mm outer diameter. During the experimental trials, the sheath was configured external to the heart with two 90° bends that correspond to the path from the femoral vein into the left atrium. The catheter was positioned inside the left atrium so that the tip was 1-2 cm from mitral annulus. The catheter controller then performed a

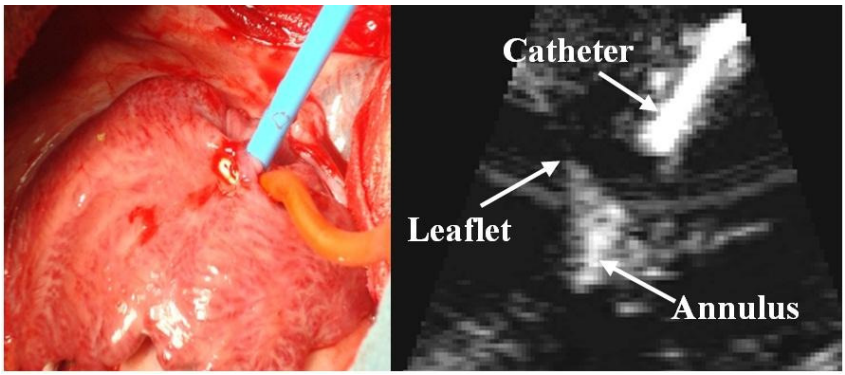


Figure 4.13 Left: Catheter tool inserted into the left atrium. Right: Ultrasound image showing catheter, mitral valve annulus, and mitral valve leaflets.

calibration routine that estimates the magnitude of the friction force in the system. Next, the image processing routines located the catheter using the Radon transform algorithm and then projected forward to find the tissue target and track its trajectory. An extended Kalman filter is used to remove any delay in the trajectory and interpolate the 3DUS information up to the 1 kHz controller rate [8]. The catheter was then servoed to maintain a constant distance between the catheter tip and the target.

### *4.4.1.* Tracking Results

The catheter system successfully tracked the mitral annulus tissue target. Figure 4.13 shows a cross section through a typical ultrasound image volume containing the catheter, mitral valve annulus, and edge of the valve leaflet. Friction compensation was used in this experiment; however, active deadzone compensation was not required because the mechanical design of the catheter system, including the selection of a guidewire and sheath with a small gap size, minimized the deadzone.

Figure 4.14 shows a plot of the typical catheter tip trajectory and the position of the mitral valve annulus. This plot was generated by manually segmenting the position

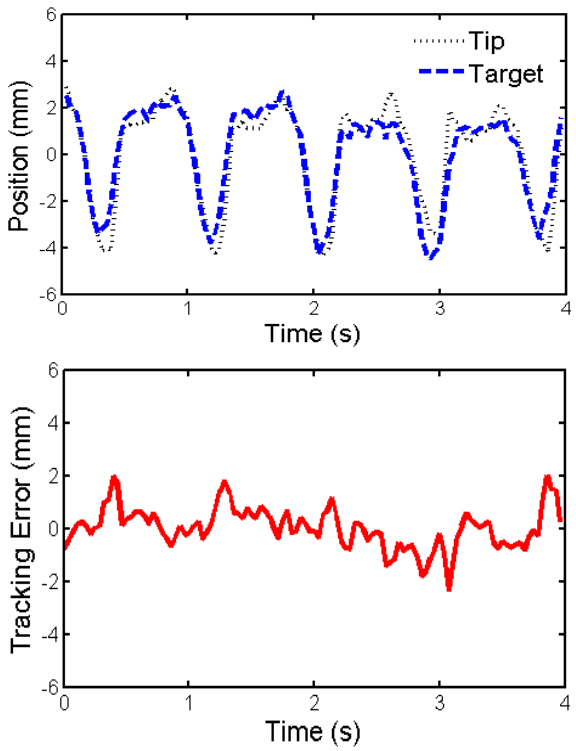


Figure 4.14 Top: Trajectory of the catheter tip and the mitral valve annulus found by manual segmentation. Bottom: The catheter trajectory tracking error. RMS tracking error was 0.77 mm.

of the catheter tip and valve structure from the 3DUS volumes three times and then averaging the values. The standard deviations of the segmented tip positions were less than 0.22 mm and the standard deviations of the segmented mitral valve annulus positions were less than 0.32 mm. Because of the seals required to prevent backflow of blood out of the heart and contain the saline in the sheath, friction compensation values as high as 2 N were required for these experiments

The image-guided catheter tracked the valve motion with RMS errors less that 1.0 mm in all experimental trials. The duration of each trial was greater than 15 s. The RMS error for the trial presented in Figure 4.14 is 0.77 mm. The tracking error shown in Figure 4.14 was caused by respiration motion not captured in the tissue tracking system,

performance limitations of the actuated catheter caused by backlash and friction, and the small beat-to-beat variations in the valve motion not compensated by the image tracking system. In comparison, the RMS tracking error for the catheter system without the compensation controller was over 8 mm due to the substantial catheter friction.

## 4.5. Discussion

This work demonstrates that robotic catheters can achieve the speed and tip position control required for intracardiac repair applications such as mitral valve annuloplasty. In addition, catheter position can be accurately controlled using real-time image guidance *in vivo*. Porcine *in vivo* studies achieved excellent tracking results, with RMS errors of less than 1 mm. These results suggest that it is feasible to use robotic catheters to enable new intracardiac repairs that are both minimally invasive and avoid the risks of stopped-heart techniques.

The major technological challenges explored in this section are the limitations on precisely controlling a guidewire inside a catheter sheath: friction and backlash. Friction increases as a function of bending angle and decreases as a function of the gap size between the guidewire and the sheath. The size of the backlash deadzone is dependent on the gap size and the bending angle. These limitations can be mitigated through mechanical design improvements, such as low-friction coatings and reducing the gap size, and control methods, including inverse and model-based backlash compensation.

To the author's knowledge, the system described here is the first robotic catheter device that can compensate for the fast motion of structures inside the heart. It is interesting to note that this approach is complementary to current commercial catheter robot systems like the Artisan Control Catheter (Hansen Medical, Mountain View CA).

The Hansen Medical catheter system achieves lateral deflection and sheath translation at roughly manual speeds and could be readily combined with the fast guidewire actuation system described here.

# Chapter 5

# Force Control

The following chapter presents the force control of the robotic catheter system. A force control feedback loop is added to the position control method presented in Chapter 4 to enable the catheter tip to apply a constant force on moving tissue targets. The control method is evaluated and demonstrated through benchtop and ultrasound-guided water tank experiments.

## 5.1. Introduction

The goal of the work presented in this chapter is to enable the catheter system to apply a constant force on the moving tissue while performing a repair task on the beating heart. Examples of clinical applications that could benefit from force control include radio frequency ablation of intracardiac tissue to treat arrhythmias and insertion of surgical anchors into the mitral valve during annuloplasty procedures [8, 22, 64]. To achieve this goal of applying a constant force, control methods designed specifically for actuated catheter systems are proposed and evaluated.

**Force Control Characteristics**

Robotic systems that have linearizable system models and slow relative motion with the environment can often achieve good performance with simple force control schemes based on force error feedback [72]. However, robotic manipulators with significant nonlinear system dynamics, such as friction, backlash, or internal compliance, or systems that interact with fast-moving environments, usually require more sophisticated control algorithms [72-75]. One example application of such a control system is the use of inner position control loops and outer force control loops to implement force control on industrial manipulators to address the friction in the joints and transmission systems [76]. Another example is the use of feedforward velocity and acceleration terms to maintain a force on fast-moving cardiac structures with a rigid handheld actuated tool, as presented in previous work by Yuen et al. [27].

The force control task presented here is limited by the friction and deadzone backlash characteristics of the robotic catheter system as well as the fast motion of the beating heart structures [34]. This work develops and demonstrates a method to enable the robotic catheter system to apply a constant force on moving target tissue. First, the force control methods are derived, evaluated, and implemented on the catheter hardware with a motion simulator target. Second, the force tracking task is demonstrated under 3DUS guidance in water tank experiments. Finally, the system performance results are analyzed to better understand how to ensure accurate and stable force control during beating heart repair procedures.

## 5.2. Control Method

The objective of the control system in this work is to apply a desired force on a fast-moving target with the robotic catheter system. A standard error-based force control law is

$$F_a = F_d + K_f (F_d - F_e) - K_v \dot{x} \tag{5.1}$$

where $F_a$ is the actuator force, $F_d$ is the desired force, $F_e$ is the force applied to the environment, $K_f$ and $K_v$ are controller gains, and $\dot{x}$ is the robot velocity [72]. However, this control approach will not work for the robotic catheter system because of the limitations identified in [34], including backlash and friction in the catheter transmission system [75, 77]. These limitations prevent the force regulator in Eqn. (5.1) from correctly responding to the force tracking error in a stable manner because the internal dynamics of the catheter obstruct the controller action from being accurately transmitted to the catheter tip. For example, as the target changes directions, the backlash in the catheter prevents the forces applied by the catheter from immediately changing. Therefore, there is a larger force tracking error that produces an even larger response from the force regulator. These controller limitations often result in instability or in the system entering a limit cycle [77].

To overcome these issues, we propose a method that uses the force error term to modulate the commanded position trajectory of the catheter. This approach is similar to the inner position loop force control approaches used to implement force control on high-friction industrial manipulators [76]. In addition to improving system stability, the use of an inner position loop also allows the controller to directly compensate for the catheter friction and backlash as these limitations are position and velocity dependent.

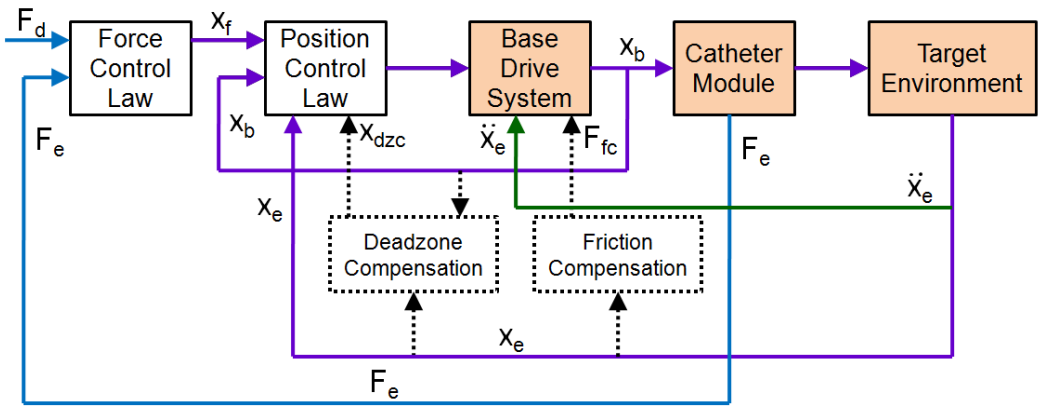


Figure 5.1 Control System Block Diagram. The blue lines indicate force values, the purple lines indicate position values, green line indicates the feedforward acceleration term, and the dotted lines indicate compensation terms.

In this force control approach, the drive system is commanded to follow a desired position, $x_d$, that is the sum of the position of the moving target $x_e$ and the position offset required to maintain the desired force $x_f$.

$$x_d = x_e + x_f \tag{5.2}$$

The force modulation term is

$$x_f = K_f(F_d - F_e) + K_{fi}\int(F_d - F_e)dt \tag{5.3}$$

where $K_f$ and $K_{fi}$ are controller gains. This control law is similar to the method presented by Chiaverini *et al* in [73]. The drive system is commanded to follow the desired position trajectory with a standard PID controller running at 1 kHz. Figure 5.1 presents a block diagram of this controller.

### *5.2.1.* Compensation Methods

While the control method presented above improves stability over conventional force control due to the inner-loop position controller, it does not alleviate the tracking

errors caused by friction and backlash. These limitations require specific compensation methods, as implemented in [34] and indicated in the block diagram in Figure 5.1 by dotted lines.

Friction compensation assumes a Coulombic friction model for the catheter and then feeds forward the friction force $F_{fc}$, based on an observer that predicts the velocity [34]. The friction force is determined during operation through an estimation routine and is dominated by the catheter system design (materials, geometry) and sheath configuration ($\theta$). Backlash compensation adds an additional term to $x_d$ that adjusts the desired base position to overcome the deadzone behavior in the catheter module (Figure 5.1). The amount of compensation, $x_{dzc}$, is determined using a catheter-specific deadzone model presented above in Eqn. (4.1). The compensation term $x_{dzc}$ is either added or subtracted from $x_d$ based on the direction of target motion and the position of the guidewire relative to the deadzone region.

In addition to these terms, a feedforward acceleration term, $\ddot{x}_e$, is added directly to the control signal, as indicated in Figure 5.1 with a green line, to "kick" the drive system actuator in situations where a step or jump in displacement is required. This feedforward acceleration is provided by the Extended Kalman Filter in the 3DUS imaged guided system [23, 25].

### *5.2.2.* Force Controller Limitations

The performance of the force control method described here is limited by a number of factors, including the accuracy of the tissue motion tracking, the compensation terms, and the unmodeled effects of the environment.

**Motion Tracking Limitations**

The most significant limitation of the controller is its dependence on accurate target motion information for motion compensation and force regulation. The controller relies on the periodic motion of the cardiac tissue to allow the predictive position estimations and feedforward acceleration terms to work properly [22]. If the tissue motion deviates greatly from the previous periodic trajectory, the desired position ($x_d$) component of the position control loop will be incorrect because the estimated position of the environment ($x_e$) will not match the real tissue motion. If the position error is great enough, the force controller will go unstable as the catheter tip is commanded to either pull away from the target or plunge through it. Possible sources of target motion tracking errors include external disturbances like arrhythmias or ectopic beats, unmodeled motions like respirations, changes in the tissue motion due to the forces applied by the catheter, and failures of the motion prediction algorithm to converge on the correct trajectory due to poor imaging quality or tool positioning [25].

**Compensation Limitations**

Another limitation of the force controller arises from changes to the physical catheter system. The controller assumes a static model for the system performance for a given catheter configuration. For example, the friction forces and backlash compensation width are fixed for each catheter position and orientation. While assuming a static catheter configuration is reasonable while operating in the constrained workspace inside the heart, other factors, such as blood clots developing between the catheter guidewire and sheath, can change the friction and backlash model parameters. To overcome this

model limitation, the backlash and friction are determined once the catheter is in position but before it has engaged the tissue to include any effects from recent changes in the system or configuration.

In certain situations, the model-predicted deadzone width must be increased to account for the deformation of the sheath and guidewire caused by significant catheter friction [34]. In this study, $x_{dzc}$ was doubled for certain trials to account for the increased deadzone width caused by significant friction values as high as 2 N.

## 5.3. Experimental Evaluation

The force control methods proposed above were first evaluated *ex vivo* to determine how well the catheter can maintain a desired force against a fast-moving target. Based on our previous studies of fast motion compensating with a catheter, the important experimental variables to examine are the catheter bend angle ($\theta$) and the speed and trajectory of the target [34]. See Figure 5.2 for a diagram of the benchtop experimental setup used to evaluate the controller designs.

The first set of experiments examined the performance of the force control schemes while interacting with a target following a 12 mm peak-to-peak, 1 Hz sinusoidal trajectory in three sheath bend configurations: 0°, 180°, and 360°. The friction, modeled as simple Coulombic friction, increases approximately linearly with bend angle [65]. The width of the backlash deadzone, described in Eqn. (4.1), is also a function of the bend angle and can be accurately predicted with the deadzone width model first presented in [65].

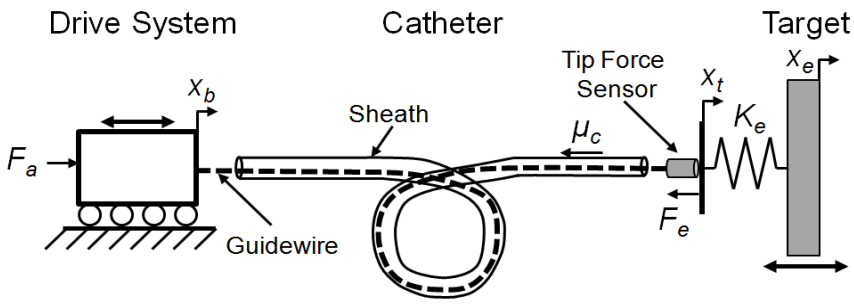


Figure 5.2 Benchtop evaluation experimental setup.

To evaluate the performance of the proposed force control methods, the system was tested with three controller configurations: 1) the force-modulated position controller in Eqn. (5.3), 2) the controller with an added friction compensation term, and 3) the controller with both friction and deadzone compensation terms. The force-modulation gains, $K_f$ and $K_{fi}$, were tuned for best stable performance and kept constant for all of the experiments.

### *5.3.1.* Force Control Methods Comparison

Figure 5.3 presents a comparison of the controller performance applying a constant force (1 N) against the motion simulator target with the catheter in a 360° bend configuration. The target was covered with compliant foam with a stiffness of approximately 0.25 N/mm to simulate cardiac tissue.

The results in Figure 5.3 demonstrate that both friction and deadzone compensation greatly improve the force tracking. Significant tracking errors can be seen when the target changes direction in both Figure 5.3b and Figure 5.3c. These errors occur because the controllers in these plots do not compensate for the deadzone region behavior. Experimentally, this behavior appears as if the tip of the catheter is delayed in

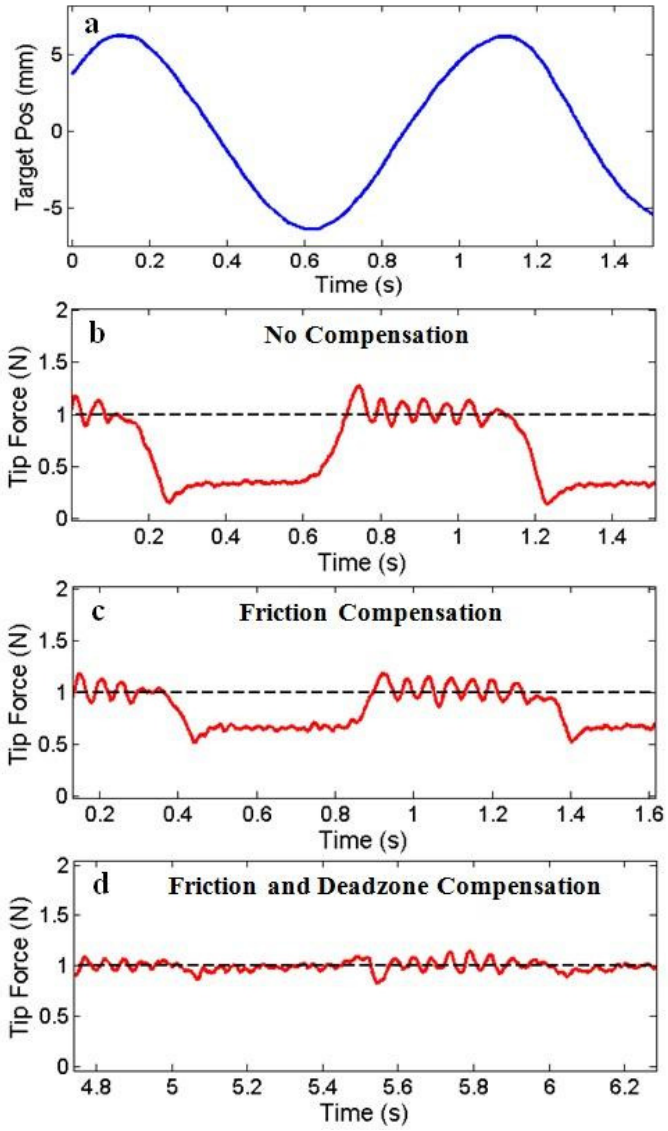


Figure 5.3 Sinusoidal trajectory comparison. (a) 1 Hz sinusoidal target trajectory, (b) the catheter tip force with only force-modulated position control, (c) with the addition of friction compensation, and (d) with the addition of both friction and deadzone compensation. The bend angle is 360°.

responding to the changes in the target trajectory. As demonstrated in Figure 5.3d, deadzone compensation significantly improves the tracking by adjusting the desired position to remove the backlash effects of the deadzone. As seen in the improvement in

performance between Figure 5.3b and Figure 5.3c, friction compensation also improves tracking by cancelling the friction resistance in the sheath.

Figure 5.4 summarizes the performance results of the three force controllers for each of the three catheter configurations. The average performance of each the controllers, presented in Figure 5.4a as the RMS deviation from the desired force, shows that the compensation terms significantly improve the catheter system's force tracking ability. For example, the RMS error for the 360° bend configuration decreases by over 45% when friction compensated was added and by almost 86% when both friction and deadzone compensated were added.

The maximum deviations from the desired force are expressed as the peak-to-peak value, the difference between the maximum and minimum tip force value during each experiment. These deviations are often greatest during the changes in the target's direction of motion (Figure 5.3). This data, presented in Figure 5.4b, clearly indicates that the compensation methods reduce the deviations from the desired force. For example, friction and backlash compensation decreased the peak-to-peak variations in the 360° bend configuration by almost 60%.

It should be noted that for the 0° catheter bend configuration, the deadzone compensation does not alter the RMS or peak-to-peak values because the catheter system has no deadzone according to the backlash model in Eqn. (4.1).

The effect of the frequency of the sinusoidal target was also investigated in this study. The target frequency was varied from 0.1 – 1.6 Hz, approximately the range of possible heart rates encountered during clinical procedures (6-96 BPM). The catheter was

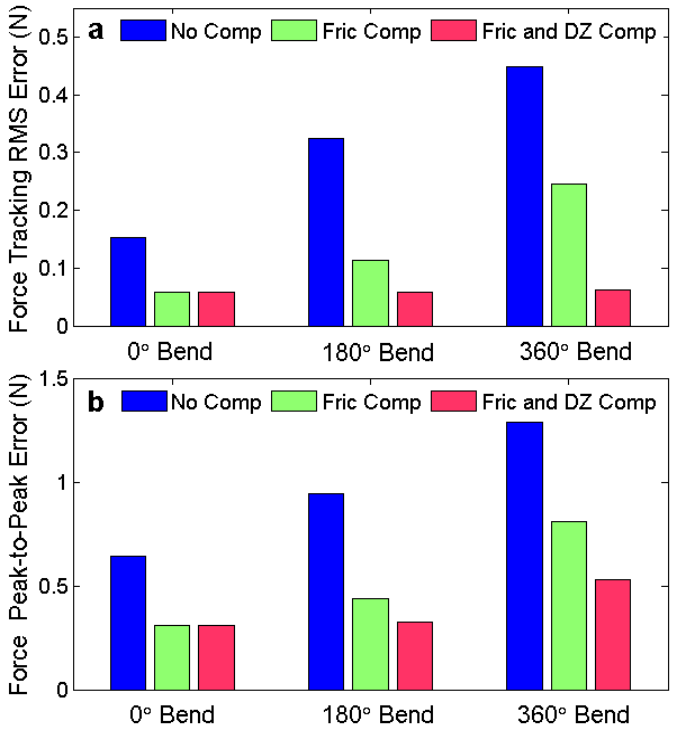


Figure 5.4 (a) Force tracking RMS error and (b) force tracking peak-to-peak error against a 1 Hz sinusoidal target as a function of bend angle for the three force control methods.

constrained in a 180° bend configuration and the control system was commanded to maintain a desired force of 1 N with and without friction and deadzone compensation.

The results of these experiments are summarized in Figure 5.5. The RMS error for both controllers was approximately constant across the frequency range, with the compensated controller performing roughly 75% better than the uncompensated controller for all of the frequencies. The peak-to-peak error increased as a function of the frequency. This trend is because as the frequency increases, the speed at which the catheter must travel through the deadzone to maintain the desired force also increases.

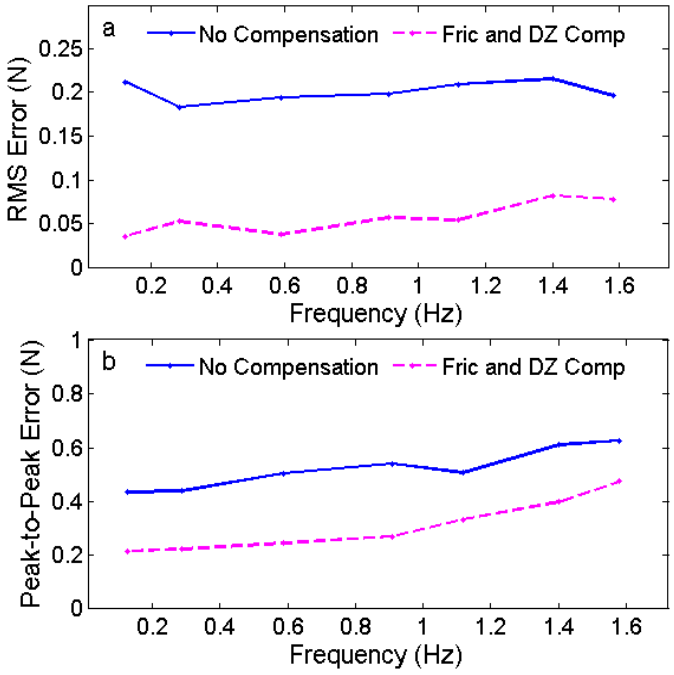


Figure 5.5 (a) Force tracking RMS error and (b) peak-to-peak error while tracking a sinusoidal trajectory as a function of the target frequency.

### *5.3.2.* Mitral Valve Trajectory

The ultimate goal of the actuated catheter system is to perform cardiac surgical repair, such as mitral valve annuloplasty, inside the heart, [9]. To simulate a mitral valve trajectory, the typical motion of a human mitral annulus was extracted from a series of 3D ultrasound volumes and used to create a motion simulator [18]. This target follows a more extreme trajectory than the sinusoidal target, with frequency components as high as 15 Hz and jumps of 15 mm in less than 100 ms (Figure 5.6a).

The catheter system was commanded to follow the mitral valve simulator while maintaining a desired force of 1 N. Initially, only modest improvements were seen when the compensation terms were added because the controller did not respond quickly enough to the rapid changes in the target trajectory. This tracking error resulted partly

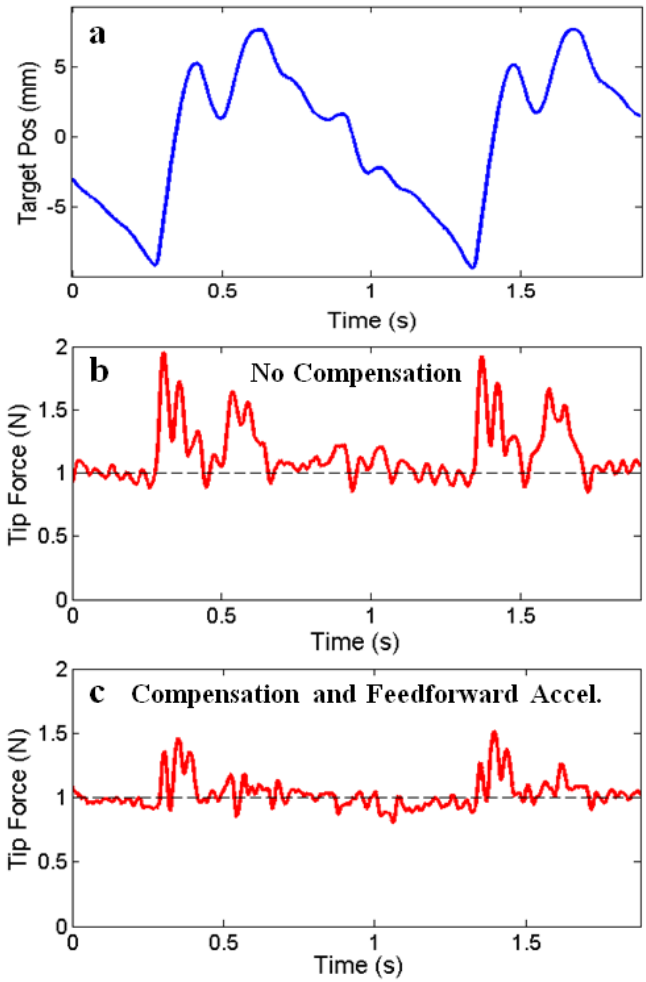


Figure 5.6 (a) The mitral valve annulus target trajectory, (b) The force tracking performance without compensating and feedforward acceleration, and (c) the performance with both compensation and feedforward acceleration.

because of the reduced position controller gains selected to maintain force stability and the saturation limits of the actuator.

To improve the trajectory tracking performance, an estimate of the desired acceleration was added to the drive system as a feedforward term. This value was generated in this experiment by a predictive autoregressive filter based on observations of previous cardiac motion cycles, as used in several previous robotic beating heart motion

compensation systems [19, 23]. This feedforward term allows for the catheter tip to start accelerating at the beginning of the larger jumps in the mitral valve trajectory before larger errors develop.

Figure 5.6 shows the catheter tip force while tracking the simulated mitral valve motion target with and without compensation and the feedforward acceleration term. The tip force RMS error for the system with only force-modulated position control was over 0.26 N. The RMS error for the controller with compensation and feedforward acceleration was 0.11 N, an improvement of approximately 55%.

### *5.3.3.* Tank Evaluation

The force controlled catheter system was also evaluated in water tank studies under 3DUS guidance to prepare for *in vivo* studies. A water tank is required to evaluate the visual servoing system because clinical ultrasound machines cannot operate in air.

**Engaging the Target**

One of the challenges of regulating the forces applied by the catheter tip to a target is the transition from operating in free space to applying the desired force on the fast-moving target**.** The process of engaging a surface is challenging because of the potential for the catheter tip to apply large and destabilizing interaction forces. Furthermore, the catheter must be able to safely retract from the target surface after the experiment is completed. To ensure that the catheter contacts the target in a controlled manner, a trapezoidal position trajectory is commanded to dictate the processes by which the tool engages and retracts from the target.

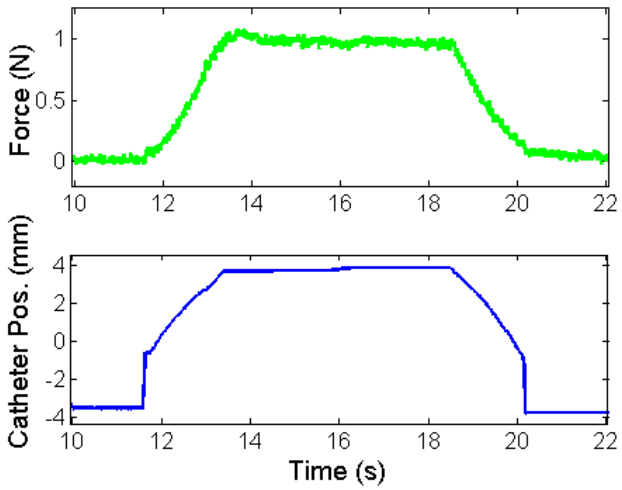


Figure 5.7 Engaging the target: The catheter engages and retracts from a static target using a trapezoidal trajectory to achieve the desired force.

It is assumed that the catheter must maintain a constant force against the tissue in order to apply a surgical technique such as ablate, resect, or staple the tissue. In the method used here, the catheter approaches the surface at a rate of 2.5-5 mm/s, applies the desired force for 5 s, and then retracts from the tissue at 5 mm/s. Figure 5.7 demonstrates engaging a static target. Any alternative engagement process is for the user to manually adjust the catheter position until it makes first contact with the moving tissue and then switch to a force control method to maintain a constant interaction force.

The process of engaging a target is further complicated when the target is quickly moving, such as the mitral valve annulus (Figure 5.6). If the approach process does not consider the motion of the target and progresses at a constant velocity, the catheter tip may collide with the target surface and result in a large spike of force and possibly system instability. To prevent this issue, the moving target is virtually stabilized relative to the catheter tip by utilizing motion compensation during the approach procedure.

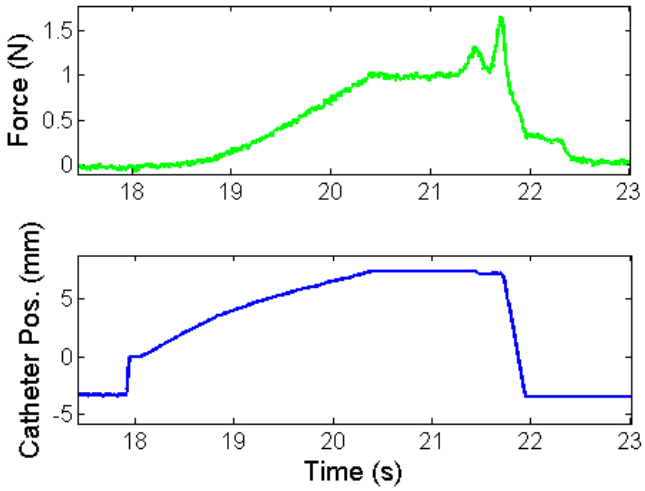


Figure 5.8 The catheter tip immediately pulls back into a safe position if the force threshold (1.5 N) is exceeded to prevent tissue damage.

To prevent damage to the tissue or tool caused by instability or unexpected forces applied to the catheter tip, the controller is instructed to pull back the catheter and enter a "safe mode" if a larger than expected force is sensed at the tip. As demonstrated in Figure 5.8, the catheter withdraws at a speed of 50 mm/s when a force spike is recorded at the tip. This force spike simulates an ectopic heart beat not anticipated by the motion compensation controller, causing the catheter tip to collide with the heart wall. The force threshold, in this case 1.5 N, determines if the controller needs to pull back the catheter into the safe mode. Other possible metrics for determining this error state in addition to a force threshold include a catheter velocity threshold to anticipate instability or limit cycles and a system power function that includes both catheter tip velocity and force.

**Tank Results**

The catheter system was evaluated using the 3DUS tracking system in a water tank interacting with both the sinusoidal and mitral valve annulus motion target. The use

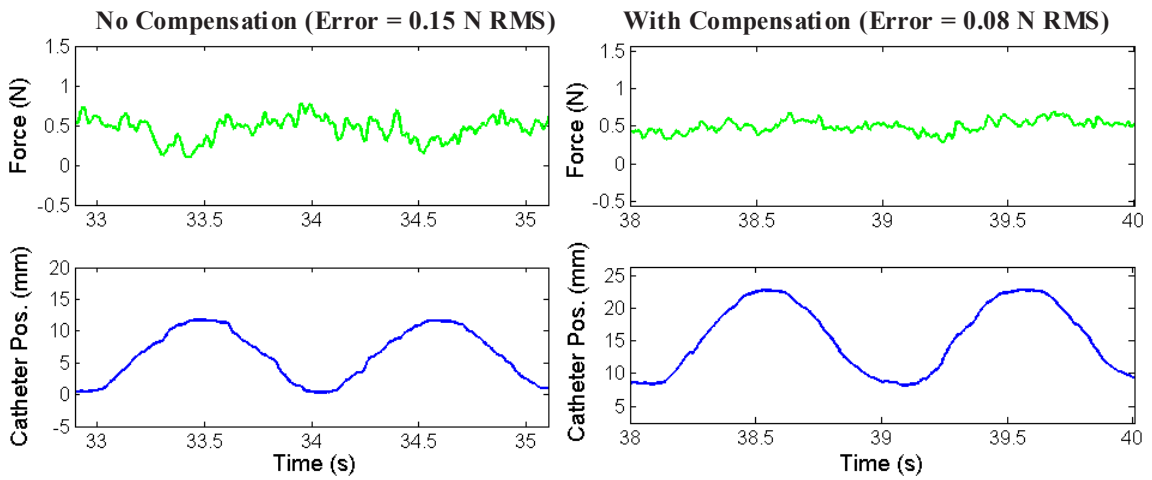


Figure 5.9 The force tracking results in a water tank under 3DUS guidance for the sinusoidal target trajectory. Left: Without deadzone or friction compensation (RMS error = 0.15 N). Right: With compensation terms (RMS error = 0.08 N).

of the 3DUS complicates the force tracking process because of the importance of the target position prediction, as discussed above in Section 5.2.2. Even in the controlled environment of the water tank experiment, the system performance varied between each trial due to the quality of the EKF tissue position prediction [25]. In spite of these limitations, performance values of 0.08 N RMS errors were achieved for the sinusoidal trajectory. Without friction and deadzone compensation, force tracking results of only 0.15 N RMS were achieved relative to the sinusoidal target (Figure 5.9). Force control performance values of 0.17 N RMS errors were achieved for the mitral valve annulus trajectory target with friction and deadzone compensation (Figure 5.10). See Figure 5.9 and Figure 5.10 for plots of the system performance in these experiments.

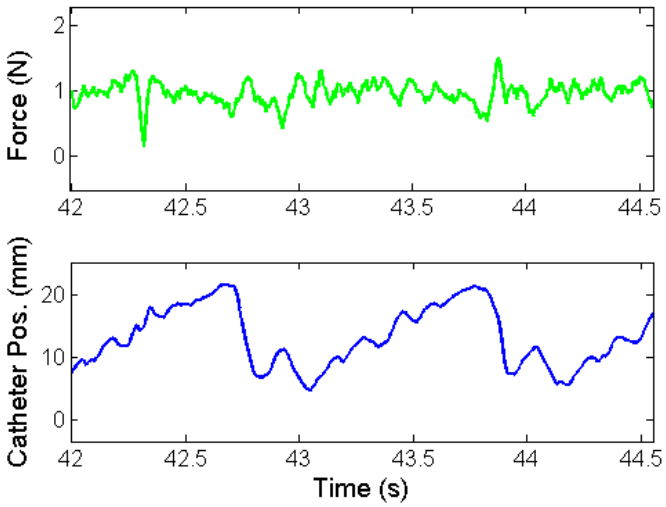


Figure 5.10 The force tracking results in a water tank under 3DUS guidance with a mitral valve annulus trajectory target with the compensation terms. Force tracking error = 0.17 N RMS.

## 5.4. Discussion

This work demonstrates that the catheter system can maintain a constant force against a moving target under 3DUS guidance with low RMS errors. In addition, the results presented above elucidate a number of important points that enable effective catheter force control. The internal performance limitations of the catheter system prevent successful use of simple force controllers. The results show that the catheter performance limitations of friction and backlash need to be compensated for to ensure successful force tracking with the catheter. This finding is especially true as the catheter sheath bend angle increases, thus increasing the size of the deadzone and the amount of friction. These two limitations can only be compensated in the position control domain because they are dependent on the catheter's position and velocity, which is one of the main reasons for using the force-modulated position controller. The peak force tracking

errors, which indicate if the catheter potentially applied tissue perforation magnitude forces, were also reduced using the compensation controller terms.

Another significant factor in catheter force control performance is the quality of the motion compensation target tracking. Because of the inner position loop structure of the force control method employed here, accurate motion tracking is essential to ensure that the catheter tip follows the target and compensates for friction and backlash. While the 3DUS motion tracking system has demonstrated impressive performance [8, 24, 25][34], it is not as accurate as the potentiometer on the benchtop simulator that provides position information (<0.1 mm error). Therefore, the target trajectory provided by the image guidance system used to control the robot position introduces some additional force tracking errors. This difference in performance can be seen in the benchtop versus the 3DUS-guided tank results, where tracking results of less than 0.05 N RMS errors were achieved on the bench while the best tracking results in the water tank were 0.08 N RMS errors.

# Chapter 6

# Haptic Evaluation

This chapter presents a study evaluating the increases to human perception provided by force feedback and the force sensing robotic catheter system. The value of haptic feedback in beating heart surgery is examined with a user study and the entire system is demonstrated with an *in vivo* experiment [78].

## 6.1. Introduction

Catheters are currently used to provide a large range of diagnostic and interventional cardiac procedures [7]. While these devices do enable intracardiac navigation and interventions, they do not increase the physician's perception of the cardiac tissue properties or the environmental conditions inside the heart. It is the objective of the work presented in this chapter to evaluate how haptics can improve human perception of tissue properties during catheter procedures.

The long, flexible nature of cardiac catheters that makes them easy to snake into the body also makes them poor at transferring force feedback information to the operator. As a catheter tool makes contact with the tissue, the contact force is balanced by the

catheter compliance and frictional losses from seals and viscous fluids. By removing these limitations and giving the clinicians tactile information about the forces at the tip of the catheter, a range of new diagnostic and interventional procedures might become possible with catheters.

Haptic feedback would also increase the information available to the clinician beyond what is currently provided by x-ray or ultrasound imaging. For example, a catheter could be used to palpate and examine tissue around a valve in the heart to determine if it is calcified or stenotic and if further procedures are required [31]. Another potential application of haptic feedback is in percutaneous device deployment. When inserting a cardiac defect closure device, haptics could inform the cardiologist if the device is positioned correctly and assess the condition of the tissue around the defect.

### *6.1.1.* Prior Work

To evaluate the efficacy of the haptic catheter system presented here, a psychophysical study was conducted to determine the stiffness of various materials using the haptic system and a manual device. The human perception of stimuli for all of the senses has been studied extensively [79]. The perception of material stiffness, which combines the tactile perception of both force and displacement, has been investigated with a number of approaches. Jones and Hunter examined a user's perception of stiffness by allowing subjects to adjust the amount of stiffness they experienced until the value matched a reference stiffness. This experiment found the substantial Weber fraction of 0.23 for human perception of stiffness [80]. Srinivasan and LaMotte investigated the tactile discrimination of material stiffness by examining the physiology of the human fingerpad [81]. This research explored how the mechanics of the fingerpad and the

tactile approach affects the human perception of different stiffness materials. LaMotte conducted further research to examine how using a stylus effected the sensations on the fingerpad and the ability to discriminate material stiffness [82].

Other researchers have used haptics to enhance the functionality of catheters. For example, the HapCath presented in [83] is an unactuated device designed to allow clinicians to perform catheterization procedures with a reduced amount of x-ray imaging by feeling the forces at the tip of the catheter. The Hansen Medical catheter also provides some amount of force feedback. The system provides the clinician with force measurements on a visual display and vibrotactile feedback though the user interface during cardiac electrophysiology procedures [84]. Haptics have also been applied to catheter training simulators to provide force feedback, which clinicians say is important for successful training [85, 86]. An example of a commercial catheter training simulator is the CathSimVR simulator (CAE, Montreal, Quebec, Canada). However, no prior work has investigated how haptics improves a user's psychophysical perception of the moving tissues inside the heart.

Previous work has also shown that motion compensation and haptic noise cancelation increase force sensitivity when interacting with moving tissue [87]. Motion compensation virtually freezes the target tissue relative to the actuated tool by commanding the end effector to match the target trajectory. This previous study used a rigid actuated instrument to investigate how motion compensation improves a user's ability to feel a moving target by removing the haptic noise caused by the motion [87]. The work presented here has extended the benefits of motion compensation to catheters, which introduces a number of new technical challenges, including the need for a

miniature catheter tip force sensor and the catheter performance limitations of friction and backlash [34, 88].

This study presents an actuated catheter system that enables haptic perception of fast-moving intracardiac structures and demonstrates the importance of haptic feedback and motion compensation in order to perceive moving tissue properties. To evaluate this system, a series of material stiffness discrimination experiments were conducted that simulate palpating moving tissue around the mitral valve. The following chapter describes the motion compensated catheter system, the haptic feedback interface, and the experimental evaluation procedure and results. Preliminary *in vivo* results that demonstrated the system operating inside the beating heart are also presented. To the author's best knowledge, the catheter system is the first device to allow haptic perception of beating cardiac tissue through the use of motion compensation. The evaluation results show that while some limitations exist, haptics and motion compensation improve a user's ability to discern material stiffness using a catheter.

## 6.2. Method

The haptic system presented here transmits force feedback from the tip of an actuated catheter tracking the fast motion of intracardiac tissue structures. The haptic interface adjusts the position offset of the motion compensation controller as it commands the actuated catheter system to compensate for the cardiac motion. In the full clinical system, the cardiologist points the catheter at the cardiac structure of interest and the 3DUS data is sent to the real-time visual servoing system that tracks the target tissue in front of the catheter tip (Figure 1.1). This trajectory is then sent to the catheter controller that compensates for the performance limitations in the catheter module to

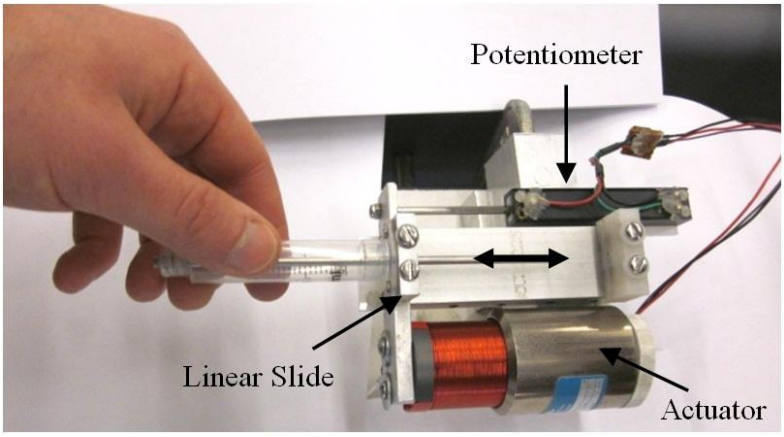


Figure 6.1 The actuated catheter haptic interface.

drive the catheter tip to track the tissue or apply a near-constant contact force on the moving intracardiac surface despite motions of 1-2 cm in under 100 ms [9, 22, 42].

In this study, a sensor on the motion simulator target provided the position information to the catheter control system to enable motion compensation instead of 3DUS imaging, which has been demonstrated in other experiments [9, 22].

### *6.2.1.* Haptic Interface

The haptic device used in this study is a single degree of freedom mechanism that allows the user to input the desired catheter position set point while reflecting the tip forces back to the user. The device, shown in Figure 6.1, consists of a linear voice coil actuator (NCC20-18-020-1X, H2W Technologies, Inc., Valencia, CA, USA), a linear potentiometer (CLP13, P3 America, San Diego, CA, USA), a linear ball slide bearing (BX4-3, Tusk Direct, Inc., Bethel, CT, USA), and a handle fabricated from a 1.4 cm diameter plastic tube.

The haptic interface operates as a bilateral force reflection interface with no delay: position feedforward and force feedback. The position input from the potentiometer on the interface is added to the motion compensation trajectory to adjust the position of the catheter end effector. In this way, the device functions like a joystick that adjusts the static position offset of the catheter. The forces measured by the catheter tip force sensor are reflected back to the user's hand through signals sent to the voice coil actuator in the haptic device. See [89] for a more detailed explanation of bilateral teleoperation.

The forces displayed by the haptic interface are linearly increased by a gain of two to improve the user's ability to differentiate softer forces from the intrinsic friction in the haptic device. The inertial effects on the interface are not addressed here because they contribute small forces relative to the force feedback at the velocities experienced in this study. Custom C++ code is used to control both the catheter drive system and the haptic interface and make measurements via a data acquisition card at 1 kHz. Commands to the actuators are amplified by a linear current amplifier (AMPAQ, Quanser Inc., Markham, Ontario, Canada). Both devices are able to provide sufficient forces (>10 N) and bandwidth (>20 Hz) for this study [22, 34].

The haptic interface was evaluated and shown to accurately display the forces sensed by the tip force sensor. Figure 6.2 shows the force output of the haptic interface measured by a load cell as a function of a sinusoidal catheter force sensor input. The limitations of the haptic interface output are primarily due to friction and stiction effects in the voice coil and potentiometer. These effects are most pronounced when the force signals change direction, resulting in the sawtooth-like profile in the force output

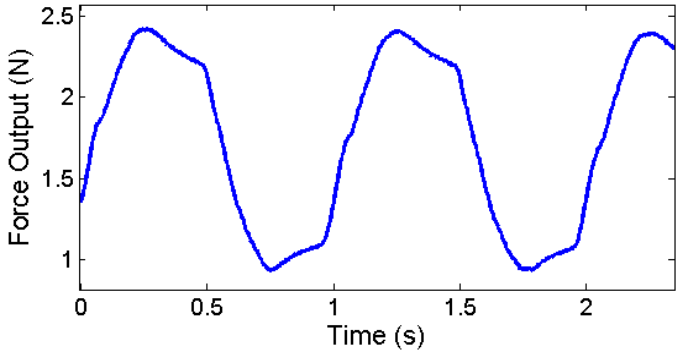


Figure 6.2 The haptic interface force output produced by a sinusoidal input to the catheter tip force sensor.

trajectory (Figure 6.2). The interface's force output is also affected by the limitations of the force sensor and the motion compensation controller. These errors introduce haptic noise to the users and may confuse the material discrimination process.

### *6.2.2.* Validation User Study

The psychophysical research technique employed in this work was the method of constant stimuli utilizing difference thresholds [79]. This method evaluates the subject's ability to differentiate between various stimuli with a series of randomized comparisons.

Five polyurethane foams were selected as material stimuli. The foams were characterized using a load cell (LCFD-1KG, Omega Engineering, Stamford CT; range: 10 N, accuracy: +/-0.015 N) and an indentation tool instrumented with a linear potentiometer (CLP13, P3 America, San Diego, CA, USA) and an indentation tip approximately the same dimensions as the catheters. Because the stiffness of the foam is nonlinear, the stiffness of each material was approximated by measuring the indentation depth caused by a 1 N force, which serves as a linear approximation of the stiffness near the average force applied by users during the experiment. The foam stiffness values

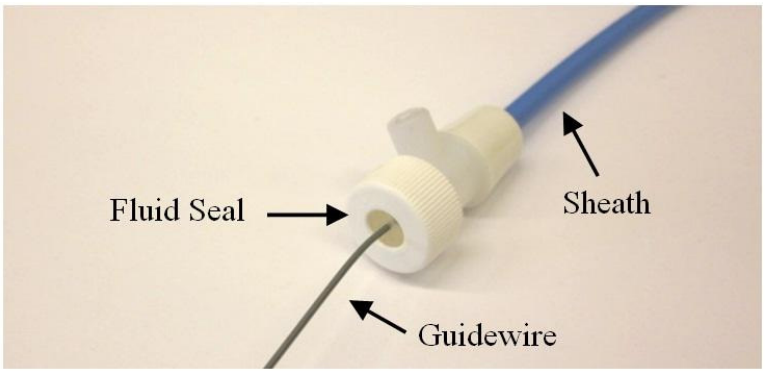


Figure 6.3 The proximal end of the manual catheter system. The manual guidewire is inserted inside the fluid seal attached to the sheath.

range from 0.17 – 0.42 N/mm, which encompasses the stiffness range of certain tissues in the human heart.

**Manual Catheter**

The manual catheter system in this experiment consisted of a clinical fixed-core straight wire guide (0.9 mm outer diameter) and a plastic sheath (4.3mm outer diameter, 3.8 mm inner diameter). The proximal end of the catheter is shown in Figure 6.3. The sheath has two fluid seals to allow the catheter to be flushed and filled with saline and to prevent blood from flowing out of the vasculature. The difference in the diameters and the seals introduced both friction and backlash to the manual catheter system. These behaviors are common in clinical catheter systems. Previous work on the robotic catheter system has shown how these limitations impact catheter performance [65].

While the passive mechanics of the actuated and manual catheter are not identical, both systems exhibit backlash and friction. However, the actuated catheter compensation controller greatly reduces the effects of these limitations as shown in [65]. Therefore, the

passive mechanics of the actuated catheter system do not significantly impact the system performance, regardless of the amount of friction or backlash.

**Study Method**

The user study employed the method of constant stimuli to examine how subjects are able to discriminate between materials of varying stiffness using the manual catheter and the haptic interface [79]. The subject group consisted of 7 subjects (6 male, 1 female), ages 24-30. None of the subjects had previous experience manipulating cardiac catheters or interacting with the haptic interface used in this study.

First, the subjects were briefed on the motivation and background of the study. After the introduction, they were shown examples of the foam materials, instructed to practice palpating them with a rigid stylus, and then trained on the two catheter devices. Training consisted of palpating the foam target with the manual and actuated guidewire with and without visual feedback. The users were then asked to compare two materials that represented the extremes of the stiffness range used in the study. If they were able to differentiate the extremes from the central control material with both catheter systems, it was determined that they were ready to proceed. Because of the subjects' unfamiliarity with both the interfaces and the palpation task, additional training was conducted on a static target using both the manual and haptic interfaces without visual feedback.

The results presented below are from the more realistic experimental setup where the target simulates the motion of the beating heart. The trajectory of the target, shown in Figure 6.4, is generated by a cam mechanism that reproduces the motion of a human

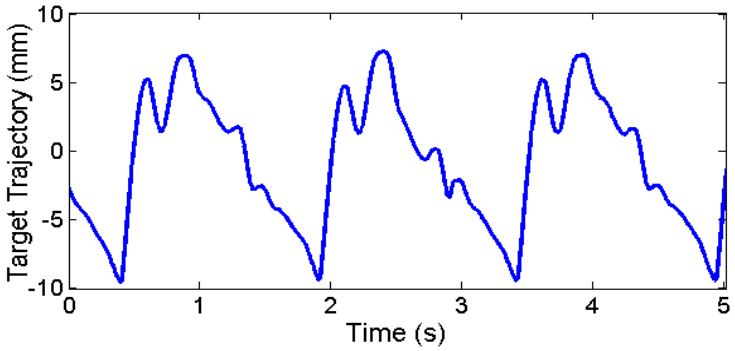


Figure 6.4 The mitral valve motion simulator trajectory.

mitral valve annulus taken from 3D ultrasound data [18]. During the study, the evaluation materials were attached to the moving target and translated along the motion trajectory.

In each trial, the subjects were presented with two materials in a randomized order to sequentially palpate: a comparison material that was varied for each trial and a control material that was held constant. Based on the interactions with the materials, the subject was then asked to state which of the two samples they perceived to be softer. They also had the option to repeat the materials if they were uncertain or could not decide which was softer. For each interface, the subjects evaluated ten pairs of materials. The forces applied to the target were recorded for the first five comparisons of each configuration. The order of the five materials and whether the control material was first or second was randomized for each user for each configuration to reduce the impact of time errors, the effect of the subject's fading mental image of the previous stimulus [79]. The five foam material samples were aligned so that they were the same height and the target was designed to allow the materials to be quickly repositioned (< 2 s) to minimize the time delays between each material evaluation trial. After all of the trials were completed, the users were asked for their feedback and evaluation confidence for both of the interfaces

on a 1-10 scale. The entire experiment took approximately 1 hour per subject and was approved by the university institutional review board (IRB).

## 6.3. Results

All of the subjects employed similar techniques to conduct the discrimination tasks. In each trial, the users slowly pushed the tool into the material and then retracted it. An example input trajectory is seen in the haptic device position plot in Figure 6.6. In addition to haptic feedback, the actuated catheter system also automatically compensates for the motion of the target to maintain a constant distance between the catheter tip and the target [34].

In the manual catheter case, the users moved the guidewire into contact with the moving target, resulting in the force profile seen in Figure 6.5. In this configuration, the target's motion caused the guidewire to buckle and apply unintended forces against the target in a cyclic manner. The subjects did not directly perceive all of the forces experienced at the guidewire tip due to the friction in the catheter and the buckling compliance of the guidewire.

The motion compensation system greatly reduces the effects of the target motion on the user's perception. As shown in Figure 6.6, the motion compensation removed the effects of the target motion and allowed the user to apply a compression force via the user-inputted displacement of the guidewire. While the users were able to apply a more controlled force on the target, they also experienced more haptic feedback from the interface. The interface transmitted both the intentionally applied contact forces and haptic noise forces created by imperfect tracking of the target trajectory. The catheter position control system is able track the target motion with less than 1 mm RMS errors

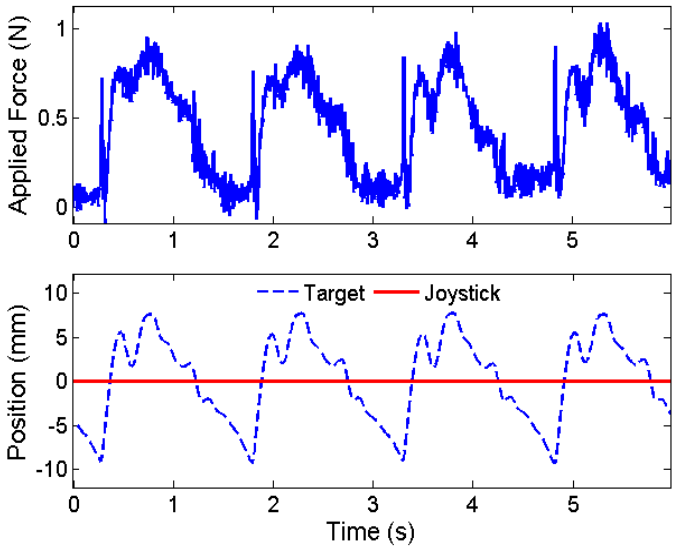


Figure 6.5 Example results using the manual catheter. (Top) The force applied to the moving target by the manual catheter. (Bottom) The target trajectory (the haptic device joystick input is not used in the manual case).

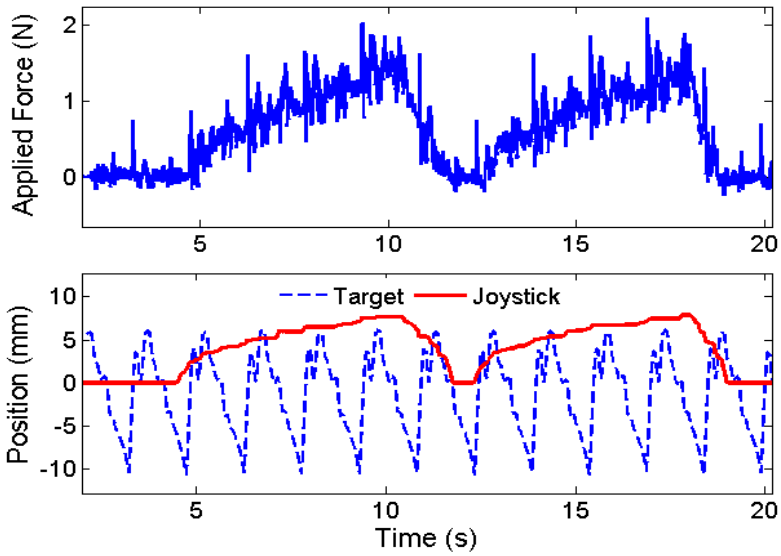


Figure 6.6 Example results using the haptic interface and motion compensated catheter. (Top) The force applied to the moving target by the actuated catheter. (Bottom) The target trajectory and haptic interface joystick position input.

[34], but these small tracking errors introduce the periodic force spikes seen in Figure 6.6.

The results for all of the subjects are plotted in Figure 6.7 and Figure 6.8. The data is expressed as the fraction of subjects who found the comparison material to be stiffer than the control material. The stiffness of control stimulus is 0.31 N/mm. For the case where the control material was compared against itself (the control-control comparison), the data is displayed as the percent of subjects that perceived the first exposure to the control material to be stiffer than the second exposure. A perfect differentiation of the materials, which is possible when directly palpating the materials with one's finger, is 0% stiffer for the two softer materials, 50% stiffer for the control-control material comparison case, and 100% stiffer for the two stiffer materials.

The cumulative results for the manual and haptic catheter configurations, presented with standard error bars in Figure 6.7 and Figure 6.8, include a number of interesting results. In the manual tool case, the subjects were unable to differentiate between soft materials and the control material any better than the control-control material comparisons. However, the subjects were able to detect the two stiffer materials slightly more than 60% of the time. The haptic interface, on the other hand, allowed the subjects to consistently identify the softer materials and recognize the stiffest material in 80% of the trials. For all of the configurations, the control-control material comparison was less than 50%, indicating that the users perceived their second interaction with the control material to be stiffer than the first exposure.

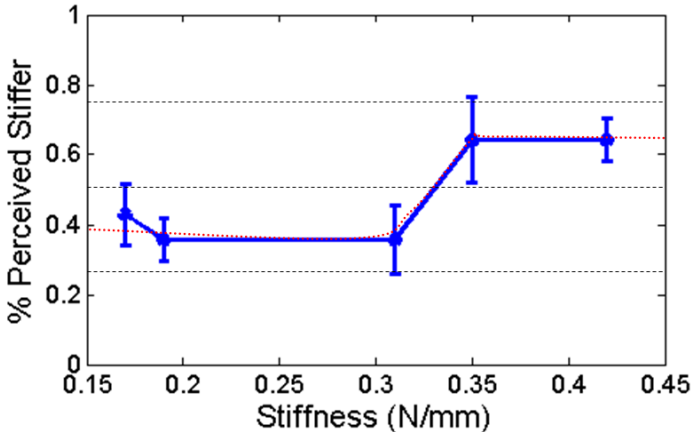


Figure 6.7 The averaged results for the manual catheter and the moving target. The error bars are the standard error.

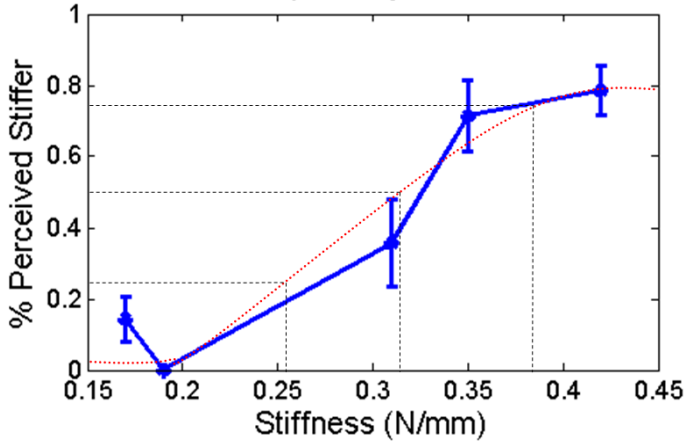


Figure 6.8 The averaged results for the actuated catheter system and the moving target with the difference thresholds indicated. The error bars are the standard error.

A method for evaluating the sensitivity of subjects to different stimuli is to determine for the lower and upper difference thresholds, the distance from the 50% stimulus value (the point of subjective equality) to the 25% and 75% stimulus values, respectively [79]. For the manual tool case, the continuous approximation of the subject data never reaches a discrimination accuracy of 25% or 75%. Thus, the upper and lower difference thresholds are both infinite (Figure 6.7). For the haptic interface results, a

lower difference threshold of 0.06 N/mm and an upper difference threshold of 0.07 N/mm were approximated from the results, as shown in Figure 6.8.

The statistical significance of the results was analyzed by performing a two-sample *t*-test on the results in Figure 6.7 and Figure 6.8 comparing the control-control probability for each interface with the probability of the other materials. For the manual catheter (Figure 6.7), the majority of the results with were not statistically significant (*p*-values < 0.05). The *p*-values from softest to hardest materials were 0.59, 1.00, 0.079, and 0.02. Only the stiffest material was distinct. The haptic interface results (Figure 6.8), on the other hand, produced almost all statistically significant *p*-values with the exception of the softest material: 0.13, 0.007, 0.03, and 0.005.

## 6.4. Discussion

This work confirms that haptic feedback and motion compensation improve a user's ability to distinguish material properties with a catheter tool. The results presented above show that the motion compensated catheter with a haptic interface enabled users to more accurately discriminate between different materials on a moving target than with a manual catheter. The upper and lower difference thresholds found for the haptic device were approximately 20% of the control material stiffness. No difference thresholds could be found for the manual catheter because the subjects were not accurate enough to achieve the 25% and 75% threshold values.

Another metric to evaluate the efficacy of the haptic system is to examine the average number of errors per user and the user confidence. Out of a total ten trials for each interface, the subjects average three incorrect selections with the manual catheter and 1.5 with the haptic catheter, a 50% improvement. Users were also more confident

with the haptic system. The average confidence value for the manual system was 50% while the average for the haptic system was 75%.

One interesting result from this study is that the users were not able to accurately distinguish the softer materials from the control material with the manual catheter as illustrated by Figure 6.7 and the high $p$-values ($p > 0.5$). One possible explanation for this trend is that the backlash and friction in the manual clinical catheter make it challenging to perceive the point of contact with the target material. Users were instructed to evaluate a material by first determining the point of initial tip contact and then exploring force-displacement relationship after that point. For the soft materials, it is unclear when the manual tool first makes contact because the initial reaction force transmitted down the length of the guidewire is overshadowed by the friction forces in the catheter. Only once significant compression of the target material has been achieved does the user to feel the reaction force from target. While this phenomenon is considerably decreased with the haptic interface, the results in Figure 6.8 do show that a small fraction of the participant had trouble sensing the contact with the softest material.

Another interesting trend is that the control-control comparison value is approximately 40% for both the manual and haptic experiments. This means that the users perceived the second interaction with the control material to be stiffer than the first interaction. One possible explanation is that the viscoelastic properties of the material altered its mechanical response after the first interaction. This trend can also be explained by user impatience and time errors introduced by pausing between each comparison. To prevent this type of biasing, the order of the comparisons was randomized to reduce time delays and material order from affecting the rest of the data.

The results presented here were shaped by the limitations of the catheter devices and interfaces used in the study. For example, the manual guidewire is able to more clearly transmit information about stiffer materials than softer materials because the friction and backlash in guidewire-sheath system cloud the tactile information created by the light contact forces. Hard materials, on the other hand, apply more substantial reaction forces with smaller deformations, which were easier for users to sense.

The haptic system experienced a different set of limitations. Users were able to perceive the light reaction forces applied by the softer materials due to the distal tip force sensing and lower friction haptic interface. However, stiffer materials were not always accurately perceived due to the compliance of the guidewire. When applying a force to the stiffer materials with the actuated catheter, the guidewire-sheath system slightly deformed and buckled under the compressive loads. This deformation appeared to the user as the deformation of the target material. The catheter and the target material act like two springs in series, thus giving the users the perception that the stiff materials are more compliant. Robotic manipulator compliance in haptic teleoperation tasks affects the user's ability to perceive the environment and is examined in detail in [90].

The catheter compliance effect is not as noticeable for materials that are much softer than the control material because the softer material compliance dominates in those cases. The compression compliance of the catheter system in this experiment is approximately 2 N/mm at 1 N of force. The compliance of the catheter, coupled with the haptic feedback noise caused by imperfect target tracking, reduced the discrimination accuracy for the stiffer materials to approximately 80% (Figure 6.8).

## 6.5. *In Vivo* Evaluation

The haptic system was also demonstrated *in vivo* during a porcine cardiac surgery. The robotic catheter with the force sensor end effector was inserted into the heart via the jugular vein and superior vena cava (SVC). Once inside the heart, the system was used to palpate the area around the tricuspid valve in the RA and the apex of the heart at the bottom of the RV. These experiments were conducted using 3DUS guidance but without motion compensation. See Section 7.2.3 for more details about the *in vivo* experiment procedure.

Figure 6.9 presents plots of the catheter tip force and haptic joystick input during two typical trials. These plots show that forces were generated at the tip of the catheter due to the motion of the haptic interface input. However, the forces experienced by the catheter were in general low in this experiment because of two factors. First, the heart tissue is soft and compliant. This is especially true in the right side of the heart where the pressure of the blood is in general lower than the left side of the heart. As a result of these tissue properties, small deformation of the tissue (<3 mm) did not result in forces above the threshold that is distinguishable from noise in the force sensor and the output of the haptic interface due to friction and other limitations in the systems.

The other factor that limited the forces experienced during the trials was the lack of sufficient bracing during the experiment. Advancing the catheter into contact with the tissue often resulted in the catheter tip slipping along the inner surface of the heart as opposed to deforming it and generating a reaction force. As a result, the user felt no haptic feedback as the tool tip was advanced, giving the impression of tissue with extremely low stiffness or the sensation that the tool was operating in free space.

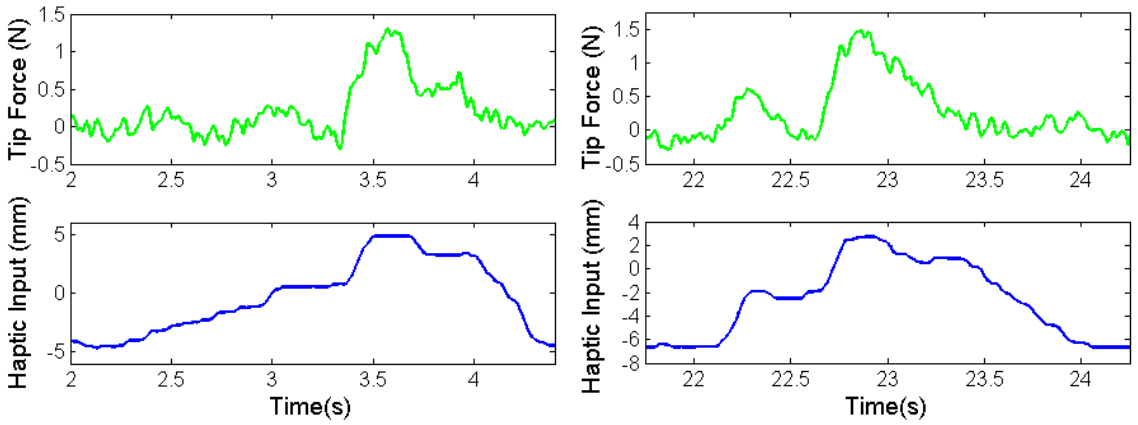


Figure 6.9 Typical forces recorded during the *in vivo* experiment as a function of the haptic interface joystick input position. Increasing the position of the haptic input results in an increase in the forces measured at the tip of the catheter.

These issues will be improved in future experiments by creating more sensitive force sensors, increasing the linear scaling gains for the haptic interface, and improving the catheter bracing to allow the catheter tip to apply greater forces against the cardiac tissue without sliding along the surface.

# Chapter 7

# Clinical Applications

This chapter presents clinical applications of the robotic catheter system. Motion compensated robotic catheters are a platform technology capable of delivering a range of therapeutics and devices to the moving tissue structures inside the heart. To further demonstrate the value of this system, two clinically relevant applications were selected: tissue resection and radio-frequency (RF) ablation. Both of these applications are surgical tasks routinely performed during cardiac interventions. The following sections describe the development of the application-specific catheter end effectors and the performance improvements provided by the robotic catheter system for these clinical applications.

## 7.1. Tissue Resection

Conventional cardiac catheters do not yet allow clinicians to interact with heart tissue with the same level of skill as in open-heart surgery. A primary reason for this limitation is that current catheters do not have the dexterity, speed, and force capabilities to perform complex tissue modifications on moving cardiac tissue. One such tissue

modification that is required to perform many procedures inside the heart, such as mitral valve repair, is tissue resection [91].

Robotic and actuated catheters are a potential solution to the limitations of conventional catheters. Current robotic cardiac catheters, such as the commercially available Artisan Control Catheter (Hansen Medical, Mountain View CA, USA) or CorPath Vascular Robotic System (Corindus Vascular Robotics, Natick MA, USA), allow for teleoperated guidance of a catheter tool inside the heart [10, 11]. These devices permit a human operator to control the positioning of a catheter *in vivo*. However, these actuated catheter technologies do not provide sufficient speeds to allow the catheters end effectors to keep up with the fast motion of intracardiac structures nor do they attempt to directly modify or resect the cardiac tissue [8, 18].

Advances have also been made in the area of tissue resection technology. Robot tissue resection is now possible in laparoscopic procedures with the daVinci surgical robotic system (Intuitive Surgical, Sunnyvale, CA, USA). This device allows for the laparoscopic resection of a large range of tissues and organs, including the prostate, lungs, and gastrointestinal system [92-94].

Tissue resection is also performed minimally invasively without the use of robotics. For example, the transurethral resection of the prostate (TURP) procedure utilizes a restroscope device, such as the Karl Storz Bipolar Restroscope System (Karl Storz Endoscopy-America Inc., El Segundo, CA, USA), to remove tissue from the prostate via the urethra using electrocautery [95]. Another example of minimally invasive tissue resection is atherectomy, a procedure where plaque or tissue is percutaneously removed from a large blood vessel using a catheter device such as the

SilverHawk Plaque Excision System (Foxhollow Technologies, Redwood City, CA USA) [96, 97]. Although these devices have demonstrated clinical efficacy for minimally invasively resecting tissue, none of the existing technologies are capable of safely resecting tissue from the fast-moving cardiac structures.

To enable resection of moving tissue inside the beating heart, a resection end effector for the motion compensating catheter system has been developed. To the best of the author's knowledge, the device presented here is the first tool that is able to apply low, controllable forces while resecting fast-moving cardiac tissue. The following sections describe the development of a resection end effector for the robotic catheter system and the evaluation of the device with a simulated cardiac tissue resection task. The results demonstrate that motion compensation enables the successful resection of tissue and reduces the forces applied by the device by almost 80%.

### *7.1.1.* Resection End Effector

To enable resection of moving tissue inside the beating heart, a resection end effector has been developed for the image-guided motion compensating catheter system described in this thesis. To the author's knowledge, the device presented here is the first tool that is able to apply low, controllable forces while resecting fast-moving cardiac tissue. The following section describes the design of the catheter resection end effector.

**Resection Tool Design**

The functional requirements of the resection tool are that it cleanly cuts tissue, applies minimal and controllable forces on the moving tissue, and can be accurately manipulated to perform resection procedures inside the intracardiac environment.

The tissue cutting approaches explored in the development of this device include a spinning cutting disk, a slicing approach that replicated the motion of a manual scalpel, and high-frequency electrosurgery approach similar to a Bovie surgical tool (Bovie Medical Corporation, Clearwater, Florida, USA). The cutting disk approach involved adding a fast spinning curricular disk blade to the tip of the catheter. Possible actuation approaches include a cable drive system, distal actuation via miniature motors, or hydraulic actuation using pressurized saline. The cutting disk approach was not selected because of the risk of entraining tissue in the spinning disk, size limitations placed on the cutting disk by the catheter sheath, and the challenge of transferring sufficient power to the tip of the catheter. The electrosurgery approach, while desirable in terms of precision and controllability, is not compatible with the intracardiac environment. The amount of heat and vapor produced by applying large amounts of current required to cut through tissue structures is not safe or feasible in the blood pool inside the heart.

As a result of this analysis and bench top prototypes of the possible approaches, the scalpel-based cutting method was selected. This approach has the benefits that it mimics standard cardiac surgery clinical practice, can be miniaturized to fit almost any size catheter, and the only actuation it requires is the positioning of the guidewire tip relative to the tissue.

The scalpel resection tool operates by slicing in the lateral direction perpendicular to the plane of the tissue surface. One possible method for generating the slicing motion is by buckling the guidewire via a pull wire, a wire running along the outside of the guidewire that can be tensioned to apply a bending moment to the tip of the guidewire.

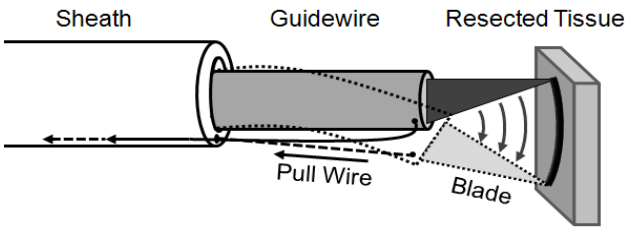


Figure 7.1 The tissue resection tool concept is actuated by a pull wire that buckles the guidewire, causing it to bend and slice through the tissue.

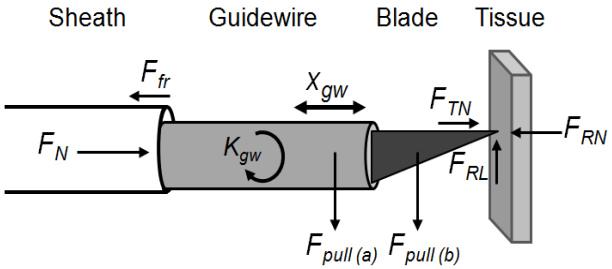


Figure 7.2 Model of the tissue resection device. The pulling force $F_{pull}$ provided by the pull wire can be applied to either (a) the guidewire or (b) the blade.

The diagram in Figure 7.1 illustrates this actuation strategy with the pull wire running through a channel along the length of the sheath.

**Resection Tool Analysis**

One challenge of the proposed device is that it requires applying a lateral force on a guidewire. Catheter guidewires are design to be rigid in compression but compliant in bending so that they can navigate the vessels to reach the heart. Figure 7.2 presents a diagram of the catheter resection process. The guidewire inside the sheath is pressed into the tissue with normal force $F_N$, resulting in a reaction force from the tissue $F_{RN}$. In order to cut the tissue, the blade must be forced downwards using a pull wire mechanism with force $F_{pull}$ applied either to the guidewire (a) or the blade (b). The location of the pull

wire force impacts the cutting efficacy of the device because the force may cause the guidewire to bend away from the tissue due to its low bending compliance, $K_{gw}$.

The resection catheter system can be modeled as a cantilever beam with two different material properties, as shown in Figure 7.3. The bending stiffness of the cutting blade is much greater than the stiffness of the guidewire in the direction of the applied force and can therefore be approximated as a rigid segment. Experimental investigation has shown that applying the pull force ($F_{pull}$) to the sheath ($l_a < 0$) or at any point between the sheath and the cutting blade tip ($0 < l_a < l_b$) causes the guidewire to buckle and the blade tip to tilt upwards, thus losing contact with the tissue. This is because a pull force not aligned with the tissue reaction force ($l_b$) causes a torque about the reaction force location, which in turn acts as a pivot relative to the tissue and causes the more compliant guidewire to tilt away from the cutting area. As a result of this behavior, the pull wire location should be as close to the cutting tip as possible ($l_a \rightarrow l_b$). Therefore, in this design the pull wire was located in the middle of the cutting blade to prevent tilting of the guidewire while still not interfering with the tissue-blade interaction.

**Prototype Design**

Based on this analysis, the design presented in Figure 7.4 was selected. A number 10 size surgical blade was attached to a 2.2 mm diameter guidewire. The guidewire was actuated in the axial direction via the drive system (Figure 3.1). Lateral direction actuation was provided by a steel pull wire attached to the center of the blade.

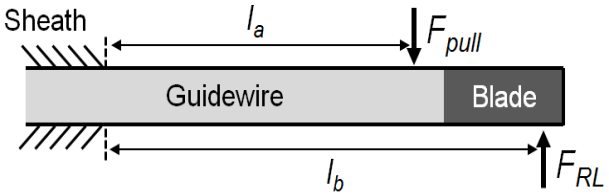


Figure 7.3 A simplified model of the resection tool mechanics

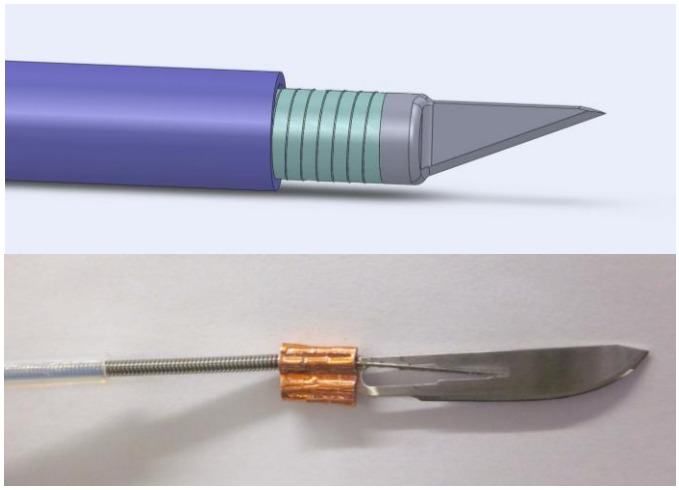

Figure 7.4 (Top) Solid model of the resection tool design and (bottom) the prototype.

In the case of this prototype, the pull wire was manually actuated, but in the clinical version the pull wire could either be manually actuated or actuated by a servo-controlled motor on the drive system module. To accommodate the motion compensation oscillations, the pull wire was passively actuated by the guidewire along the direction of fast servoing until it was laterally actuated to provide the resection motion. The bending and twisting mechanism described above in Section 3.1.4 were not integrated with this prototype. A retractable cover will also be required for the clinical version to prevent unintentional puncture of tissue while positioning the device.

### *7.1.2.* Evaluation Method

The efficacy of the resection device was evaluated with the task of resecting a piece of tissue on a moving target. In this experiment, a piece of bovine tissue was attached to a single DOF motion simulator that followed a human mitral valve annulus trajectory segmented from human ultrasound data [18]. The trajectory simulates the large motion of the human mitral valve moving at 60 beats per minute (Figure 6.4).

The evaluation task called for the user to control a joystick input to approach the moving tissue with the resection tool, apply a normal force to the tissue, and then manually actuate the pull wire to move the blade laterally and slice through the tissue. This task was carried out using the actuated catheter with and without motion compensation. To evaluate the normal forces applied by the catheter on the tissue, a force sensor was integrated into the motion simulator (LCFD-1KG, Omega Engineering, Stamford CT, range: 10 N, accuracy: 0.015 N). In this experiment, the target position was taken directly off a potentiometer on the motion simulator instead of the *in vivo* 3DUS image guidance system.

### *7.1.3.* Resection Results

The motion compensated resection tool successfully resected the tissue. Motion compensation allowed the cutting blade to track the trajectory of the tissue while the pull wire forced the scalpel blade through the tissue. The manual resection device, on the other hand, failed to completely or cleanly cut the tissue. Figure 7.5 illustrates how the two approaches cut the tissue. The manual, non-motion compensated tool was only able to stab and puncture the tissue because it did not track the motion of the tissue target.

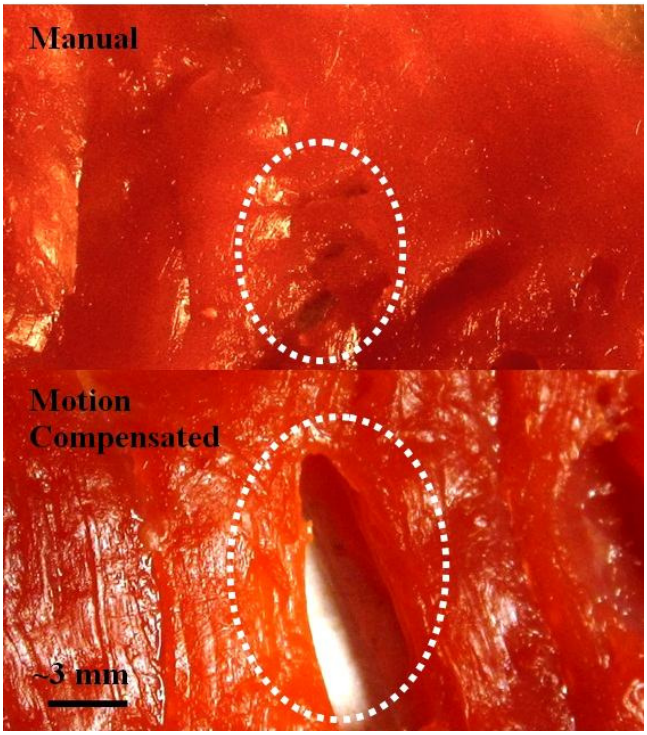


Figure 7.5 Tissue resection experiment results. (Top) The manual tool punctured the tissue a number of times but did not successfully cut the tissue. (Bottom) The motion compensated tool cleanly resected the tissue.

When the user advanced the blade towards the tissue, it collided repeatedly but was not able to slice the tissue. The motion compensated device was able to cleanly and evenly slice the tissue because the compensation allowed the blade to maintain a constant position relative to the tissue. Once the user advanced the blade to a sufficient cut depth, the pull wire was drawn and the blade cleanly cut through the tissue.

These results are reinforced by the normal force values applied to the tissue during the experiments. As shown in Figure 7.6, the resection tool without motion compensation applied considerably more force on the tissue than the motion compensated tool. Motion compensation reduced the RMS force value by 77% (0.77 N vs. 3.31 N) and the peak force values by almost 70% (1.82 N vs. 5.81 N).

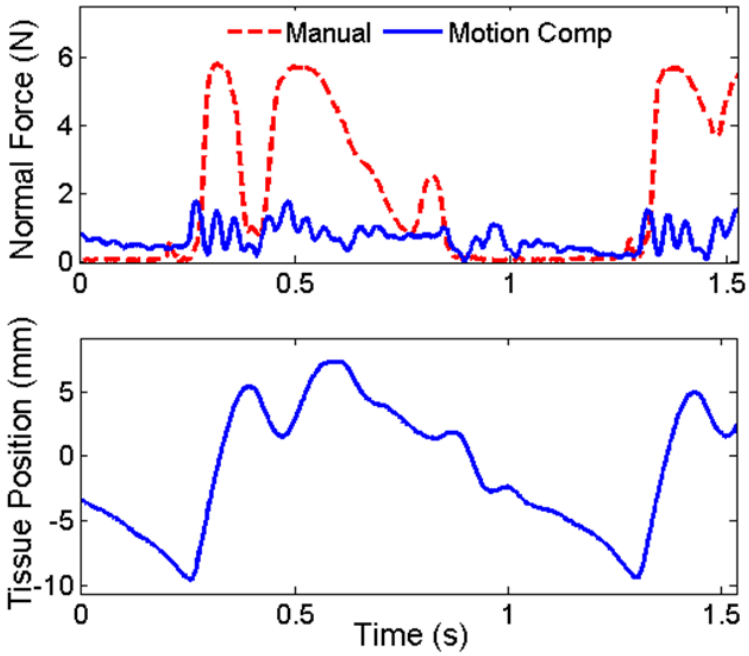


Figure 7.6 (Top) Normal forces applied to the tissue by the manual catheter and the motion compensated catheter. (Bottom) The cardiac motion simulator trajectory.

### *7.1.4.* Discussion

These results show that motion compensation enables safe and effective resection of fast-moving tissue structures inside the heart. Without the use of motion compensation, the resection blade was unable to make a clean, straight cut in the tissue and the end effector applied quadruple the force on the tissue. Previous work has demonstrated that the actuated catheter system is able to successfully track and compensate for the fast cardiac motion using 3DUS guidance [34].

This work demonstrates the possibility of resecting tissue inside the beating heart; however, a number of technological advances are required to make this device clinically feasibility. One of the biggest remaining challenges is how to provide the clinician with clear, real-time images of the cardiac structures with enough resolution to allow for

accurate repair procedures. In additional to better imaging, more tools will be required to perform complete surgeries. For example, end effectors to approximate and affix tissue will be required to perform annuloplasty procedures [91]. Finally, strategies for safely using these tools *in vivo* will need to be explored and perfected before clinical trials can proceed.

## 7.2. Cardiac Ablation

Ablation is used by interventional cardiologists and cardiac surgeons to destroy cardiac conduction pathways that contribute to arrhythmias, or irregular heart beat abnormalities [64]. Ablation damages the cardiac tissue by heating it up to a high enough temperature to kill the cells that make up the tissue. A common form of ablation technology is radio frequency (RF) ablation, where alternating current (AC) is applied directly to the tissue by an electrode at radio frequencies (approximately 500 kHz) [64]. The basic components of a RF ablation system are a power supply that generates the RF current, an ablation electrode that is connected to the RF generator via a wire, and a return electrode pad that completes the conduction path back to the RF generator. In order to perform a cardiac RF ablation, the return electrode is applied to the exterior of the body (often the back), and the ablation electrode is placed in contact with the tissue to be ablated. The system is the turned on for a period of time with a fixed power level until the tissue is sufficiently heated to stop the electrical conduction pathway.

### *7.2.1.* Ablation End Effector

A custom ablation electrode end effector was developed for the robotic catheter system. The goal of the ablation tool is to enable the catheter system to apply RF energy

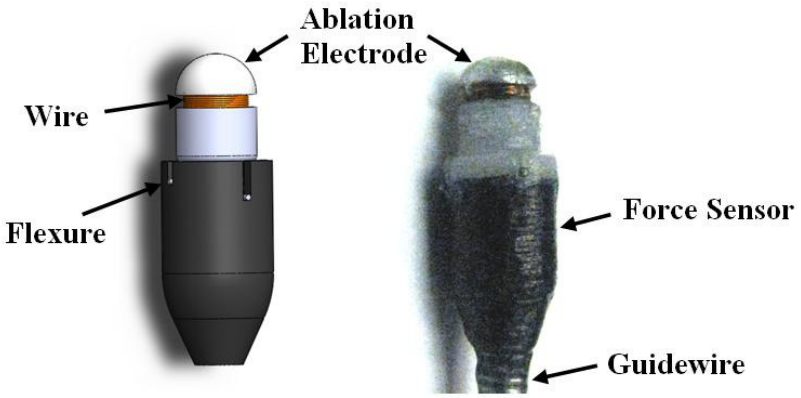


Figure 7.7 Ablation end effector solid model (left) and prototype (right).

to the fast-moving tissue inside the heart while apply a constant normal force. The functional requirements of the ablation end effector are to sense forces, to ablate tissue using a clinical RF generator with the same efficacy as conventional ablation catheters, and to be robust enough to operate in the intracardiac environment.

Figure 7.7 presents a solid model and image of the ablation sensor design. The device consists of a force sensor similar to the one described in Section 3.2, a stainless steel electrode, and a fine wire that runs down the length of the catheter to the RF generator. The ablation tool body is approximately 6 mm in diameter and approximately 15 mm in length. The force sensor achieves similar performance to the sensor presented above in Section 3.2 and the ablation electrode functions identically to commercial RF ablation catheters, such as the Medtronic RF Marinr MCXL (Medtronic, Minneapolis, Minnesota, USA). Figure 7.8 presents examples of the ablation lesions created with this tool on porcine tissue while operating with a RF generator (Stockert 70, Biosense Webster, Diamond Bar, California, USA). The ablation end effector is able to destroy the tissue using the same power and time settings as the clinically available Medtronic catheter.

Figure 7.8 Tissue sample ablated with the catheter force sensing RF ablation tool. The lesions are approximately 4 mm in diameter

The cardiac ablation end effector was evaluated both *ex vivo* in a water tank and *in vivo*. RF ablation is used to destroy pathological electrical conduction pathways in the cardiac walls and septa that cause arrhythmias [64]. These arrhythmia-inducing areas can occur in almost any part of the heart; therefore, a catheter ablation device must be able to maintain good ablation contact against all of the intracardiac surfaces [64][98].

### *7.2.2. Ex Vivo* Evaluation

The robotic ablation catheter was first evaluated in a water tank experiment to examine the ability of the system to maintain good ablation electrode contact against a surface while applying a constant force. A number of studies have demonstrated that cardiac ablation efficacy is directly related to the forces applied by the catheter tip and the quality of the electrode-tissue contact [84, 98-100]. Manually operated catheters do not adequately ablate tissue if they are bouncing or sliding on the tissue surface, in poor contact due to low forces, or creating tissue perforations due to large contact forces [99, 100]. The objective of this *ex vivo* evaluation was to demonstrate that the robotic catheter

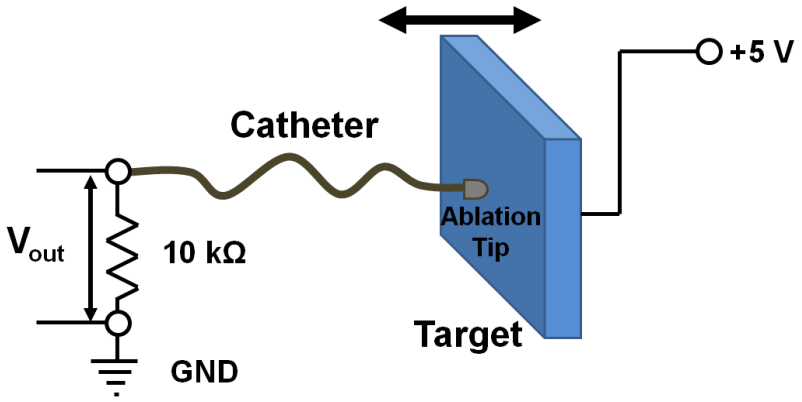


Figure 7.9 The *ex vivo* ablation catheter experimental setup. The moving target was connected to a 5 V DC signal and the catheters were instrumented with a voltage divider to measure the ablation resistance. Resistance measurements were used to evaluate tip contact quality for both a manual catheter and the robotic catheter system.

system can improve ablation quality by maintaining good contact while applying a constant force.

**Method**

The system was evaluated by commanding the catheter to maintain a constant contact force against a moving target. The target was composed of a conductive pad used as the current return path electrode in clinical ablation procedures (REM Polyhesive II Patient Return Electrode, Tyco Healthcare, Gosport, UK) backed with compliant foam (thickness: 25 mm, approximate stiffness: 0.1 N/mm). The target translated along a 12 mm amplitude sinusoidal trajectory at a frequency of approximately 1 Hz (60 BPM).

For a given power setting the ablation current, and therefore the efficacy of tissue destruction, is determined by the impendence between the electrode and the tissue surface. Cardiac ablation systems operate in the radio frequency range, approximately 500 kHz [64]. It is impractical to directly measure the ablation current impendence at

this operating frequency; therefore, the DC resistance values were measured instead. To measure the resistance, 5 V DC was applied to the patient return electrode and a voltage divider was created at the proximal end of the catheters to measure the ablation resistance (Figure 7.9). As the contact between the catheter and the target changed due to variations of the contact force or tip position, the resistance between the catheter electrode and the return electrode pad also changed. This resistance, $R_{abl}$, can be calculated from the resulting output of the voltage divider, $V_{out}$:

$$R_{abl} = \frac{5V}{V_{out}} \times 10k\Omega - 10k\Omega \tag{5.1}$$

$$= \left( \frac{5V}{V_{out}} - 1 \right) \times 10k\Omega$$

The evaluation experiment was conducted on the sinusoidal moving target using both the robotic catheter and a commercial manual ablation catheter (RF Marinr MCXL, Medtronic, Minneapolis, Minnesota, USA). For the manual catheter, a load cell was also added to the target to record the forces applied by the catheter tip (Omega Engineering LCFD-1KG, Stamford, CT, USA). The robotic catheter ablation tip contains a force sensor, as described above. The robotic system was operated under force control with 3DUS guidance, described in detail in Chapter 5. Both catheters were rigidly braced 100 mm from the ablation tip at orientations perpendicular to the plane of the moving target. The manual catheter was positioned so its ablation electrode was able to remain in contact for the entire target trajectory (Figure 7.10). While this experimental setup allows for a fair comparison of the manual and robotic catheter systems, it does not accurately approximate the exact mechanics of intracardiac ablation, including the

**Manual Catheter** **Robotic Catheter**

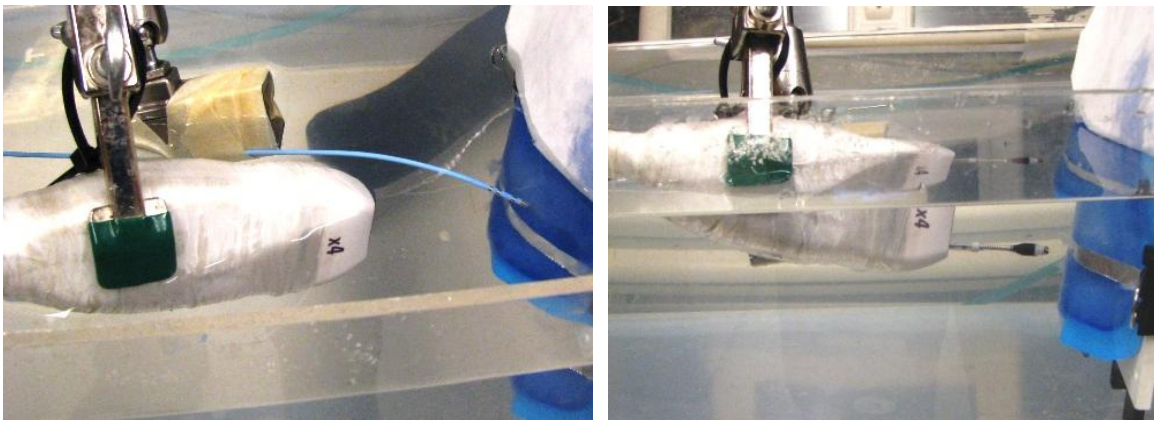

Figure 7.10 The ablation experiment water tank setup for the manual catheter system (left) and the robotic catheter system (right). Both images show the catheters, the white 3DUS imaging probe, and the blue motion target.

compliance of the vessels in the heart and the tool orientation relative to the moving tissue structures.

**Results**

Figure 7.11 presents the results of the experiment. The manual catheter was not able to apply a constant force or maintain a constant resistance. The reason for this poor performance was because the motion of the target caused the ablation tip to slide and tilt relative to the target surface as the motion simulator pushed on the manual catheter and caused it to buckle. Catheter compliance is a desirable feature in manual catheters because it prevents them from applying large forces and perforating cardiac tissue. However, this bending compliance makes it challenging to achieve reliable ablation

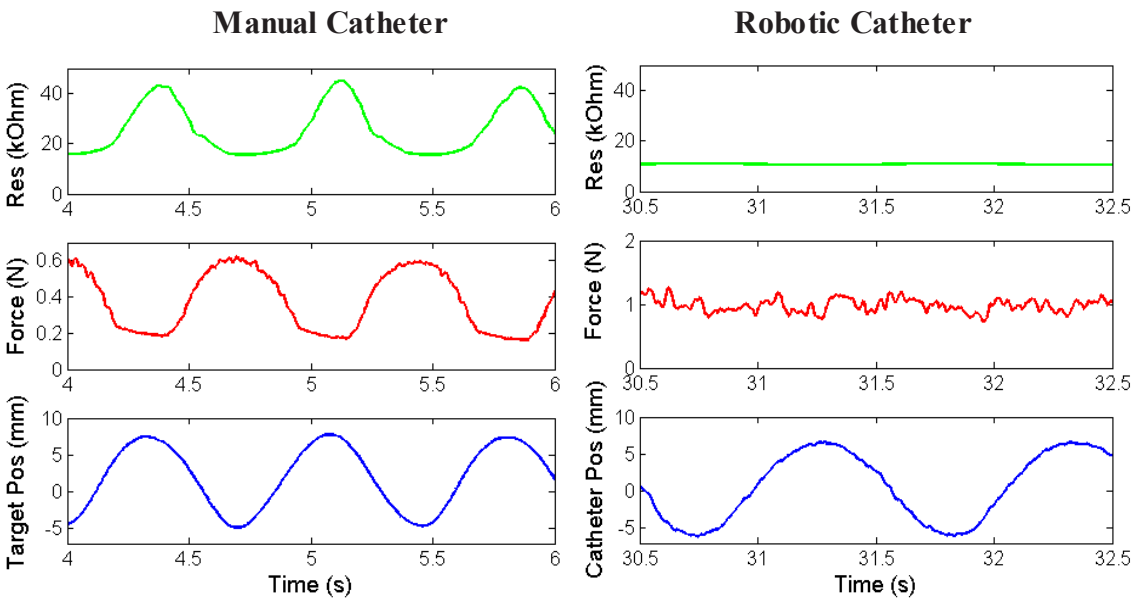


Figure 7.11 A comparison of the electrical resistance and interaction forces between a conductive target and a manual catheter (left) and the robotic catheter system (right). The manual catheter applies a force and resistance that vary with the motion of the target. In contrast, the robotic catheter achieves consistent electrical contact with the moving target while applying a constant force.

performance. As shown in Figure 7.11, the manual catheter generated peak-to-peak resistance values of over 20 kOhm and peak-to-peak force values of 0.4 N.

The robotic catheter, in contrast to the manual catheter, achieved almost constant resistance values while maintaining a desired force of 1 N with a force tracking error of 0.11 N RMS. The RMS variation of the resistance value was 0.25 kOhms, 97% less than the RMS variation of 9.88 kOhm for the manual catheter system. The robotic catheter was able to achieve this level of performance because the 3DUS-guided motion compensation system and the force control algorithm enabled the ablation tip to maintain consistent contact with the target despite the fast motion.

### *7.2.3. In Vivo* Evaluation

In addition to the *ex vivo* evaluations, the robotic ablation system was also tested *in vivo*. The system was examined as part of a porcine animal surgery. To introduce the catheter into the heart, a surgical cutdown was performed on the jugular vein of a 75 Kg pig. An introducer sheath (Large Check-Flo Introducer, 18 French, Cook Medical Inc., Bloomington, Indiana, USA) was first inserted into the jugular vein and guided through the superior vena cava (SVC) into the RA. After being flushed with saline to prevent any air bubbles from being introduced into the heart, the robotic catheter system was inserted into the RA via the introducer sheath. Under 3DUS guidance, the catheter was positioned at the apex of the RV by manually adjusting the catheter insertion depth through the introducer sheath and bending the catheter sheath using the bending mechanism described in Section 3.1.4. Final positioning of the ablation end effector was achieved during the experiment using the joystick user interface.

The ablation end effector and catheter system was able to apply RF energy with similar values to what is experienced during clinical RF ablation procedures [64]. The ablation energy was provided by the RF generator (Stockert 70, Biosense Webster, Diamond Bar, California, USA). Further experiments will be conducted to evaluate the *in vivo* efficacy of the ablation end effector and to compare the robotic catheter system to the performance of manual ablation catheters.

### *7.2.4.* Discussion

The results presented above demonstrate that the robotic catheter system is able to successfully ablate tissue. The system was able to apply a constant force while

maintaining a constant ablation resistance with the ablation end effector on a moving target. It should also be noted that this experiment was conducted under 3DUS motion tracking and guidance. The *in vivo* results show that the ablation system is capable of applying RF energy to the inside of the heart with impedance and power values similar to clinical ablation catheter systems. These results also confirm that the catheter system is compatible with standard cardiac catheter approaches and techniques.

The *ex vivo* results in Section 7.2.2 show that the robotic ablation catheter system offers a number of advantages over current manual catheters, including the ability to apply a constant force while maintaining consistent ablation contact. However, there are a number of limitations in this initial validation study due to the challenges of accurately simulating *in vivo* cardiac ablation in a laboratory setting. First, measuring the DC resistance of the contact does not consider the electrical frequency response of the cardiac tissue at the 500 kHz frequency used by the RF energy generator. In addition, the system was tested in water instead of electrically-conductive blood or saline, which alters the electrode conduction properties. Finally, the experimental setup did not simulate a realistic catheter *in vivo* configuration and the mechanics of the vascular approach and cardiac tissue. These limitations will be corrected in future research.

The preliminary *in vivo* results demonstrate that the ablation end effector is capable of ablating tissue in certain situations without the assistance of force control or motion compensation. This static catheter approach was successful despite the lack of robotic actuation because the compliant heart wall deformed around the ablation tip during the procedure. This tissue deformation resulted in large and potentially damaging forces because the significant axial stiffness of the actuated guidewire prevented the

catheter from deflecting during tissue contact. While no force values were recorded during the ablation procedure, it was clear from visual inspection that the inner wall of the heart was abraded and bruised because of the catheter tip-tool interaction forces. Force control and motion compensation will allow catheter systems to maintain good ablation contact while regulating the applied forces at a safe level to prevent any additional tissue damage.

While these initial *in vivo* results demonstrate the feasibility of the robotic ablation approach, further work is required to find the optimal ablation settings and evaluate the quality of the ablation therapy. In future experiments, the duration and amount of energy applied during each ablation application will be experimentally evaluated to determine the most affective settings to modify the cardiac tissue. To find these values, cardiac electrophysiologists who specialize in ablation will be consulted and cadaver studies will be conducted to select appropriate ablation settings and experimental evaluation techniques.

# Chapter 8

# Conclusions

This thesis presents the design and evaluation of robotic catheters for beating heart surgery. First, the intracardiac environmental conditions were examined to understand the forces, displacements, and tissue stiffness values experienced by an intracardiac device while interacting with the fast-moving structures inside the heart (Chapter 2). These results and insights were used to develop the mechanical design of the system, including end effectors and intracardiac bracing strategies (Chapter 3). The robotic catheter system was analyzed to determine how best to control the tip position of the catheter (Chapter 4) and to regulate the forces the catheter tip applies to the moving tissue structures (Chapter 5). These control strategies were investigated on the bench, in a water tank simulator, and *in vivo*. Finally, clinically relevant applications of the system were examined. These applications included a haptic study of users' perception of the stiffness of moving tissue (Chapter 6) and two clinical procedures: tissue resection and RF ablation (Chapter 7). This work provides a solid foundation for the development of robotic catheters and the design of 3DUS-guided and motion compensating tools to improve cardiac repair.

The contribution of this work is the elucidation of the benefits and challenges of performing surgery on the beating heart with a robotic catheter. Specific contributions include:

- Establishing the forces involved in beating heart surgery
- Mechanical design of catheter-based surgical systems
- Position and force control of motion compensated catheters
- Exploration of clinical applications of the system, including haptics and ablation

## 8.1. Design and Control Insights

This work has produced a number of conclusions and insights regarding the challenges of implementing beating heart surgery using a robotic catheter system.

**Bracing**

Catheter bracing is required inside the heart to allow the catheter system to apply substantial forces without deflecting away from the tissue surface. Bracing strategies can be as simple as a rigid sheath or as complicated as a deployable structure that expands to fill the atrium, as shown in Figure 3.10. The bracing approach used in the *in vivo* experiments presented here was to support the catheter via a larger introducer sheath inserted into the heart. This approach is not optimal, as the introducer sheath is only as stable and static as the vessels and tissue structures around the heart that it is inserted through. However, the introducer sheath does provide some support against the contractile forces inside the heart. The data presented in Chapter 2 shows that a catheter tool will experience significant displacements and forces while interacting with the major

heart valves. Therefore, bracing will be required not only to allow the catheter to apply forces, but also to remain in a stable position relative to the moving tissue structures.

**Catheter Performance Limitations: Friction and Backlash**

The main challenges to accurate catheter tip position and force control are the performance limitations of friction and backlash. These effects are investigated in detail in Chapter 4. Because of the control method's dependence on a feedforward model of the catheter tip position, the accuracy of the catheter tip desired trajectory tracking will always be limited by the accuracy of the catheter transmission system model. The control method presented here assumes a static model; however, in reality a model that constantly updates the backlash and friction properties based on the catheter configuration and external conditions would be more accurate. For the experimental evaluation presented here a static friction and backlash model was sufficient because catheter configuration and environment were not rapidly changing as is sometimes the case inside the heart, especially while repositioning tissues or applying large forces.

**Real-Time Tip Position Sensing**

The feedforward control approaches utilized in this work, including the inverse and model-based deadzone compensation presented in Chapter 4, have their limitations. It is not always possible to assume that a model of a mechanical transmission system will predict the output for a given input. A better approach to accurately controlling the catheter tip position would be to provide real-time position sensing for the catheter tip. This would allow for closed-loop control based on position feedback from the distal tip of

the catheter and not the proximal end at the actuator drive system. Tip position sensing would allow for a more traditional adaptive controller scheme to be used that could adapt to the variations in the catheter system performance. Real-time tip position tracking is infeasible at this time, however, due to technical limitations including latencies and limited resolution of potential tracking technologies like 3DUS imaging and EM trackers.

**Haptic Feedback**

Simple haptic feedback has limited value for catheter procedure guidance. The catheter force sensor used in this work only provides single DOF force information and thus can only measure forces applied to the catheter tip along the length of the tool. Lateral forces are not sensed at present. As a result, many of the forces involved in surgical procedures, such as cutting, approximating, and affixing tissue, cannot be perceived by the user. One area where haptic feedback might be useful is for augmenting the poor quality of some 3DUS imaging. The haptic interface could inform the clinician when the tool first makes contact with the tissue and thus prevent the clinician from accidentally puncturing the tissue or applying unwanted forces.

**Clinical Applications**

The robotic catheter system has the capacity to deliver a number of procedure-specific end effectors. The eventual goal of the system is to use multiple, coordinated robotic catheters to complete more complex surgical tasks, such as closing heart defects and repairing damaged valve leaflets and chordae. This level of performance, however, will require significant improvements in imaging and robot control. In the meanwhile,

the robotic catheter system can make the greatest contribution by improving the success of currently conducted procedures, such as ablating moving cardiac structures (Section 7.2) and deploying percutaneous implants. For example, the deployment of the MitralClip mitral valve repair system (Abbott Laboratories, Abbott Park, Illinois, USA), which requires grabbing the moving mitral valve leaflets, could be made easier if it used the 3DUS-guided motion compensation system employed in this research.

## 8.2. Future Work

A number of improvements can be made to the robotic catheter system in the areas of mechanical design and control. The system can also be applied to new medical applications, including neurosurgery and peripheral vascular disease.

**Mechanical Design**

The areas where the mechanical design of the current robotic catheter system could be improved include the limited DOF of the actuation system, the lack of sophisticated intracardiac bracing, and new end effectors for more complex surgical procedures.

Additional fast-servoed degrees of freedom would allow the catheter to track cardiac tissue with complex three dimensional trajectories. This would expand the range of tissue structures that can be treated with the robotic catheter system to almost any part of the intracardiac surface. Increasing the actuated DOF could be accomplished by adding rotational and linear servo motors to the bending and twisting mechanism in Figure 3.3.

As described in detail in Section 3.3, bracing inside the heart is essential for accurately applying forces and interacting with the moving tissue structures. Possible bracing technologies include variable stiffness sheaths, inserting stiffening wires through the sheath into the vessels connected to the heart, or deploying actively stabilizing structures inside the heart chambers. All of these options need to be explored further and evaluated *in vivo*.

Finally, more sophisticated end effectors must be developed to realize the goal of completing complicated surgeries on the beating heart solely with robotic catheters. Potential new end effectors including stapling devices, suturing tools, and tissue grasping and manipulating tools would allow for major structural repairs and modifications of the cardiac tissue. The main challenge of developing these tools is miniaturizing existing technologies and integrating them with the catheter system. Possible manufacturing technologies include metal microelectromechanical systems (MEMS) [101] and smart composite microstructure (SCM) manufacturing [102].

**Control**

The current limitations of the robotic catheter control system are accurate position control of the catheter tip and the 3DUS image servoing system. As described above in Section 8.1, the model-based feedforward position control of the catheter tip is not able to adapt to changes in the environment or catheter configuration. This shortcoming could be overcome with accurate tip position measurements.

An ideal method to measure the catheter tip position is the 3DUS system; however, the current ultrasound systems are limited by low resolution, noise, and

substantial latencies [24, 29]. Improved imaging would not only improve catheter control, but also would allow for more complex tissue motions to be tracked. For example, an arbitrary point on the ventricle wall could be tracked for RF ablation therapy. This is an ongoing area of research that requires innovations to improve both the 3DUS technology and the computer vision algorithms to enable tracking of less distinct objects and features in the ultrasound images.

**New Applications**

In addition to the clinical applications described in this thesis, the robotic catheter system could be adapted for a number of medical procedures and therapies. In the area of cardiac surgery, the system could be used to deploy prosthetic valves, suture annuloplasty rings to improve valve function, and repair or reattach chordae and other parts of the subvalvular apparatus. Beyond the heart, the catheter system could also be used to treat peripheral vascular disease in other parts of the body. For example, the catheter system could be used to reconstruct occluded vessels or reposition stents in the appendages. The system would use 3DUS guidance to track vascular structures and force control to regulate tool-tissue interactions and perform effective surgical repairs.

In addition to vascular and cardiac applications, the robotic catheter system could also be used to perform minimally invasive surgery on the brain. The catheter could be introduced into the cranium through a small hole in the skull and navigated around the brain lobes into the folds and other open areas inside the skull. These procedures could benefit from 3DUS guidance, motion compensation to respond to the motions of the brain physiology, and force control to guarantee safety. The same end effectors designed to

perform surgery inside the heart could be repurposed to remove brain tumors and repair damaged vessels. Haptic feedback could also be integrated to allow clinicians to more accurately interact with organs and tissue structures.

All of these applications will be explored in future work to identify medical challenges where the robotic catheter system could make the greatest impact and provide the greatest improvements to patient care.

# References

[1] H. C. Kung, D. L. Hoyert, Xu J. and S. L. Murphy, "Deaths: final data for 2005," *National Vital Statistics Reports,* vol. 56, 2008.

[2] J. M. Murkin, W. D. Boyd, S. Ganapathy, S. J. Adams and R. C. Peterson, "Beating heart surgery: why expect less central nervous system morbidity?" *The Annals of Thoracic Surgery,* vol. 68, pp. 1498-1501, 10, 1999.

[3] G. W. Roach, M. Kanchuger, C. M. Mangano, M. Newman, N. Nussmeier, R. Wolman, A. Aggarwal, K. Marschall, S. H. Graham and C. Ley, "Adverse cerebral outcomes after coronary bypass surgery," *N. Engl. J. Med.,* vol. 335, pp. 1857-1864, 1996.

[4] M. J. Mack, "Pro: beating-heart surgery for coronary revascularization: is it the most important development since the introduction of the heart-lung machine?" *Ann. Thorac. Surg.,* vol. 70, pp. 1774, 2000.

[5] R. Ascione, C. T. Lloyd, M. J. Underwood, A. A. Lotto, A. A. Pitsis and G. D. Angelini, "Economic outcome of off-pump coronary artery bypass surgery: a prospective randomized study," *Ann. Thorac. Surg.,* vol. 68, pp. 2237-2242, 1999.

[6] B. Gersak and Z. Sutlic, "Aortic and mitral valve surgery on the beating heart is lowering cardiopulmonary bypass and aortic cross clamp time," in *Heart Surg Forum,* 2002, pp. 182-186.

[7] D. S. Baim, Ed., *Grossman's Cardiac Catheterization, Angiography, and Intervention*. Philadelphia, PA: Lippincott Williams & Wilkins, 2005.

[8] S. G. Yuen, S. B. Kesner, N. V. Vasilyev, P. J. del Nido and R. D. Howe, "3D ultrasound-guided motion compensation system for beating heart mitral valve repair," in *Medical Image Computing and Computer-Assisted Intervention,* 2008.

[9] S. B. Kesner, S. Yuen and R. Howe, "Ultrasound servoing of catheters for beating heart valve repair," *Information Processing in Computer-Assisted Interventions,* pp. 168-178, 2010.

[10] D. B. Camarillo, C. F. Milne, C. R. Carlson, M. R. Zinn and J. K. Salisbury, "Mechanics Modeling of Tendon-Driven Continuum Manipulators," *Robotics, IEEE Transactions on,* vol. 24, pp. 1262-1273, 2008.

[11] R. Beyar, "Navigation within the heart and vessels in clinical practice," *Ann. N. Y. Acad. Sci.,* vol. 1188, pp. 207-213, 2010.

[12] B. Knight, G. M. Ayers and T. J. Cohen, "Robotic positioning of standard electrophysiology catheters: A novel approach to catheter robotics," *J. Invasive Cardiol.,* vol. 20, pp. 250-253, 2008.

[13] J. Jayender, M. Azizian and R. V. Patel, "Autonomous Image-Guided Robot-Assisted Active Catheter Insertion," *Robotics, IEEE Transactions on,* vol. 24, pp. 858-871, 2008.

[14] J. Jayender, M. Azizian and R. V. Patel, "Bilateral telemanipulation of a flexible catheter in a constrained environment," in *Robotics and Automation, 2008. ICRA 2008. IEEE International Conference on,* 2008, pp. 649-654.

[15] T. Fukuda, S. Guo, K. Kosuge, F. Arai, M. Negoro and K. Nakabayashi, "Micro active catheter system with multi degrees of freedom," in *Robotics and Automation, 1994. Proceedings., 1994 IEEE International Conference on,* 1994, pp. 2290-2295 vol.3.

[16] S. Guo, T. Fukuda, K. Kosuge, F. Arai, K. Oguro and M. Negoro, "Micro catheter system with active guide wire," in *Robotics and Automation, 1995. Proceedings., 1995 IEEE International Conference on,* 1995, pp. 79-84 vol.1.

[17] P. Kanagaratnam, M. Koa-Wing, D. T. Wallace, A. S. Goldenberg, N. S. Peters and D. W. Davies, "Experience of robotic catheter ablation in humans using a novel remotely steerable catheter sheath," *Journal of Interventional Cardiac Electrophysiology,* vol. 21, pp. 19-26, 2008.

[18] D. T. Kettler, R. D. Plowes, P. M. Novotny, N. V. Vasilyev, P. J. del Nido and R. D. Howe, "An active motion compensation instrument for beating heart mitral valve surgery," in *Intelligent Robots and Systems, 2007. IROS 2007. IEEE/RSJ International Conference on,* 2007, pp. 1290-1295.

[19] O. Bebek and M. Cavusoglu, "Intelligent control algorithms for robotic assisted beating heart surgery," *IEEE Trans. on Robotics,* vol. 23, pp. 468–480, 2007.

[20] R. Ginhoux, J. Gangloff, M. de Mathelin, L. Soler, M. M. A. Sanchez and J. Marescaux, "Active filtering of physiological motion in robotized surgery using predictive control," *Robotics, IEEE Transactions on,* vol. 21, pp. 67-79, 2005.

[21] Y. Nakamura, K. Kishi and H. Kawakami, "Heartbeat synchronization for robotic cardiac surgery," in *IEEE International Conference on Robotics and Automation,* 2001, pp. 2014–2019.

[22] S. G. Yuen, D. T. Kettler, P. M. Novotny, R. D. Plowes and R. D. Howe, "Robotic motion compensation for beating heart intracardiac surgery," *The International Journal of Robotics Research,* vol. 28, pp. 1355, 2009.

[23] S. G. Yuen, P. M. Novotny and R. D. Howe, "Quasiperiodic predictive filtering for robot-assisted beating heart surgery," in *Robotics and Automation, 2008. ICRA 2008. IEEE International Conference on,* 2008, pp. 3875-3880.

[24] P. M. Novotny, J. A. Stoll, P. E. Dupont and R. D. Howe, "Real-time visual servoing of a robot using three-dimensional ultrasound," in *Robotics and Automation, 2007 IEEE International Conference on,* 2007, pp. 2655-2660.

[25] S. G. Yuen, N. V. Vasilyev, P. J. del Nido and R. D. Howe, "Robotic tissue tracking for beating heart mitral valve surgery," *Med. Image Anal.,* 2010.

[26] M. F. Newman, J. L. Kirchner, B. Phillips-Bute, V. Gaver, H. Grocott, R. H. Jones, D. B. Mark, J. G. Reves and J. A. Blumenthal, "Longitudinal assessment of neurocognitive function after coronary-artery bypass surgery," *N. Engl. J. Med.,* vol. 344, pp. 395-402, 2001.

[27] S. G. Yuen, D. P. Perrin, N. V. Vasilyev, P. J. del Nido and R. D. Howe, "Force tracking with feed-forward motion estimation for beating heart surgery," *Robotics, IEEE Transactions on,* vol. 26, pp. 888-896, 2010.

[28] P. M. Novotny, J. A. Stoll, N. V. Vasilyev, P. J. Del Nido, P. E. Dupont, T. E. Zickler and R. D. Howe, "GPU based real-time instrument tracking with three-dimensional ultrasound," *Med. Image Anal.,* vol. 11, pp. 458-464, 2007.

[29] P. Novotny, J. Cannon and R. Howe, "Tool localization in 3D ultrasound images," *Medical Image Computing and Computer-Assisted Intervention-MICCAI 2003,* pp. 969-970, 2003.

[30] W. H. Lewis, "Gray's anatomy of the human body," *Lea & Febiger,* 1936.

[31] L. H. Cohn, *Cardiac Surgery in the Adult.* New York, NY: McGraw-Hill Medical Publishing, 2008.

[32] P. T. L. Chiam and C. E. Ruiz, "Percutaneous transcatheter mitral valve repair: a classification of the technology," *JACC Interventions,* vol. 4, pp. 1, 2011.

[33] J. Zeitlhofer, S. Asenbaum, C. Spiss, A. Wimmer, N. Mayr, E. Wolner and L. Deecke, "Central nervous system function after cardiopulmonary bypass," *European Heart Journal,* vol. 14, pp. 885, 1993.

[34] S. B. Kesner and R. D. Howe, "Position Control of Motion Compensation Cardiac Catheters," *Robotics, IEEE Transactions on,* pp. 1-11, 2011.

[35] T. A. Timek, S. L. Nielsen, D. T. Lai, D. Liang, G. T. Daughters, N. B. Ingels Jr and D. C. Miller, "Effect of chronotropy and inotropy on stitch tension in the edge-to-edge mitral repair," *Circulation,* vol. 116, pp. I276-81, Sep 11, 2007.

[36] S. L. Nielsen, D. D. Soerensen, P. Libergren, A. P. Yoganathan and H. Nygaard, "Miniature C-shaped transducers for chordae tendineae force measurements," *Annals of Biomedical Engineering,* vol. 32, pp. 1050-1057, 08/01, 2004.

[37] M. O. Jensen, H. Jensen, M. Smerup, R. A. Levine, A. P. Yoganathan, H. Nygaard, J. M. Hasenkam and S. L. Nielsen, "Saddle-shaped mitral valve annuloplasty rings experience lower forces compared with flat rings," *Circulation,* vol. 118, pp. S250-5, Sep 30, 2008.

[38] A. Carpentier, D. H. Adams and F. Filsoufi, *Carpentier's Reconstructive Valve Surgery.* Maryland Heights, MI: Saunders Elsevier, 2010.

[39] S. J. Crick, M. N. Sheppard, S. Y. Ho, L. Gebstein and R. H. Anderson, "Anatomy of the pig heart: comparisons with normal human cardiac structure," *J. Anat.,* vol. 193 (Pt 1), pp. 105-119, Jul, 1998.

[40] P. Hunter, A. McCulloch and H. Ter Keurs, "Modeling the mechanical properties of cardiac muscle," *Prog. Biophys. Mol. Biol.,* vol. 69, pp. 289-331, 1998.

[41] Y. Fung, *Biomechanics: Mechanical Properties of Living Tissues.* New York, NY: Springer, 1993.

[42] S. B. Kesner and R. D. Howe, "Force control of flexible catheter robots for beating heart surgery," in *Robotics and Automation (ICRA), 2011 IEEE International Conference on,* 2011, pp. 1589-1594.

[43] C. R. Wagner, D. P. Perrin, R. D. Howe, N. Vasilyev and P. J. Del Nido, "Force feedback in a three-dimensional ultrasound-guided surgical task," in *Haptic Interfaces for Virtual Environment and Teleoperator Systems, 2006 14th Symposium on,* 2006, pp. 43-48.

[44] E. Wilson, Z. Yaniv, D. Lindisch and K. Cleary, "A Buyer's guide to electromagnetic tracking systems for clinical applications," in *Proceedings of SPIE on Medical Imaging: Visualization, Image-Guided Procedures, and Modeling,* 2008, pp. 69182B-1.

[45] J. G. Webster, *Tactile Sensors for Robotics and Medicine.* New York: John Wiley & Sons, Inc., 1988.

[46] E. Sachs, M. Cima, P. Williams, D. Brancazio and J. Cornie, "Three-dimensional printing: rapid tooling and prototypes directly from a CAD model," *Journal of Engineering for Industry(Transactions of the ASME)(USA),* vol. 114, pp. 481-488, 1992.

[47] P. Polygerinos, A. Ataollahi, T. Schaeffter, R. Razavi, L. D. Seneviratne and K. Althoefer, "MRI-compatible intensity-modulated force sensor for cardiac catheterization procedures," *Biomedical Engineering, IEEE Transactions on,* vol. 58, pp. 721-726, 2011.

[48] P. Polygerinos, D. Zbyszewski, T. Schaeffter, R. Razavi, L. D. Seneviratne and K. Althoefer, "MRI-compatible fiber-optic force sensors for catheterization procedures," *Sensors Journal, IEEE,* vol. 10, pp. 1598-1608, 2010.

[49] U. X. Tan, B. Yang, R. Gullapalli and J. P. Desai, "Design and development of a 3-axis MRI-compatible force sensor," in *Robotics and Automation (ICRA), 2010 IEEE International Conference on,* 2010, pp. 2586-2591.

[50] T. Duerig, A. Pelton and D. Stöckel, "An overview of nitinol medical applications," *Materials Science and Engineering: A,* vol. 273, pp. 149-160, 1999.

[51] V. M. Measurements Group, *Strain Gage Based Transducers: Their Design and Construction*. Loveland, CO: Group Publishing, 1988.

[52] F. T. S. Yu and S. Yin, *Fiber Optic Sensors*. New York, NY: Marcel Dekker, 2002.

[53] M. C. Yip, S. G. Yuen and R. D. Howe, "A robust uniaxial force sensor for minimally invasive surgery," *Biomedical Engineering, IEEE Transactions on,* vol. 57, pp. 1008-1011, 2010.

[54] P. J. Kyberd and P. H. Chappell, "A force sensor for automatic manipulation based on the Hall effect," *Measurement Science and Technology,* vol. 4, pp. 281, 1993.

[55] A. M. Dollar and R. D. Howe, "A robust compliant grasper via shape deposition manufacturing," *Mechatronics, IEEE/ASME Transactions on,* vol. 11, pp. 154-161, 2006.

[56] Objet Geometries Ltd., "FullCure870 VeroBlack Data Sheet," vol. 2010, 2010.

[57] W. J. Book, S. Le and V. Sangveraphunsiri, "Bracing strategy for robot operation," in *Proceedings of RoManSy '84: The Fifth CISM-IFToMM Symposium,* Udine, Italy, 1984, .

[58] H. West, "Kinematic Analysis for the Design and Control of Braced Manipulators," 1986.

[59] J. Y. Lew and W. J. Book, "Bracing Micro/Macro manipulators control," in *Proceedings of 1994 IEEE ICRA,* San Diego, CA, 1994, .

[60] J. Zupancic and B. Tadej, "Comparison of position repeatability of a human operator and an industrial manipulating robot," *Computers in Biology and Medicine,* vol. 28, pp. 415, 1998.

[61] R. L. Hollis and R. Hammer, "Real and virtual coarse-fine robot bracing strategies for precision assembly," in *Proceedings of 1992 IEEE ICRA,* Nice, France, 1992, .

[62] A. Fields, K. Youcef-Toumi and H. Asada, "Flexible Fixturing and Automatic Drilling of Sheet Metal Parts Using a Robot Manipulator," *Robotics & Computer-Integrated Manufacturing,* vol. 5, pp. 371, 1989.

[63] S. Kim, M. Spenko, S. Trujillo, B. Heyneman, D. Santos and M. R. Cutkosky, "Smooth Vertical Surface Climbing With Directional Adhesion," *IEEE Trans. on Robotics,* vol. 24, pp. 64, 2008.

[64] S. K. Huang, S. K. S. Huang and D. J. Wilber, *Radiofrequency Catheter Ablation of Cardiac Arrhythmias: Basic Concepts and Clinical Applications.* Wiley-Blackwell, 2000.

[65] S. B. Kesner and R. D. Howe, "Design and control of motion compensation cardiac catheters," in *Robotics and Automation (ICRA), 2010 IEEE International Conference on,* 2010, pp. 1059-1065.

[66] M. Kaneko, T. Yamashita and K. Tanie, "Basic considerations on transmission characteristics for tendon drive robots," in *Advanced Robotics, 1991. 'Robots in Unstructured Environments', 91 ICAR., Fifth International Conference on,* 1991, pp. 827-832 vol.1.

[67] A. Nahvi, J. M. Hollerbach, Y. Xu and I. W. Hunter, "An investigation of the transmission system of a tendon driven robot hand," in *Intelligent Robots and Systems '94. 'Advanced Robotic Systems and the Real World', IROS '94. Proceedings of the IEEE/RSJ/GI International Conference on,* 1994, pp. 202-208 vol.1.

[68] G. Palli and C. Melchiorri, "Model and control of tendon-sheath transmission systems," in *Robotics and Automation, 2006. ICRA 2006. Proceedings 2006 IEEE International Conference on,* 2006, pp. 988-993.

[69] M. Nordin and P. Gutman, "Controlling mechanical systems with backlash - a survey," *Automatica,* vol. 38, pp. 1633-1649, 2002.

[70] E. K. Bassett, A. H. Slocum, P. T. Maslakos, H. I. Pryor, O. C. Farokhzad and J. M. Karp, "Design of a mechanical clutch-based needle-insertion device," *PNAS,* vol. 106, pp. 5540-5545, 2009.

[71] B. Armstrong-Helouvry, P. E. Dupont and C. Canudas De Wit, "A survey of analysis tools and compensation methods for control of machines with friction," *Automatica,* vol. 30, pp. 1083-1138, 1994.

[72] B. Siciliano and L. Villani, *Robot Force Control.* Kluwer Academic Publishers, 1999.

[73] S. Chiaverini, B. Siciliano and L. Villani, "A survey of robot interaction control schemes with experimental comparison," *Mechatronics, IEEE/ASME Transactions on,* vol. 4, pp. 273-285, 1999.

[74] S. Eppinger and W. Seering, "Introduction to dynamic models for robot force control," *Control Systems Magazine, IEEE,* vol. 7, pp. 48-52, 1987.

[75] S. Eppinger and W. Seering, "Understanding bandwidth limitations in robot force control," in *Robotics and Automation. Proceedings. 1987 IEEE International Conference on,* 1987, pp. 904-909.

[76] J. Maples and J. Becker, "Experiments in force control of robotic manipulators," in *Robotics and Automation. Proceedings. 1986 IEEE International Conference on,* 1986, pp. 695-702.

[77] W. Townsend and J. Salisbury Jr, "The effect of coulomb friction and stiction on force control," in *Robotics and Automation. Proceedings. 1987 IEEE International Conference on,* 1987, pp. 883-889.

[78] S. B. Kesner and R. D. Howe, "Discriminating tissue stiffness with a haptic catheter: Feeling the inside of the beating heart," in *IEEE World Haptics Conference ,* 2011, pp. 13-18.

[79] G. A. Gescheider, *Psychophysics: Method and Theory.* Hillsdale, NJ: Lawrence Erlbaum Associates, Inc., 1976.

[80] L. A. Jones and I. Hunter, "A perceptual analysis of stiffness," *Experimental Brain Research,* vol. 79, pp. 150-156, 1990.

[81] M. A. Srinivasan and R. H. LaMotte, "Tactual discrimination of softness," *J. Neurophysiol.,* vol. 73, pp. 88-101, 1995.

[82] R. H. LaMotte, "Softness discrimination with a tool," *J. Neurophysiol.,* vol. 83, pp. 1777, 2000.

[83] T. Meiß, C. Budelmann, T. A. Kern, S. Sindlinger, C. Minamisava and R. Werthschutzky, "Intravascular palpation and haptic feedback during angioplasty," in *EuroHaptics Conference, 2009 and Symposium on Haptic Interfaces for Virtual Environment and Teleoperator Systems. World Haptics 2009. Third Joint,* 2009, pp. 380-381.

[84] Y. Okumura, S. Johnson and D. Packer, "An analysis of catheter tip/tissue contact force-induced distortion of three-dimensional electroanatomical mapping created using the Sensei robotic catheter system," *Heart Rhythm,* vol. 4, pp. S318, 2007.

[85] A. G. Gallagher and C. U. Cates, "Virtual reality training for the operating room and cardiac catheterisation laboratory," *The Lancet,* vol. 364, pp. 1538-1540, 2004.

[86] S. L. Dawson, S. Cotin, D. Meglan, D. W. Shaffer and M. A. Ferrell, "Designing a Computer-Based Simulator for Interventional Cardiology Training," *Catheterization and Cardiovascular Interventions,* vol. 51, pp. 522-527, 2000.

[87] S. G. Yuen, K. A. Dubec and R. D. Howe, "Haptic noise cancellation: Restoring force perception in robotically-assisted beating heart surgery," in *Haptics Symposium, 2010 IEEE,* 2010, pp. 387-392.

[88] S. B. Kesner and R. D. Howe, "Design Principles for Rapid Prototyping Forces Sensors Using 3-D Printing," *Mechatronics, IEEE/ASME Transactions on,* pp. 1-5, 2011.

[89] P. F. Hokayem and M. W. Spong, "Bilateral teleoperation: An historical survey," *Automatica,* vol. 42, pp. 2035-2057, 2006.

[90] M. Tavakoli and R. D. Howe, "Haptic effects of surgical teleoperator flexibility," *The International Journal of Robotics Research,* vol. 28, pp. 1289-1302, 2009.

[91] W. R. Chitwood Jr, L. Nifong, J. E. Elbeery, W. H. Chapman, R. Albrecht, V. Kim and J. A. Young, "Robotic mitral valve repair: trapezoidal resection and prosthetic annuloplasty with the da Vinci surgical system," *J. Thorac. Cardiovasc. Surg.,* vol. 120, pp. 1171, 2000.

[92] J. Bodner, H. Wykypiel, G. Wetscher and T. Schmid, "First experiences with the da Vinci (TM) operating robot in thoracic surgery," *European Journal of Cardio-Thoracic Surgery,* vol. 25, pp. 844-851, 2004.

[93] P. C. Giulianotti, N. C. Buchs, G. Caravaglios and F. M. Bianco, "Robot-assisted lung resection: outcomes and technical details," *Interactive CardioVascular and Thoracic Surgery,* vol. 11, pp. 388, 2010.

[94] T. A. D'Amico, "Robotics in thoracic surgery: Applications and outcomes," *J. Thorac. Cardiovasc. Surg.,* vol. 131, pp. 19, 2006.

[95] V. Malhotra, "Transurethral resection of the prostate," *Anesthesiol. Clin. North America,* vol. 18, pp. 883-897, 2000.

[96] K. N. Garratt, U. P. Kaufmann, W. D. Edwards, R. E. Vlietstra and D. R. Holmes Jr, "Safety of percutaneous coronary atherectomy with deep arterial resection," *Am. J. Cardiol.,* vol. 64, pp. 538-540, 1989.

[97] F. Ikeno, T. Hinohara, G. C. Robertson, M. Rezaee, P. G. Yock, B. Reimers, A. Colombo, E. Grube and J. B. Simpson, "Early experience with a novel plaque excision system for the treatment of complex coronary lesions," *Catheterization and Cardiovascular Interventions,* vol. 61, pp. 35-43, 2004.

[98] J. M. Kalman, A. P. Fitzpatrick, J. E. Olgin, M. C. Chin, R. J. Lee, M. M. Scheinman and M. D. Lesh, "Biophysical characteristics of radiofrequency lesion formation in vivo: dynamics of catheter tip-tissue contact evaluated by intracardiac echocardiography," *Am. Heart J.,* vol. 133, pp. 8-18, 1997.

[99] D. Shah, H. Lambert, A. Langenkamp, Y. Vanenkov, G. Leo, P. Gentil-Baron and B. Walpoth, "Catheter tip force required for mechanical perforation of porcine cardiac chambers," *Europace,* vol. 13, pp. 277, 2011.

[100] D. C. Shah, H. Lambert, H. Nakagawa, A. Langenkamp, N. Aeby and G. Leo, "Area Under the Real-Time Contact Force Curve (Force-Time Integral) Predicts Radiofrequency Lesion Size in an In Vitro Contractile Model," *J. Cardiovasc. Electrophysiol.,* vol. 21, pp. 1038-1043, 2010.

[101] E. J. Butler, C. Folk, A. Cohen, N. V. Vasilyev, R. Chen, P. J. del Nido and P. E. Dupont, "Metal MEMS tools for beating-heart tissue approximation," in *Robotics and Automation (ICRA), 2011 IEEE International Conference on,* 2011, pp. 411-416.

[102] R. Wood, S. Avadhanula, R. Sahai, E. Steltz and R. Fearing, "Microrobot design using fiber reinforced composites," *Journal of Mechanical Design,* vol. 130, pp. 052304, 2008.